Arctic spring and summertime aerosol optical depth baseline from long-term observations and model reanalyses - Part 1: climatology and trend

Peng Xian[1], Jianglong Zhang[2], Norm T. O'Neill[3], Travis D. ~~Toth[3]~~Toth[4], Blake Sorenson[2], Peter R. ~~Colarco[4]~~Colarco[5], Zak ~~Kipling[5], Norm T. O'Neill[6]~~Kipling[6], Edward J. Hyer[1], James R. Campbell[1], Jeffrey S. Reid[1] and Keyvan ~~Ranjbar[6]~~Ranjbar[3, a]

[1]Naval Research Laboratory, Monterey, CA, USA.
[2]Department of Atmospheric Sciences, University of North Dakota, Grand Forks, ND
[3]~~NASA Langley Research Center, Hampton, Virginia, USA.~~
[4]~~NASA Goddard Space Flight Center, Greenbelt, MD, USA.~~
[5]~~European Centre for Medium-Range Weather Forecasts, Reading, UK.~~
[6]~~Département[3]~~Département de géomatique appliqué, Université de Sherbrooke, Sherbrooke, Québec, Canada
[4]NASA Langley Research Center, Hampton, Virginia, USA.
[5]NASA Goddard Space Flight Center, Greenbelt, MD, USA.
[6]European Centre for Medium-Range Weather Forecasts, Reading, UK.
[a]now at: Flight Research Laboratory, National Research Council Canada, Ottawa, ON, Canada

Correspondence: Peng Xian (peng.xian@nrlmry.navy.mil)

Abstract

We present an Arctic aerosol optical depth (AOD) climatology and trend analysis for 2003-2019 spring and summertime periods derived from a combination of multi-agency aerosol reanalyses, remote sensing retrievals, and ground observations. This includes the U.S. Navy Aerosol Analysis and Prediction System ReAnalysis version 1 (NAAPS-RA v1), the NASA Modern-Era Retrospective Analysis for Research and Applications, version 2 (MERRA-2), and the Copernicus Atmosphere Monitoring Service ReAnalysis (CAMSRA). Space-borne remote sensing retrievals of AOD are considered from the Moderate Resolution Imaging Spectroradiometer (MODIS), the Multi-angle Imaging SpectroRadiometer (MISR), and Cloud-Aerosol Lidar with Orthogonal Polarization (CALIOP). Ground-based data include sun photometer data from Aerosol Robotic Network (AERONET) sites and oceanic Maritime Aerosol Network (MAN) measurements. Aerosol reanalysis AODs and space-borne retrievals show consistent climatological spatial patterns and trends for both spring and summer seasons over the lower-Arctic (60-70°N). Consistent AOD trends are also found for the high Arctic (north of 70°N) from reanalyses. The aerosol reanalyses yield more consistent AOD results than climate models, verify well with AERONET, and corroborate complementary climatological and trend analysis. Speciated AODs are more variable than total AOD among the three reanalyses, and a little more so for March-May (MAM) than for June-August (JJA). Black Carbon (BC) AOD in the Arctic comes predominantly from biomass burning (BB) sources in both MAM and JJA, and BB overwhelms anthropogenic sources in JJA for the study period.

AOD exhibits a multi-year negative MAM trend, and a positive JJA trend in the Arctic during 2003-2019, due to an overall decrease in sulfate/anthropogenic pollution, and a significant JJA increase in BB smoke. Interannual Arctic AOD variability is significantly large, driven by fine-mode, and specifically, BB smoke, with both smoke contribution and interannual variation larger in JJA than in MAM. It is recommended that climate models should account for BB emissions and BB interannual variabilities and trends in Arctic climate change studies.

1. Introduction

The Arctic is warming faster than the overall global climate, a phenomenon widely known as Arctic amplification (Serreze and Francis 2006; Serreze and Barry 2011). This has led to rapid changes in regional sea ice properties. September sea ice coverage is shrinking at an unprecedented rate (Comiso 2012; Meier et al., 2014). Younger and thinner ice is replacing thick multi-year sea ice (Kwok and Rothrock 2009; Hansen et al, 2013; Rosel et al. 2018). Mechanisms contributing to sea ice changes include increased anthropogenic greenhouse gases (Notz and Stroeve 2016; Dai et al., 2019), sea ice-albedo feedback (Perovich and Polashenski 2012), increased warm and moist air intrusion into the Arctic (Boisvert et al. 2016; Woods et al., 2016; Graham et al. 2017), radiative feedbacks associated with cloudiness and humidity (Kapsch et al. 2013; Morrison et al. 2018), and increased ocean heat transport (Nummelin et al., 2017; Taylor et al. 2018). However, one of the least understood factors of Arctic change is the impact of aerosols on sea ice albedo and concentration (IPCC ~~2013~~2021).

Atmospheric aerosol particles from anthropogenic and natural sources reach or can be found in the Arctic region ~~through both~~as the result of long-range transport and local emissions~~, affecting~~ respectively. This affects regional energy balance through both direct and indirect radiative processes (Quinn et al., 2008; Engvall et al., 2009; Flanner, 2013; Sand et al., 2013; Markowicz et al., 2021; Yang et al., 2018). Aerosol particles influence cloud microphysical properties as cloud condensation nuclei (CCN) and/or ice ~~nuclei (IN~~nucleating particles (INP), affecting cloud albedo, lifetime, phase, and probability of precipitation (e.g., Lubin and Vogelmann, 2006; Lance et al., 2011; Zamora et al, 2016; Zhao and Garrett 2015; Bossioli et al., 2021). Additionally, deposition of light-absorbing aerosol species such as dust and black/brown carbon on the surface of snow and ice can trigger albedo feedbacks and facilitate melting and prolong melting seasons (Hansen & Nazarenko, 2004; Jacobson, 2004; Flanner et al., 2007; Skiles et al., 2018; Dang et al., 2017; Kang et al., 2020). However, the impact of aerosol particles on polar climate change is still not well characterized, and their relative importance compared to other warming factors is difficult to isolate and quantify.

Climate modeling studies show that due to stronger feedback processes between the atmosphere-ocean-sea-ice-land the Arctic region is more sensitive to local changes in radiative forcing than tropical and mid-latitude regions (Shindell and Faluvegi 2009; Sand et al., 2013). ~~On the other hand~~Furthermore, there seems to be an emerging agreement on a higher sensitivity of Arctic clouds by aerosol particles than lower-latitude regions due to the very low aerosol amounts compared to lower latitudes (Prenni et al., 2007; Mauritsen et al. 2011; Birch et al., 2012; Coopman et al., 2018; Wex et al., 2019). Both underscore the important role aerosol particles may play in the

93 Arctic weather and climate, and the urgency to better quantify the amount of aerosols in
94 the Arctic.

95 A variety of atmospheric aerosol species exist in the Arctic region. Anthropogenic
96 pollution contributes significantly to the formation of the Arctic haze, which generally
97 occurs in later winter and spring due to wintertime build-up in the shallow boundary
98 layer with effective transport and reduced removal (e.g., Law and Stohl, 2007; Quinn et
99 al., 2008). Biomass burning (BB) smoke, originating from wildfires in boreal North
100 America and Eurasia, are often observed and/or modeled being transported into the
101 Arctic (Eck et al. 2009; Eckhardt et al. 2015; Stohl et al. 2007; Warneke et al. 2009;
102 Iziomon et al., 2006; Evangeliou et al. 2016; Kondo et al., 2011; Brieder et al., 2014;
103 Markowicz et al. 2016; Khan et al., 2017; Engelmann et al., 2021). Airborne dust,
104 emitted from exposed sand or soils due to glacier retreat (Bullard et al., 2016; Groot
105 Zwaaftink et al., 2016), are likely on the rise as the Arctic warms. Dust can also
106 originate from lower latitude deserts, e.g., Sahara and Asia, and arrive in the Arctic
107 through long-range transport (Stone et al, 2007; Breider et al., 2014; AboEl-Fetouh et
108 al., 2020). As the Arctic sea-ice melts and the ice-free surface increases, emissions of
109 sea salt and biogenic aerosols (e.g., from dimethylsulfide; Dall et al., 2017; Gabric et al.,
110 2018) are expected to increase. There are also ultrafine particles nucleated from
111 gaseous precursors, though in small amounts (Baccarini et al., 2021; Abbatt et al.,
112 2019).

113 Because of the harsh surface environment endemic to the Arctic, aerosol field
114 measurements are limited in comparison with the mid-latitude and tropical
115 environments. Despite an increasing number of field campaigns carried out over the
116 past two decades (e.g., review by Wendisch et al., 2019; and more recently the
117 MOSAiC, https://mosaic-expedition.org) and their usefulness in improving process-level
118 understanding, field measurement periods tend to be short and limited to certain areas
119 and thus are not necessarily representative spatially and temporally of the whole Arctic.
120 There are many Arctic-aerosol optical property studies that are based on long-term site
121 measurements (e.g., Herber et al., 2002; Tomasi et al., 2007; Eck et al., 2009; Glantz et
122 al., 2014; Ranjbar et al., 2019; AboEl-Fetouh et al., 2020), however, the). The number
123 of sites is, however, limited and of irregular spacing (mostly located at the northern edge
124 of the North American, Eurasian continents, and the Svalbard region).

125 Climate models that are not well constrained by observations exhibit large variations in
126 basic aerosol optical properties, with: one finds, for example, an order of magnitude
127 difference in simulated regional aerosol optical depth (AOD) and large differences in the
128 simulated seasonal cycle of AOD over the Arctic (e.g., Glantz et al., 2014; Sand et al.,
129 2017). TheseSuch results will not reduce the uncertainty in the radiative impact of
130 aerosols through direct (including surface albedo effect) and indirect forcings in the
131 Arctic climate. Impacts of aerosols and clouds, overall, constitute one of the largest

132 sources of uncertainty in climate models (IPCC 2013). This is apparently exacerbated in
133 a warming Arctic (Goosse et al., 2018). A modeling study by DeRepentigny et al. (2021)
134 shows that the inclusion of interannually varying BB emissions, compared with only
135 climatological emissions, results in simulations of large Arctic climate variability and
136 enhanced sea ice loss. This finding suggests the sensitivity of climate relevant
137 processes to aerosol interannual variability in the Arctic.

138 In this paper, we present an AOD climatology and trend analysis for the 2003-2019
139 Arctic spring and summertime, based on a combination of multi-national interagency
140 aerosol reanalyses, satellite remote sensing retrievals, and ground observations. We
141 define the Arctic and the high-Arctic as regions north of 60°N and 70°N respectively.
142 The lower-Arctic is defined as regions between 60°N-70°N. To reference lower-latitude
143 source influences, the area of 50°N-90°N is included for context.

144 There are clear advantages to using aerosol reanalyses of chemical transport models in
145 comparison with climate models for Arctic aerosol studies. Smoke emissions are
146 frequently updated (hourly rather than monthly BB smoke emission sources for
147 example) while satellite observations of both meteorological and aerosol data are also
148 incorporated into those aerosol reanalyses through data assimilation. High-latitude fires
149 are strongly influenced by weather patterns including large-scale transport patterns
150 (e.g., Flannigan and Harrington 1998; Skinner et al. 1999). Thus, BB smoke in
151 particular, is more realistically accounted for in aerosol reanalyses.

152 To our knowledge, this is the first time aerosol reanalysis products are evaluated and
153 compared over the Arctic. The goal of the study is to provide a baseline of AOD
154 distribution, magnitude, speciation, and interannual variability over the Arctic during the
155 sea ice melting season. Statistics of Arctic extreme AOD events is provided in a
156 companion paper (Part 2). The baseline can be used for evaluating aerosol models,
157 calculating aerosol radiative forcing, and providing background information for field
158 campaign data analysis and future field campaign planning in a larger climate context.
159 This paper is organized as follows: Sect. 2 and 3 introduce the data sets and methods
160 respectively. Sect. 4 verifies the reanalyses. Results are reported in Sect. 5.
161 Discussions and conclusions are provided in Sect. 6 and 7.

162
163 **2. Data**
164 A combination of aerosol reanalyses, satellite-based aerosol remote sensing data, and
165 ground-based aerosol measurements are used to describe source dependent AOD and
166 its trend over the Arctic during spring (March-May, ie., MAM) and summertime (June-
167 August, ie., JJA). Note that "MAM" and "JJA" are meant to represent convenient and
168 informative acronyms for springtime and summertime. In the sections where we discuss
169 MAM and JJA trends we refer to, respectively, year to year trends of springtime and

170 ~~summertime AODs (not seasonal trends from March to April to May or June to July to~~
171 ~~August averaged over the multi-year sampling period).~~i.e., MAM) and summertime (i.e.,
172 JJA). The aerosol reanalyses include the Navy Aerosol Analysis and Prediction System
173 reanalysis (NAAPS-RA; Lynch et al., 2016) developed at the Naval Research
174 Laboratory, the NASA Modern-Era Retrospective Analysis for Research and
175 Applications, version 2 (MERRA-2; Randles et al., 2017), and the Copernicus
176 Atmosphere Monitoring Service ReAnalysis (CAMSRA; Inness et al., 2019) produced at
177 ECMWF. The remote sensing data include AOD retrievals from the Moderate
178 Resolution Imaging Spectroradiometer (MODIS; Levy et al., 2013), the Multi-angle
179 Imaging SpectroRadiometer (MISR; Kahn et al., 2010), and Cloud-Aerosol Lidar with
180 Orthogonal Polarization (CALIOP). Sun photometer data from Aerosol Robotic Network
181 ~~(AERONET; Holben et al., 1998)~~ sites and oceanic Maritime Aerosol Network
182 ~~(~~measurements were employed as key validation components (respective citations of
183 AERONET; Holben et al., 1998 and MAN, Smirnov et al., 2009~~) measurements.~~).
184 Overviews of remote sensing techniques for Arctic aerosols can be found in Tomasi et
185 al. (2015) and Kokhanovsky et al. (2020). The analysis period is focused on 2003-2019,
186 when all three aerosol reanalyses are available. A summary of the datasets is provided
187 in Appendix A.
188
189 2.1 MODIS AOD
190
190 AOD data from MODIS on Terra and Aqua was based on Collection 6.1 Dark Target
191 and Deep Blue retrievals (Levy et al., 2013). Additional quality control and some
192 corrections were applied as described in Zhang and Reid 2006, Hyer et al. 2011, Shi et
193 al. 2011, and Shi et al. 2013, and were updated for the Collection 6.1 inputs. The 550
194 nm quality-assured and quality-controlled MODIS C6 AOD data ~~(550 nm)~~ are a level 3
195 product that is produced at 1°x1° latitude/longitude spatial and 6-hrly temporal
196 resolution. Those 6-hrly (averaged) MODIS AOD data were then monthly-binned in
197 order to study long-term aerosol climatology and trends. ~~Seasonal~~Seasonnally-binned
198 (year to year) means and trends were derived only when the total count of 1°x1° degree
199 and 6-hrly data ~~was greater than~~exceeded 10 for a season.
200
201 2.2 MISR AOD
202 The MISR instrument onboard the Terra satellite platform provides observations at nine
203 different viewing zenith angles across four different spectral bands ranging from 446 to
204 866 nm. These instrumental configurations facilitate AOD retrievals over bright surfaces,
205 such as desert regions (Kahn et al., 2010). MISR Version 23 AOD data at 558 nm
206 (Garay et al., 2020) were analyzed ~~between Jan 2003 and December 2019.~~. No MISR
207 AOD is available over Greenland due to snow and ice coverage. Monthly gridded MISR
208 AOD data were created by averaging only MISR data with 100% clear pixels~~,~~ (as

209 defined by each pixel's 'cloud screening parameter'~~,~~) at a spatial resolution of 1°~~x1~~x 1°
210 latitude/longitude. Only monthly grid cells whose number of ~~MODIS~~MISR 100%-cloud-
211 clear AODs was greater than 20 were used to derive the climatology and trend.
212
213 2.3 CALIOP AOD

214 Cloud-Aerosol Lidar with Orthogonal Polarization (CALIOP), the primary instrument on
215 the Cloud-Aerosol Lidar and Infrared Pathfinder Satellite Observations (CALIPSO)
216 satellite, is a polarization-sensitive lidar that operates at two wavelengths (532 and 1064
217 nm; Winker et al. 2003). It has, since its launch in 2006, collected a continuity of vertical
218 aerosol and cloud profiles. We primarily ~~utilized~~used daytime and nighttime 532 nm
219 aerosol extinction coefficient data from the Version 4.2 (V4.2) Level 2 (L2) aerosol
220 profile product (Kim et al., 2018). The product resolution is 5 km in horizontal~~/~~ and 60 m
221 in vertical ~~resolution) (Kim et al., 2018), with the V4.2 L2.~~ The aerosol layer product was
222 used for quality assurance (QA) procedures. The CALIOP aerosol profiles are~~, as~~
223 ~~implemented and described in detail in past studies,~~ rigorously QAed before analysis
224 (Campbell et al. 2012; Toth et al. 2016; 2018). Only cloud-free CALIOP profiles are
225 used~~, as~~: this was determined through the atmospheric volume description (AVD)
226 parameter included in the aerosol profile product (i.e., ~~we implemented a strict cloud~~
227 ~~screening procedure for which~~ we excluded CALIOP profiles with any range bin
228 classified as cloud by the AVD parameter). A significant portion of CALIOP aerosol
229 profile data consists of retrieval fill values (-9999s, or RFVs) that are, in part, due to the
230 minimum detection limits of the lidar. In fact, ~~for some areas in the Arctic region,~~ over
231 80% of CALIOP profiles consist entirely of RFVs in some Arctic regions (Toth et al.
232 2018). These result in zero-valued column AODs ~~being equal to zero: including them:~~
233 their inclusion in ~~the~~ composites would artificially lower the mean AOD. They were thus
234 excluded from our analysis. We also tested retaining AOD=0 values in our analysis and
235 that did not change the AOD trends (see more discussions in section 6). Lastly, the
236 cloud-free QAed profiles without AOD=0 profiles were used to compute mean CALIOP
237 AODs at 2° x 5° latitude/longitude resolution. To ensure spatial and temporal
238 representation, ~~seasonal~~seasonally-binned means and trends were derived only when
239 the total count of gridded data ~~is~~in any season exceeded 20.

240 2.4 AERONET
241 The AErosol RObotic NETwork (AERONET) is a ground-based global sun photometer
242 network. AERONET instruments measure sun and sky radiance ~~at several~~
243 ~~wavelengths,~~in spectral bands ranging from the near-ultraviolet to the ~~near~~short-wave-
244 infrared. This network has been providing daytime aerosol-property measurements ~~of~~
245 ~~aerosol properties~~ since the 1990s (Holben et al., 1998; Holben et al., 2001). Only
246 cloud-screened, quality-assured version 3 Level 2 AERONET data (Giles et al., 2019)
247 are used in this study.

248

249 The 500 nm fine mode (FM) and coarse ~~model~~mode (CM) AODs from the Spectral
250 Deconvolution Method (SDA) of O'Neill et al. (2003), along with the FM spectral
251 derivative at 500 nm are used to extrapolate FM AOD to 550 nm. ~~It is assumed the~~
252 (assuming equal CM AOD at 500 ~~nm~~ and 550 nm ~~are equal.~~). Total AOD is simply the
253 sum of FM and CM AODs. The SDA product is an AERONET product that has been
254 verified using in situ measurements (see for example Kaku et al., 2014) and a variety of
255 co-located lidar experiments (see, for example, Saha et al., 2010 and Baibakov et al.,
256 2015). The FM and CM separation is effected spectrally: this amounts to a separation of
257 the FM and CM optical properties associated with their complete FM and CM particle
258 size distributions. This optical separation, characterized by the ratio of FM AOD to total
259 AOD at 550 nm is referred to as the fine mode fraction (FMF). An analogous FM and
260 CM AOD separation in terms of a cutoff radius applied to a retrieved or measured
261 particle size distribution is referred to as the sub-micron fraction (SMF; where the
262 numerator of the SMF is the FM AOD associated with the AOD contribution of particles
263 below a cutoff radius). The SMF is the basis for separating FM and CM components in
264 the AERONET (AOD & sky radiance) inversion. The SDA algorithm and the AERONET
265 inversion generate FM and CM AODs that are moderately different (see, for example,
266 Sect. 4 of Kleidman et al., 2005). The advantage of the SDA is its significantly
267 ~~higher~~shorter intersampling time and thus retrieval ~~resolution (~ a few minutes versus ~~~
268 ~~an~~numbers (~ 20 / hour vs ~ 1 / hour for the AERONET inversion~~) and thus retrieval~~
269 ~~numbers,~~), its independence from a variable cut off radius and its greater operational
270 generality (being applicable to other networks such as the MAN sunphotometer
271 network).

272

273 AERONET data were binned into 6-hr intervals centered at normal synoptic output
274 times of the reanalyses (0, 6, 12, and 18 UTC) and then averaged within the bins. ~~The~~
275 ~~monthly~~Monthly-mean temporal representativeness was rendered more likely by only
276 including means with more than 18 6-hr data bins. Ten AERONET sites (Table 1, Fig. 1)
277 were selected based on regional representativeness (coupled with the reality of the
278 sparsity of AERONET sites in the Arctic), the availability of data records between Jan
279 2003 and Dec 2019 ~~(the main study period),~~, and for easier comparison with other
280 Arctic studies (e.g., Sand et al., 2017). To explore the potential impact of different
281 sampling resolutions on the results (e.g., Balmes et al., 2021), we generated daily AOD
282 statistics (Table S1) that could be compared with Table 1 ~~6hrly~~6 hrly statistics. In
283 general, the mean and median of MAM or JJA AODs (including total, FM and CM
284 AODs) at the ten AERONET sites change very slightly (mostly 0.00, or <=0.01). The
285 daily AOD standard deviation was less than its ~~6hrly~~6 hrly analogue.

286

287 We found that thin clouds could occasionally be identified and retrieved as CM aerosols
288 in level 2, version 3 AERONET data. These retrievals were manually removed by
289 identifying such thin clouds using Terra and Aqua visible-wavelength imagery from
290 NASA Worldview and comparing 6-hrly NAAPS-RA with AERONET AODs. CM AODs
291 greater than the 3-sigma level were then also removed (as per AboEl-Fetouh et al.,
292 2020).
293
294 2.5 MAN AOD
295 The Marine Aerosol Network (MAN) is a hand-held Microtops sun photometer (research
296 vessel based) counterpart to AERONET employed for: ocean measurements in
297 areasare acquired where no-land based AERONET site can exist (Smirnov et al., 2009,
298 2011). The products share AERONET product nomenclature and data processing is
299 similar to that of AERONET. Level 2 data above 70°N for the period of 2003-2019 were
300 employed in this study. SDA-based FM and CM AOD at 550 nm were derived and
301 averaged over 6-hr time bins.
302
303 2.6 NAAPS AOD reanalysis v1
304 The Navy Aerosol Analysis and Prediction System (NAAPS) AOD ReAnalysis (NAAPS-
305 RA) v1 provides 550 nm, global-scale, speciated AODAODs at a global scale with 1°x1°
306 degreex 1° spatial and 6-hrly temporal resolution for the years 2003-2019 (Lynch et al.,
307 2016). This NAAPS-based reanalysis is based on NAAPS withincorporates assimilation
308 of quality-controlled retrievals of AOD from, MODIS and MISR AOD retrievals (Zhang et
309 al., 2006; Hyer et al., 2011; Shi et al., 2011). AODs from anthropogenic and biogenic
310 fine aerosol species (ABF,; a non-BB sources mixture of sulfate, black carbon or BC,
311 organic aerosols and secondary organic aerosols from non-BB sources), dust, biomass-
312 burningBB smoke, and sea salt aerosols are available. The aerosol source functions
313 were tuned to obtain the best match between the model FM and CM AODs and the
314 AERONET AODs for 16 regions globally. Wet deposition processes were constrained
315 with satellite-derived precipitation (Xian et al., 2009). The reanalysis reproduces the
316 decadal AOD trends found using standalone satellite products (e.g., Zhang et al., 2010;
317 2017 who excluded polar regions due to lack of verification data).

318 2.7 MERRA-2 AOD reanalysis

319 NASA Modern-Era Retrospective Analysis for Research and Applications, version 2
320 (MERRA-2) includes an aerosol reanalysis, which scheme that incorporates AOD
321 assimilation of AOD from a variety of remote sensing data sources, including MODIS
322 and MISR after 2000. The aerosol module used for MERRA-2 is the Goddard
323 Chemistry, Aerosol Radiation and Transport model (GOCART; Chin et al. 2000; Colarco
324 et al., 2010), which). It provides simulations of sulfate, black and organic carbon, dust

325 and sea salt aerosols. A detailed description and global validation of the AOD reanalysis
326 product can be found in Randles et al. (2017) and Buchard et al. (2017). For this study,
327 monthlyMonthly mean speciated AODs and total AOD at 550 nm with 0.5° latitude and
328 0.625° longitude spatial resolution were used for this study.

329 2.8 CAMSRA AOD reanalysis

330 The Copernicus Atmosphere Monitoring Service (CAMS) Reanalysis (CAMSRA, Inness
331 et al., 2019) is a new ECMWF-led global reanalysis of atmospheric composition
332 produced at the ECMWF.(Inness et al., 2019). It followed on the heels of the MACC
333 reanalysis (Inness et al., 2013) and CAMS interim reanalysis (Flemming et al., 2017).
334 The dataset covers the period of 2003–2020 and is being continued forextended to
335 subsequent years. The model is driven by the Integrated Forecasting System (IFS)
336 used at ECMWF for weather forecasting and meteorological reanalysis (but at a coarser
337 resolution). It incorporates additional modules activated for prognostic trace gases and
338 aerosol species (, including dust, sea salt, organic matter, black carbon and sulfate) and
339 trace gases. The radiative impact of aerosol particles and ozone on meteorology is
340 included. Satellite retrievals of total AOD at 550 nm are assimilated from MODIS for the
341 whole period, and from the Advanced Along-Track Scanning Radiometer for 2003–
342 2012, using a 4D variational data assimilation system with a 12-hour data assimilation
343 window along with meteorological and trace gas observations. The speciated AOD
344 products are available at a 3-hourly with monthly temporal resolution and a ~0.7° spatial
345 resolution, and monthly mean AODs at 550 nm were used in this study. Model
346 development has generally improved the speciation of aerosols compared with earlier
347 reanalyses, and evaluation against AERONET globally is largely consistent over the
348 period of the reanalysis.

349 2.9 Multi-reanalysis-consensus (MRC) AOD

350 All three of the individual reanalyses are largely independent in their underlying
351 meteorology and in their aerosol sources, sinks, microphysics, and chemistry. They
352 were also generated through data assimilation (DA) of satellite and/or ground-based
353 observations of AOD. The assimilation methods, and the assimilated AOD observations,
354 including the treatments of the observations prior to assimilation (quality control, bias
355 correction, aggregation, and sampling, etc.), often differ. There is, on the other hand,
356 consistent use of MODIS data with its daily global spatial coverage.

357 Based on the three aerosol reanalysis products described above, we made an MRC
358 product following the multi-model-ensemble method of the International Cooperative for
359 Aerosol Prediction (ICAP, Sessions et al., 2015; Xian et al., 2019). The MRC is a
360 consensus mean of the three individual reanalyses, with a 1°x1° degree spatial and
361 monthly temporal resolution. Speciated AODs and total AOD at 550 nm for 2003-2019

362 are available. This new product is validated here, along with the three component
363 reananlysis members, using ground-based Arctic AERONET observations. Validation
364 results in terms of bias, RMSE, and coefficient of determination (r^2) for monthly-mean
365 total, FM and CM AODs are presented in Tables 2, 3, 4. The MRC, in accordance with
366 the ICAP multi-model-consensus evaluation result, is found to generally be the top
367 performer among all of the reanalyses for the study region.

368 2.10 Fire Locating and Modeling of Burning Emissions (FLAMBE) v1.0
369
370 FLAMBE is a biomass-burning emission inventory derived from a satellite-based active
371 fire hotspot approach (Reid et al., 2009; Hyer et al., 2013). FLAMBE can take satellite
372 fire products from either geostationary sensors, which offer faster refresh rates and
373 observation of the full diurnal cycle, or polar orbiters, which have a greater sensitivity.
374 There are significant daily sampling biases and additional artifacts ~~from~~induced by day
375 to day shifts in the orbital pattern for polar-orbiting satellites (e.g., Heald et al., 2003,
376 Hyer et al., 2013). However, the polar-only version of FLAMBE, which employed
377 MODIS-based fire data, is more appropriate for reanalysis and trend analysis. This is
378 because multiple changes in the geostationary constellation over the ~~stud~~study period
379 posed a challenge in terms of smoke source-function consistency. The FLAMBE
380 MODIS-only smoke source was also used in the NAAPS-RA v1 because of the same
381 temporal consistency requirement. FLAMBE ~~show~~shows similar BB emission trends as
382 the ~~time series of~~ yearly BB emission time series for the Arctic region based on other
383 inventories for a similar study period (using BC emission of Fig. 2 in McCarty et al.,
384 2021). These inventories include the Global Fire Assimilation System (GFAS; Kaiser et
385 al., 2012), and the Global Fire Emission Dataset (GFED; Randerson et al., 2006; van
386 derWerf et al., 2006).
387
388   **3. Method**

389 The Arctic AOD climatology and trends are analyzed in this study using remote sensing
390 products derived from MODIS, MISR, CALIOP, and AERONET (each sensor typically
391 generating aerosol products of different native wavelengths). The 550 nm AOD was
392 employed as the benchmark parameter ~~for this study~~ since the three aerosol reanalyses
393 AODs and the MODIS AOD are all available at 550 nm while the 558nm and 532nm
394 AODs of MISR and CALIOP are appreciably close to 550 nm. AERONET and MAN
395 modal AODs at 550 nm were derived using the SDA method as described in Sect. 2.4
396 and 2.5. Arithmetic means were employed for all the data processing in order to be
397 consistent with the arithmetic statistics that are usually reported in the literature and with
398 the arithmetic statistics of the monthly data from the aerosol reanalyses. Various studies
399 have shown that geometric statistics are more representative of AOD histograms (see,
400 for example, Hesaraki et al., 2017 and Sayer et al., 2019). However, Hesaraki et al.

401 (2017) showed that arithmetic statistics could be employed to readily estimate
402 geometric statistics[1]. This option effectively renders the reporting of arithmetic or
403 geometric statistics less critical.

404 The species of interest are ~~biomass burning (~~BB~~)~~ smoke, ~~anthropogenic and biogenic~~
405 ~~fine aerosols (~~ABF~~)~~ in NAAPS, and its ~~equivalent~~analogue of sulfate for MERRA-2 as
406 well as CAMSRA and dust and sea salt aerosols. Anthropogenic aerosol particles, as
407 ~~an~~ external climate ~~forcer~~forcers, have drawn some attention in climate studies (e.g.,
408 Wang et al., 2018; Ren et al., 2020; Yang et al., 2018; Sand et al., 2016; Eckhardt et al.,
409 2015; Brieder et al., 2017). However, BB smoke, which can be both natural and
410 anthropogenic in origin, has been shown to be the largest contributor (over the last two
411 decades) to Arctic summer AOD and concentration (Evangeliou et al. 2016; Sand et al.
412 2017 for modelling studies and Eck et al. 2009; Eckhardt et al. 2015; Stohl et al. 2007;
413 Warneke et al. 2009 for observational-based studies). Recent BC measurements ~~of BC~~
414 in Arctic snow also show a strong association with BB based on modelled tracer
415 correlations ~~and~~with measured optical properties of snow (Hegg et al., 2009; Doherty et
416 al., 2010; Hegg et al., 2010; Khan et al., 2017). A climate modeling study recently found
417 that much larger Arctic climate variability and enhanced sea ice melting were introduced
418 using BB emissions with interannual variability as opposed to fixed climatological
419 monthly-mean BB emissions (DeRepentigny et al., 2021), a result that underscored the
420 importance of quantifying the magnitude and interannual variability of BB smoke in
421 Arctic climate forcing estimates. Thus BB smoke AOD is separated out from the total
422 AOD as a singularly important species in this study.

423 The separation of species in this analysis is a bit arbitrary since the representation of
424 different aerosol types and sources in each reanalysis is slightly different. The NAAPS
425 model is unique compared to other reanalyses and operational models in that it carries
426 aerosol species by source rather than chemical speciation. For example, biomass
427 burning ~~and a combined~~ ABF are carried as separate species and permit explicit
428 hypothesis testing about the sources, sinks, and optical properties. Conversely,
429 MERRA-2 and CAMSRA carry organic carbon (OC)/organic matter (OM), ~~black carbon~~
430 ~~(~~BC~~)~~ and various inorganic species combining a multitude of anthropogenic, biogenic
431 and ~~open~~ biomass burning source pathways. In this study the sum of OC/OM and BC
432 AOD is used to approximate BB smoke AOD from CAMSRA and MERRA-2. The ratio of
433 BC AOD to the sum of BC and OC/OM AOD is, on average, about 10% for areas north
434 of 60°N ~~on average~~ for both MERRA-2 and CAMSRA for both MAM and JJA (the single
435 exception to this is that the MERRA-2 ratio is about ~~20~~18% in MAM). The ratios change
436 little for area >70°N and area >80°N.

---

[1] with an erratum: the equation (2) transformation to geometric mean should be $\tau_{g,x} = \frac{<\tau_x>}{\exp\left(\frac{\ln^2 \mu_x}{2}\right)})$

437 It is worth noting that ~~all~~ the three reanalyses use either hourly~~/~~ or daily BB smoke
438 emission inventories: inventories that ~~use~~employ dynamic smoke sources detected by
439 polar-orbiting satellites. Examples include FLAMBE (Reid et al., 2009) for NAAPS-RA,
440 Quick Fire Emissions Dataset (QFED) for MERRA-2 after 2010 (GFED with monthly BB
441 emission before 2010~~,~~ as per Randerson et al., 2006~~;~~ and van derWerf et al., 2006),
442 and Global Fire Assimilation System (GFAS, Kaiser et al., 2012) for CAMSRA. This is
443 expected to yield a better spatial and temporal representation of BB smoke emissions
444 compared to climate models which use monthly mean BB inventories (e.g., Sand et al.,
445 2017).

446 We also assume all dust and sea salt are CM, while other model aerosol species,
447 including ABF in NAAPS-RA, sulfate in MERRA-2 and CAMSRA, BB smoke in NAAPS-
448 RA, ~~black carbon~~BC and ~~organic carbon~~OC/OM in MERRA-2 and CAMSRA are FM
449 aerosol particles. This approximation (the sequestering of dust and sea salt to the
450 ~~coarse mode~~CM regime) is based on the fact that FM dust and sea salt only contribute
451 a small portion of the total dust or sea salt AOD at 550 nm. For example, FM ~~mode~~dust
452 represents about 30% and 39% of total dust AOD globally in MERRA-2 and CAMSRA
453 respectively. The numbers are 17% and 10% for sea salt. ~~While~~NAAPS-RA makes the
454 simplifying microphysical assumption that all dust and sea salt are CM. ~~This usage~~
455 ~~renders the FM~~

456 For verification purpose, bias, root-mean-square deviation (RMSE) and ~~CM bulk aerosol~~
457 ~~comparisons more tractable (with~~coefficient of determination (denoted r^2) of reanalysis
458 AODs compared to AERONET/MAN AODs are calculated. r^2 equals the square of the
459 ~~rider~~Pearson correlation coefficient between the observed and the modeled AODs.
460 When estimating contributions of individual species to total AOD interannual variability,
461 r^2 is calculated as the square of the Pearson correlation coefficient between the
462 seasonally-binned modeled speciated AOD and total AOD. In that ~~we must remain~~
463 ~~conscious of any artificial separation that might~~form, r^2 provides the percentage of
464 "explained variance" of total AOD by a speciated AOD. The statistical definition and
465 interpretation of r^2 can be ~~created by any FM or CM oversimplification).~~ found
466 https://en.wikipedia.org/wiki/Coefficient_of_determination.

467 The significance test for trend analysis applies the same calculation method as in Zhang
468 et al. (2010; 2017), an approach which, in turn, was based on the method of
469 Weatherhead et al. (1998). This trend analysis method requires a continuous time
470 series of data.

471 **4. Comparison of AODs from aerosol reanalyses and AERONET**

472 The number of AERONET observations are tied to the increase in the number of
473 daylight hours and are therefore more numerous during the summer than in the spring.

474   This translates to their generally being more temporally representative of 6 hr or daily
475   means in JJA. As a consequence, we preferentially used a JJA climatology to illustrate
476   reanalyses vs AERONET comparisons. Fig. 1 shows the 2003-2019 mean JJA FM and
477   CM AODs from AERONET and the speciated AODs from NAAPS-RA, MERRA-2, and
478   CAMSRA (all at 550 nm).. All three aerosol reanalyses appear to capture the total AOD
479   magnitudes to varying extents. The AERONET retrievals show that total AOD during the
480   Arctic JJA season is dominated by contributions from FM aerosols. Large FM AOD
481   values (generally indicative of strong BB smoke influence) are found in Yakutsk and
482   Tiksi in Siberia, and Bonanza Creek in Alaska. CM aerosols also contribute a
483   substantial fraction, varying from a minimum of 15% in regions close to BB smoke
484   sources to a maximum of ~25% at the Norwegian Sea and Greenland Sea coastal sites
485   (Hornsund, Andenes, and Ittoqqortoormitt): these sites are likely impacted by sea salt
486   aerosols lifted by North Atlantic cyclonic events. NAAPS-RA produces AERONET-
487   comparable FM and total AODs in general while showing a tendency to overestimate
488   CM AODs (see Table 2 for explicit biases). The other two reanalyses (MERRA-2 and
489   CAMSRA) produce higher FM AOD and total AOD and lower CM AOD compared to
490   AERONET (see also Table 2).

491   Differences exist between the three reanalyses with respect to the FM and CM
492   partitioning of aerosol species. For example, sea salt aerosols always dominate in the
493   CAMSRA (dust + sea salt) CM: this comment even applies to some inland sites (e.g.,
494   Bonanza-Creek) and implies a modeling issue. Dust is the dominant CM species in
495   NAAPS-RA and MERRA-2. This latter result was foundis true at all AERONET site
496   positions: it is likely attributable to elevated dust layers transported from lower latitudes
497   (Stone et al, 2007; Jacob et al., 2010; Breider et al., 2014; Aboele-Fetouh et al., 2020).
498   The proportional contribution of dust to total AOD is theat its largest in NAAPS-RA: a
499   result that could have contributed to its high bias in CM AOD (Table 2). The contribution
500   of organic matter to FM AOD is generally larger in CAMSRA than in the other two
501   reanalyses. On the whole, BB smoke is the largest contributing species to total JJA
502   AOD over the Arctic. This is consistent across all the reanalyses except for some sites
503   in NAAPS-RA (e.g., Andenes, Hornsund, and Kangerlussuaq where ABF AOD is
504   slightly larger than BB smoke AOD). This can be partially due to the different types of
505   speciation employed in NAAPS-RA: ABF includesrepresents anthropogenic and
506   biogenic pollution aerosols, including. The latter category includes sulfate, BC and (with
507   the exception of BB aerosols) organic aerosols of all origins (except for biomass burning
508   aerosols).. It is also worth noting that mean AERONET AODs are, in general, higher
509   (0.01-0.02, and can be ~0.1 higher for the sites close to BB sources) than their median
510   counterparts (Table 1) as well as their geometric means. This is because AOD
511   histograms are typically more lognormal than normal in form (asymmetric linear-AOD
512   histograms with positively skewed tails as per, for example, Hesaraki et al., 2017):
513   arithmetic means are, accordingly, often driven by extreme (>95% percentile for

514 example) AOD events. Because these extreme events constitute an important part of
515 the Arctic aerosol environment, the AOD means are presented here.

516

517
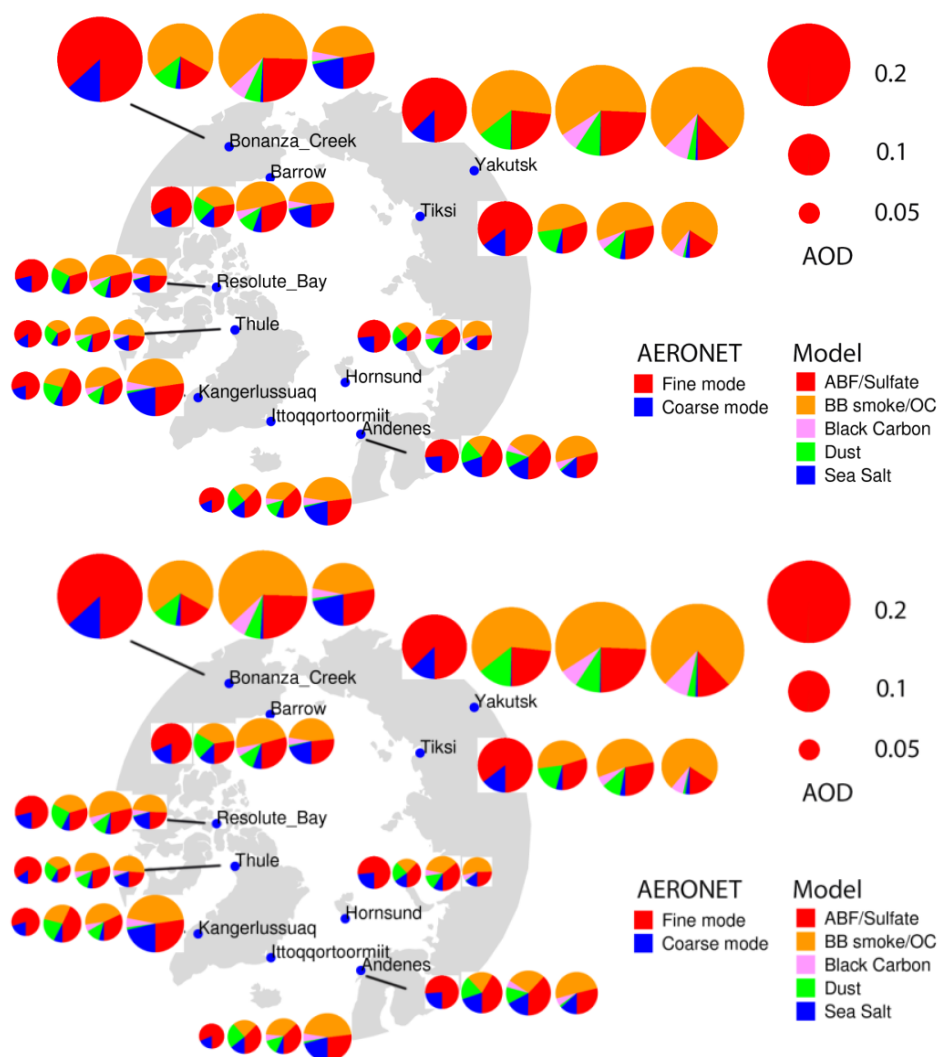
518 **Figure 1.** Polar projection map showing the locations of the AERONET Arctic sites
519 (small solid blue circles) used in this study. Long-term (2003-2019) JJA-mean FM and
520 CM AODs at 550 nm from AERONET (leftmost circle of each group of four circles) and
521 respectively, the speciated pie-charts of 550 nm AODs from NAAPS-RA, MERRA2, and

522 CAMSRA for each site. Warm colors (red, orange, and pink) represent ~~fine mode~~FM
523 and cool colors (green and blue) represent ~~coarse mode.~~CM. Circle size varies with
524 AOD magnitude (see the key to the top right).
525

526 **Table 1.** Geographical coordinates of AERONET sites used in this study~~,~~ and
527 ~~seasonal~~seasonally-binned mean, median and standard deviation of the total AOD and
528 SDA-derived FM and CM AOD at 550nm for MAM and JJA based on 2003-2019 data
529 when available. "n" represents the number of 6-hrly AERONET data.
530

sites	latitude	longitude	elev (m)	region	MAM (mean|median|std)			n	MAM FMF		JJA (mean|median|std)			n	JJA FMF	
					total AOD	FM AOD	CM AOD		mean	median	total AOD	FM AOD	CM AOD		mean	median
Hornsund	77.0°N	15.6°E	12	Svalbard	0.10|0.09|0.05	0.07|0.06|0.04	0.03|0.02|0.03	846	0.71	0.75	0.08|0.06|0.07	0.06|0.04|0.07	0.02|0.01|0.02	971	0.77	0.83
Thule	76.5°N	68.8°W	225	Greenland	0.08|0.07|0.05	0.06|0.05|0.03	0.03|0.01|0.04	1,009	0.75	0.81	0.07|0.05|0.07	0.06|0.04|0.06	0.01|0.01|0.02	1,509	0.85	0.88
Kangerlussuaq	67.0°N	50.6°W	320	Greenland	0.07|0.06|0.04	0.05|0.04|0.02	0.02|0.02|0.03	957	0.69	0.72	0.07|0.05|0.05	0.05|0.04|0.05	0.01|0.01|0.02	1,768	0.77	0.78
Ittoqqortoormiit	70.5°N	21.0°W	68	Greenland	0.06|0.05|0.04	0.04|0.04|0.02	0.02|0.01|0.03	545	0.72	0.78	0.06|0.04|0.04	0.05|0.03|0.05	0.01|0.01|0.02	1,280	0.80	0.81
Andenes	69.3°N	16.0°E	379	Norway	0.08|0.07|0.05	0.05|0.04|0.03	0.03|0.02|0.03	821	0.67	0.71	0.08|0.07|0.05	0.06|0.05|0.05	0.02|0.01|0.02	1,008	0.75	0.78
Resolute_Bay	74.7°N	94.9°W	35	Nunavut	0.10|0.08|0.09	0.07|0.06|0.04	0.03|0.02|0.03	520	0.73	0.78	0.08|0.05|0.10	0.06|0.04|0.10	0.02|0.01|0.03	1,178	0.78	0.83
Barrow	71.3°N	156.7°W	8	Alaska	0.11|0.09|0.07	0.08|0.06|0.05	0.03|0.02|0.04	605	0.73	0.77	0.10|0.07|0.15	0.08|0.05|0.15	0.02|0.01|0.02	1,155	0.79	0.82
Bonanza_Creek	64.7°N	148.3°W	353	Alaska	0.10|0.08|0.09	0.06|0.04|0.08	0.04|0.03|0.04	953	0.61	0.60	0.21|0.09|0.36	0.18|0.06|0.35	0.03|0.02|0.03	1,717	0.75	0.76
Tiksi	71.6°N	129.0°E	17	Siberia	0.10|0.10|0.03	0.08|0.08|0.03	0.02|0.01|0.02	39	0.80	0.82	0.13|0.08|0.18	0.11|0.07|0.17	0.02|0.01|0.02	449	0.80	0.85
Yakutsk	61.7°N	129.4°E	119	Siberia	0.15|0.11|0.15	0.11|0.08|0.13	0.04|0.02|0.04	1,516	0.76	0.80	0.16|0.09|0.24	0.14|0.07|0.24	0.02|0.01|0.02	2,579	0.81	0.84
MAN	>70°N	-		Arctic Ocean	0.11|0.10|0.06	0.06|0.06|0.04	0.04|0.04|0.03	85	0.62	0.62	0.06|0.05|0.07	0.04|0.03|0.07	0.02|0.02|0.01	435	0.66	0.67

531

532 Table 1 provides the geographical coordinates of the ten AERONET sites and the
533 ~~(arithmetic)~~ mean, median and standard deviation of the total, FM and CM AODs at 550
534 nm for both MAM and JJA based on available ~~2003-2019~~ data (the availability of
535 AERONET data can be appreciated from the monthly time series in Fig. 2). Analogous
536 MAN statistics are provided in the last row of Table 1 (see also Fig. S1 for geographical
537 distributions of MAN measurements). The seasonal mean total AOD for Resolute Bay,
538 the Greenland sites, Hornsund and the MAN measurements are < ~ 0.1 (0.06-0.10)
539 while the Alaskan and Siberian site values are >~ 0.1 (0.10 to 0.15 with Bonanza
540 Creek displaying a substantially larger JJA value of 0.21). All sites, except Bonanza
541 Creek, tend to have moderately higher median AOD in MAM: this is consistent with
542 other Arctic sunphotometer studies (Tomasi et al., 2015; Xie et al., 2018). The lesser
543 values in JJA ~~decrease~~, according to the reanalyses (Fig. 4 and 5), is related to higher
544 FM ABF/sulfate and/or CM dust and sea salt in MAM. This AOD seasonal difference
545 may have evolved in the past two decades with a decreasing trend in ABF/sulfate as
546 discussed in Sect. 5.3. The ~~seasonal~~ mean AOD is greater in JJA than in MAM for
547 Yakutsk, Tiksi and Bonanza Creek: this is likely due to strong FM AOD variations
548 associated with BB smoke events (see, for example, the discussions concerning the
549 seasonal competition between FM AOD smoke and FM AOD Arctic haze, in AboEl-
550 Fetouh et al., 2020). The standard deviations of the total and FM AODs are also high for
551 those three sites.

552 The Table 1 median and mean of the FMF vary, respectively, between 0.60 to 0.88 and
553 0.61 to 0.85 with higher FMF in JJA than in MAM. ~~The MAM to JJA increase~~The MAN

554 measurements have higher CM AODs and lower FMF compared to AERONET
555 measurements, due to possible contributions from sea salt aerosols. The MAM to JJA
556 increase in FMF for all sites and MAN is coherent with the month-to-month increase of
557 AboEl-Fetouh et al., (2020) although their 550 nm arithmetic means tend to be larger
558 (monthly-binned extremes of 0.81 to 0.98). Most, or at least a significant part of this
559 difference is likely attributable to differences between our FMF (SDA) separation of the
560 product and the SMF (AERONET-inversion) separation of AboEl-Fetouh et al.'s
561 climatology: the. The SMF is generally larger than the FMF because it tends to attribute
562 a fraction of the CM particle size distribution and thus a fraction of the CM AOD to the
563 FM AOD (see, for example, the 550 nm SMF vs FMF comparisons Section 4 of
564 Kleidman et al., 2005). More discussions about the differences in terms of FMF vs. SMF
565 and arithmetic vs. geometric statistics are available in the supplement material.

566 **Table 2.** Total, FM and CM AOD bias of CAMSRA, MERRA-2, NAAPS-RA and their
567 consensus mean MRC compared to AERONET monthly data.

sites	Bias-total AOD				Bias-FM AOD				Bias-CM AOD			
	CAMSRA	MERRA2	NAAPS-RA	MRC	CAMSRA	MERRA2	NAAPS-RA	MRC	CAMSRA	MERRA2	NAAPS-RA	MRC
Hornsund	-0.02	0.01	0.00	0.00	-0.01	0.01	-0.01	0.00	-0.01	0.01	0.02	0.00
Thule	0.00	0.02	0.00	0.01	0.01	0.02	-0.01	0.01	-0.01	0.00	0.01	0.00
Kangerlussuaq	0.02	0.02	0.02	0.02	0.03	0.02	0.02	0.02	-0.01	0.00	0.02	0.00
Ittoqqortoormiit	0.04	0.03	0.02	0.03	0.04	0.02	0.00	0.02	0.00	0.01	0.02	0.01
Andenes	0.03	0.04	0.02	0.03	0.03	0.02	0.00	0.02	0.00	0.02	0.02	0.01
Resolute_Bay	0.01	0.02	0.01	0.01	0.03	0.02	0.00	0.02	-0.02	0.00	0.01	0.00
Barrow	0.02	0.03	0.00	0.02	0.04	0.03	-0.01	0.02	-0.02	0.00	0.02	0.00
Bonanza_Creek	0.06	0.04	0.00	0.03	0.09	0.05	0.00	0.05	-0.02	-0.01	0.00	-0.01
Tiksi	0.02	0.02	-0.01	0.01	0.04	0.02	-0.01	0.02	-0.02	0.00	0.01	0.00
Yakutsk	0.03	0.04	0.01	0.03	0.05	0.05	0.00	0.03	-0.02	0.00	0.01	-0.01
mean	0.02	0.03	0.01	0.02	0.04	0.03	0.00	0.02	-0.01	0.00	0.01	0.00
median	0.02	0.03	0.01	0.02	0.04	0.02	0.00	0.02	-0.02	0.00	0.02	0.00

568

569 **Table 3.** Same as Table 2, except for RMSE.

sites	RMSE-total AOD				RMSE-FM AOD				RMSE-CM AOD			
	CAMSRA	MERRA2	NAAPS-RA	MRC	CAMSRA	MERRA2	NAAPS-RA	MRC	CAMSRA	MERRA2	NAAPS-RA	MRC
Hornsund	0.04	0.02	0.02	0.02	0.03	0.02	0.02	0.02	0.02	0.01	0.02	0.01
Thule	0.02	0.03	0.02	0.02	0.03	0.03	0.02	0.02	0.02	0.01	0.02	0.01
Kangerlussuaq	0.03	0.03	0.03	0.03	0.04	0.02	0.02	0.02	0.01	0.01	0.02	0.01
Ittoqqortoormiit	0.04	0.03	0.02	0.03	0.05	0.03	0.01	0.02	0.01	0.01	0.02	0.01
Andenes	0.03	0.04	0.03	0.03	0.03	0.03	0.02	0.02	0.01	0.02	0.03	0.02
Resolute_Bay	0.03	0.04	0.02	0.03	0.04	0.04	0.02	0.03	0.02	0.01	0.02	0.01
Barrow	0.05	0.05	0.03	0.04	0.06	0.04	0.03	0.03	0.02	0.01	0.02	0.01
Bonanza_Creek	0.11	0.10	0.07	0.08	0.12	0.10	0.06	0.08	0.03	0.02	0.01	0.02
Tiksi	0.05	0.04	0.02	0.03	0.06	0.04	0.02	0.03	0.02	0.01	0.01	0.01
Yakutsk	0.07	0.07	0.04	0.06	0.08	0.07	0.04	0.06	0.03	0.01	0.01	0.01
mean	0.05	0.05	0.03	0.04	0.05	0.04	0.03	0.03	0.02	0.01	0.02	0.01
median	0.04	0.04	0.03	0.03	0.05	0.04	0.02	0.03	0.02	0.01	0.02	0.01

570

571 **Table 4**. Same as Table 2, except for r^2.

sites	r2-total AOD				r2-FM AOD				r2-CM AOD			
	CAMSRA	MERRA2	NAAPS-RA	MRC	CAMSRA	MERRA2	NAAPS-RA	MRC	CAMSRA	MERRA2	NAAPS-RA	MRC
Hornsund	0.23	0.78	0.75	0.73	0.35	0.73	0.71	0.67	0.27	0.45	0.55	0.56
Thule	0.50	0.47	0.73	0.64	0.52	0.45	0.70	0.62	0.01	0.26	0.44	0.41
Kangerlussuaq	0.48	0.54	0.42	0.53	0.52	0.52	0.35	0.52	0.00	0.57	0.16	0.35
Ittoqqortoormiit	0.68	0.75	0.67	0.79	0.63	0.81	0.76	0.83	0.24	0.36	0.14	0.35
Andenes	0.67	0.63	0.68	0.71	0.68	0.66	0.64	0.71	0.10	0.23	0.21	0.21
Resolute_Bay	0.52	0.51	0.67	0.63	0.53	0.49	0.73	0.62	0.02	0.06	0.03	0.05
Barrow	0.33	0.68	0.70	0.62	0.45	0.76	0.69	0.68	0.05	0.27	0.41	0.41
Bonanza_Creek	0.81	0.78	0.80	0.83	0.83	0.79	0.82	0.85	0.06	0.43	0.45	0.46
Tiksi	0.77	0.80	0.87	0.84	0.82	0.82	0.90	0.86	0.02	0.20	0.10	0.15
Yakutsk	0.70	0.70	0.80	0.77	0.78	0.71	0.80	0.80	0.01	0.41	0.42	0.42
mean	0.57	0.66	0.71	0.71	0.61	0.67	0.71	0.72	0.08	0.32	0.29	0.34
median	0.60	0.69	0.72	0.72	0.58	0.72	0.72	0.70	0.04	0.32	0.31	0.38

572

573
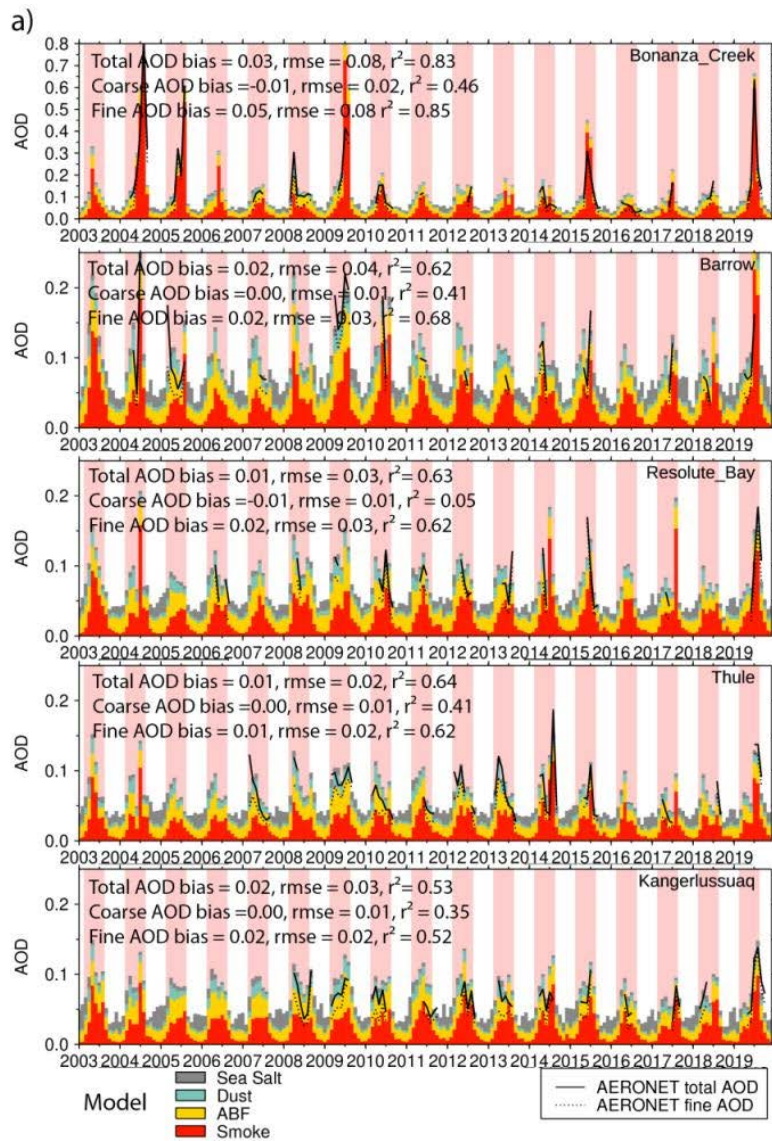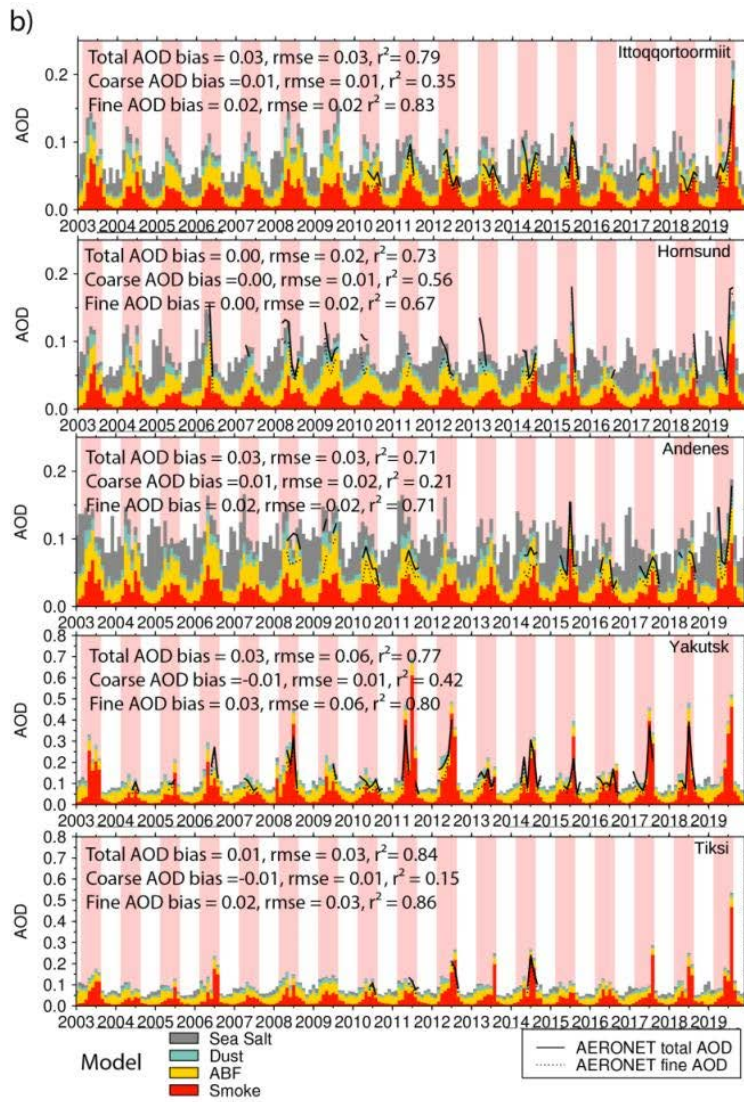
574
575 **Figure 2.** Monthly-binned time series of FM, CM, and total AERONET AODs and MRC
576 speciated AOD at a) Bonanza Creek, Barrow, Resolute_Bay, Thule, Kangerlussuq, and
577 b) Ittoqqortoormitt, Hornsund, Andenes, Yakutsk, and Tiksi sites. The JJA periods are
578 highlighted with pink shading for easy reading. The legends of each time series show
579 MRC bias, RMSE and r^2. Monthly mean AERONET AODs is obtained only when the
580 total number of 6-hr data exceeds 18 to ensure temporal representativeness.

581 Fig. 2 shows the time series of monthly mean FM, CM and total AODs from the ten
582 AERONET stations (CM AOD can be inferred from the difference between total AOD
583 and FM AOD) and the speciated AODs from MRC ~~(recall the approximation of assigning~~
584 ~~dust and sea salt to the CM, and ABF/sulfate and smoke to the FM). The MRC monthly-~~
585 ~~binned~~ . Bias, RMSE, and r^2 verification statistics ~~at the ten~~versus AERONET ~~sites are~~
586 ~~given in the Fig. 2 legends. Verification statistics~~for monthly-binned data of individual
587 aerosol reanalysis members and the MRC ~~based on monthly data~~ are presented in
588 Tables 2, 3, and 4 ~~for bias, RMSE, and r^2~~ respectively. The MRC is consistently biased
589 slightly high for FM AOD across all sites and about neutral for CM AOD for most. As a
590 result, total AOD tends to bias slightly high, with biases ranging from 0.00 to 0.03.
591 RMSE values range from 0.02 to 0.03 for most sites, except for Bonanza Creek,
592 Yakutsk and Barrow with RMSE values of 0.06, 0.05 and 0.04 (driven mainly by FM
593 variations). The r^2 values range from 0.53 to 0.84, with FM AOD r^2 values ranging from
594 much higher to marginally higher than the CM AOD values. This is understandable as
595 FM AOD displays large variabilities (which models are more capable of capturing) while
596 CM AOD displays relatively low values and smaller absolute variabilities on seasonal
597 and interannual time scales. Also, emissions of CM aerosols like dust and sea salt, are
598 driven dynamically by model or reanalysis surface winds where the surface wind
599 dependency increases exponentially in amplitude: the simulation of this dependency
600 has been a challenge to all global aerosol models (Sessions et al., 2015; Xian et al.,
601 2019).

602 Our previous experience with multi-reanalysis and multi-model ensembles indicates, in
603 general, that the consensus of multi-reanalyses or multi-models show better verification
604 scores than individual component members (Sessions et al., 2015; Xian et al., 2019;
605 Xian et al., 2020). However, these studies are based on more global analyses for which
606 the Arctic impact is relatively weak because of the sparsity of observational Arctic data.
607 Tables 2, 3 and 4 indicate that the Arctic is rather unique inasmuch as the MRC is not
608 necessarily the top AOD-estimation performer. NAAPS-RA generally has moderately
609 better bias, RMSE and r^2 verification scores for the total and FM AODs compared to
610 MERRA-2 and CAMSRA while CM AOD does not perform as well. In previous MRC and
611 multi-model consensus evaluations, all component members either performed
612 comparably in terms of AOD RMSE, bias and r^2 or the number of multi models was
613 relatively larger (e.g., 5 to 6 for the International Cooperative for Aerosol Prediction
614 multi-model consensus). This study is the first time that all three developing centers
615 have systematically evaluated their AOD reanalysis performance on an Arctic-wide
616 climate scale.

617 **5. Seasonal Analysis**

618   In this section we present spring and summertime Arctic AOD climatologies derived
619   from space-borne remote sensing retrievals and aerosol reanalyses. We then present
620   the seasonal cycle, interannual variability and trends of total and speciated AODs.

621   5.1 Spring and Summertime AOD Climatology for the Arctic
622   5.1.1 Space-based remote sensing AOD climatology
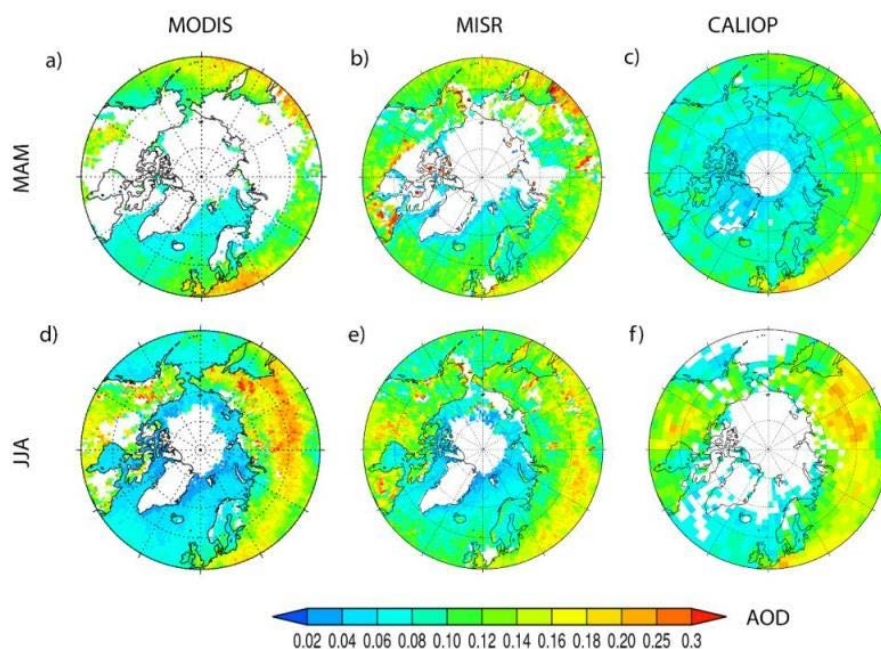
623
624   **Figure 3.** Satellite-derived, mean climatological MAM (upper) and JJA (lower) MODIS
625   AOD at 550 nm (left), MISR AOD at 558 nm (middle), and CALIOP AOD at 532 nm
626   (2006-2019, right). These are based onThe averaging period for MODIS C6 DT+DB and
627   MISR AOD v23 overwas 2003-2019, and while the CALIOP AOD overperiod was 2006-
628   2019. White area meansThe white areas correspond to a lack of data. The latitude
629   circles are at 50°, 60°, 70° and 80° N.

630   Bright, snow- and ice-covered surfaces, large solar zenith angles (SZA) (to the extreme
631   of sub-horizon SZAs during the polar night), and extensive cloud coverage result in limited
632   (quality assured) Arctic aerosolAOD retrievals by passive-basedfrom sensors like MODIS
633   and MISR. The latitude limit of an active, downward-looking, polar-orbiting sensor like
634   CALIOP on CALIPSO results in a polar region profile gap above 82°N. Known CALIOP
635   issues of CALIOP with retrieval filled values (RFVs) (Toth et al., 2018) and high noise to
636   low signal ratioto noise over the Arctic during the summertime also limit its aerosol

637 retrievals ~~near~~during the ~~Arctic~~JJA season. These challenges ~~are reflected as not~~translate
638 to substantial data ~~coverage (Fig. 3) ~~free MAM and JJA areas in the high Arctic and
639 Greenland~~, and over large regions of~~ as well as North America and Siberia in ~~both March-~~
640 ~~April-May (MAM) and June-July-August (JJA) in the AOD climatology maps based on~~ the
641 MODIS, MISR, and CALIOP~~. Compared to MAM, JJA has~~ AOD climatology maps of Fig.
642 3. JJA shows significantly larger ~~data coverage from~~ MODIS and MISR area coverage
643 over higher latitudes as aerosol retrievals from MODIS and MISR are ~~based on~~
644 ~~reflected~~acquired in continuous or nearly continuous sunlight~~. Also, when snow and sea~~
645 ~~ice~~ conditions. The summertime melt ~~in summer, darker~~season means a greater
646 presence of ice- and snow- free ocean and land surfaces ~~that are suitable~~as required for
647 ~~applying~~ passive-~~based aerosol retrieval methods are exposed. MAM data coverage for~~
648 ~~CALIOP is more than that of JJA due to less solar contamination during the night than~~
649 ~~during daytime for lidars~~ satellite-based AOD retrievals. Nevertheless, the long operation
650 time of these sensors (about two decades) provides sufficient data to construct a~~a~~n AOD
651 climatology, as well as emissions climatology for the near Arctic and the midlatitude
652 regions where most sources of Arctic aerosols reside.

653 In general, the Fig. 3 AOD patterns ~~from the~~are similar for all three sensors ~~are similar.~~
654 ~~High.~~ Higher AODs of 0.15-0.25 ~~appear~~can be observed in the 50°N-65°N latitude belt
655 over land~~, i.e.,~~. These are associated with large ~~areas of~~ boreal and subarctic areas in
656 Siberia, east and central Europe and North America ~~sector~~ in both spring and summer~~,~~
657 ~~with AOD.~~ AODs, mostly higher than 0.2 over Siberia in JJA~~,~~ are associated with biomass
658 burning events ~~(Fig. 3).~~. The average AOD over water is considerably lower, ranging from
659 0.02 to 0.12, with lower AOD over the north Atlantic and relatively ~~high~~higher AOD in the
660 northeast Pacific influenced by outflows from the Eurasian Continent~~, and lower AOD~~
661 ~~over the north Atlantic, and the~~. The lowest AODs (0.02-0.06) occur over the Arctic
662 Ocean~~. It is also visible that~~ AOD over water is slightly higher in MAM than in JJA, which
663 is consistent with other observation-based studies within the Arctic circle (e.g., Tomasi et
664 al., 2015~~),~~). This result is possibly related to higher pollution levels from the upstream
665 continents in MAM. CALIOP AOD exhibits a~~spatial patterns~~ similar ~~spatial pattern as~~to
666 MODIS and MISR. ~~Additionally, AOD~~AODs over Greenland ~~is on the order of~~(unique to
667 CALIOP) range from 0.02-0.06~~, and is a minimum compared to other regions due~~: these
668 minimal values are attributable to its high elevations (nearly 2km on average).
669 ~~AOD~~CALIOP-derived AODs over Siberia and North America ~~is~~are distinctively higher in
670 JJA than in MAM ~~based on CALIOP.~~. This seasonal difference ~~can (~~also ~~be~~ seen ~~with~~by
671 MISR ~~and can be explained by~~) is attributable to seasonal boreal fire activities, i.e., boreal
672 fire is generally more active in JJA than in MAM (Giglio et al., 2013). The seemingly larger
673 ~~seasonal~~ JJA vs MAM CALIOP difference ~~in CALIOP than in MODIS and MISR~~ over
674 Siberia and North American as compared with MODIS and MISR could also be
675 associated with different averaging times (2006-2019 vs. 2003-2019~~, and Fig. 2~~) as well
676 as data sampling rate~~, as the~~. The swath for MODIS and MISR is on the order of a few

677 hundred to a few thousand kilometers, while the ~~swath~~"beam diameter" for CALIPSO is
678 on the order of 70m (~~see e.g.,~~Winker et al., 2009; Colarco et al., 2014).While MODIS and
679 MISR yield more valid retrievals during JJA than MAM, the CALIOP data samples more
680 during MAM due to decreased signal to noise ratio during the summer (c.f. O'Neill et al.,
681 2012).

682 5.1.2 Arctic AOD climatology derived from aerosol reanalyses

683 Fig. 4 and 5 show spatial distributions of 2003-2019 mean total AOD and speciated
684 AOD from the three aerosol reanalyses and their consensus mean for spring and
685 summer respectively. Although there is limited AOD data available for ~~DA~~data
686 assimilation in the Arctic, lower latitude ~~aerosols, whose AOD is~~AODs that are
687 assimilation constrained ~~with DA,~~can affect Arctic AOD through transport and thus
688 exert an indirect Arctic AOD constraint ~~there~~. Additionally, all the reanalyses use
689 satellite-fire-hotspot-based BB emissions with fine temporal resolution (hourly to daily~~),~~
690 ~~which exert~~). This exerts a source constraint, especially temporally (emission magnitude
691 differs more than timing among the different models). As a result, there are
692 ~~good~~significant similarities in the spatial distributions of total AODs among the three
693 reanalyses. For example, MAM total AOD values are, for all reanlyses, high in the 50°N-
694 65°N belt over the ~~Eurasia~~Eurasian continent and its downwind Pacific region (values of
695 0.16-0.30), low ~~and on~~(of the order of 0.1 or less) for regions north of 70°N, and at a
696 minimum over Greenland ~~for MAM~~. The high AODs over boreal North America and
697 ~~Siberia~~the Siberian BB regions are more prominent in JJA compared to MAM. In
698 general, we would note that the distribution patterns and total AOD magnitude ~~of total~~
699 ~~AOD~~ are comparable to ~~those derived~~available retrievals from MODIS, MISR, and
700 CALIOP ~~where available to a large extent~~.
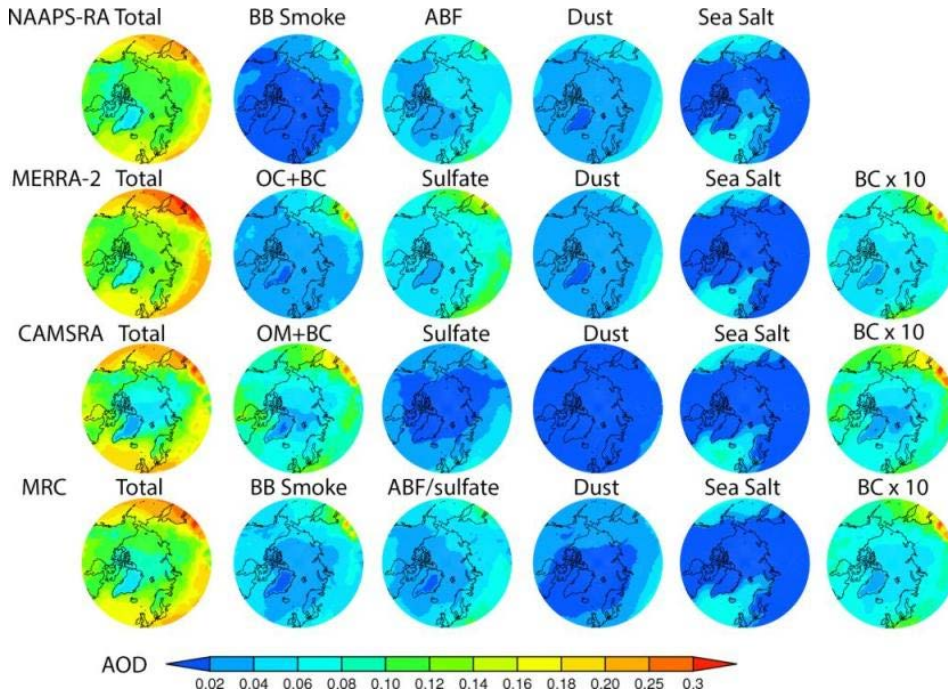
701
702 **Figure 4**. 2003-2019 Climatological MAM-mean total and speciated AOD at 550 nm
703 from NAAPS-RA, MERRA-2 and CAMSRA over the Arctic. As MERRA2 and CAMSRA
704 do not have a biomass-burning-induced single aerosol species, the sum of the organic
705 carbon (OC)/organic matter (OM) and black carbon (BC) AODs is used to approximate
706 biomass-burning smoke AOD. The ratio of BC to the sum of BC and OC/OM in MAM for
707 area >60°N is about 18% for MERRA-2 and 10% for CAMSRA. The ratios change little
708 for area >70°N and area >80°N.
709
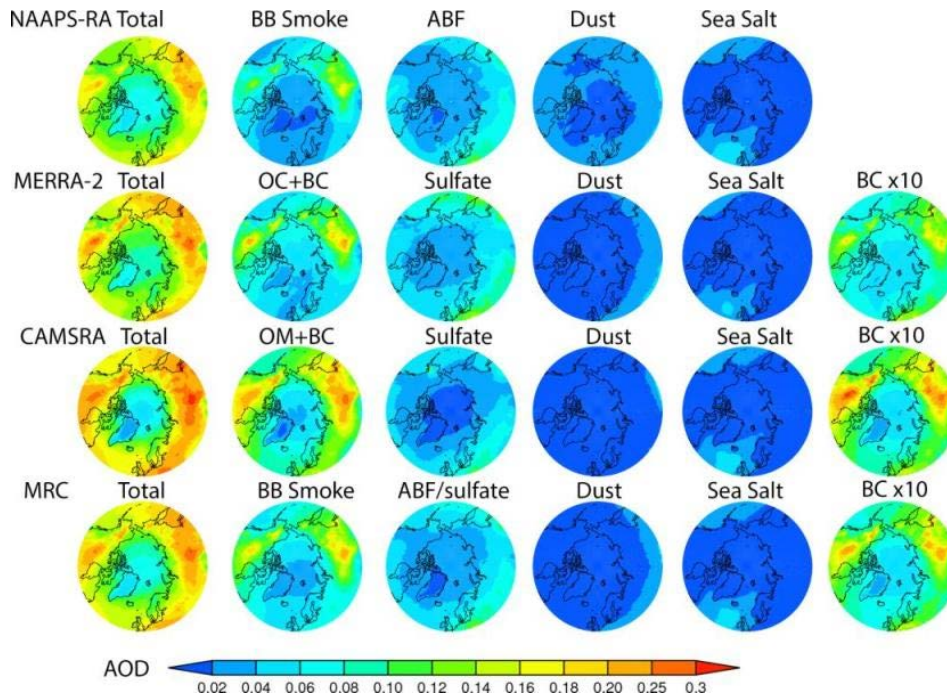
710
711 **Figure 5**. Same as Figure 4, except for JJA. ~~The ratio of BC to the sum of BC and~~
712 ~~OC/OM in JJA is between 10%-11% for area >60°N for both MERRA2 and CAMSRA.~~
713 ~~This ratio changes little for area >70°N and area >80°N.~~

714 Speciated AODs have more variability than total AOD among the three reanalyses, and
715 a little more so for MAM than for JJA ~~(Figas shown in Figs~~. 4, 5, 6~~). This is~~
716 ~~understandable.~~ The lesser JJA variability follows because passive Arctic-AOD
717 retrievals ~~of AOD~~ are more available in summer ~~than in spring near the Arctic,~~ and
718 ~~therefore~~ reanalyses ~~have~~ are therefore more ~~observational constraints in summer.~~
719 ~~While~~constrained by those observations. The lesser total AOD ~~is~~variability is the result
720 of it being constrained through data assimilation~~, however,~~ while speciated AOD is not
721 ~~and models must~~ : the latter AODs rely on ~~their~~model physics and boundary ~~conditions.~~
722 ~~The MRC shows that~~ condition constraints. In general BB smoke and ABF/sulfate ~~are~~
723 AODs largely dominate dust and sea-salt during MAM and JJA. The MRC MAM results
724 show similar ~~in magnitude for the Arctic in MAM.~~BB smoke and ABF/sulfate
725 magnitudes. However, ~~by model,~~the NAAPS-RA and MERRA-2 results suggest ~~the~~ an
726 ABF/sulfate dominance ~~of ABF/sulfate~~ over BB smoke~~, and~~ while CAMSRA suggests
727 the reverse ~~for CAMSRA. Based on the.~~ The high ~~bias of~~ FM AOD ~~verified with~~ vs
728 AERONET ~~(Sect. 4, Table 2),~~ bias of CAMSRA ~~possibly overestimates OC~~(Table 2)

729   suggests OM and BC, and hence BB smoke. overestimation. BB smoke becomes the
730   dominant rival species in JJAover ABF/sulfate as summertime boreal BB activity
731   increases in summer on average and ABF/sulfate turns to the 2nd place overall. The
732   strengthening of. The increase in smoke AOD from spring to summer is a consistent
733   feature across all the reanalyses despite that(while CAMSRA tends to have, singularly,
734   shows significantly higher BB smoke AOD and lower sulfate AOD compared to the other
735   two reanalyses in both seasons. ABF/sulfate AOD level is slightly higher in MAM than in
736   JJA for MRC (from slightly less than 0.04 to about 0.03 for 60-90°N regional average). A
737   ). All reanalyses show a June minimum in total AOD (Fig. 6). This is apparent from all
738   reanalyses, associated with ainduced by general decrease inpost-springtime
739   ABF/sulfate, dust and sea salt AODs after springtime and before severe BB activities
740   inreductions coupled with increased July and August BB activities. The spatial
741   distributions of seasonal mean BC AOD from MERRA-2 and CAMSRA greatly resemble
742   those of smoke AOD, and (arguably more so for JJA than MAM, except over Europe.).
743   This suggests a dominant role of the BB sourcesources over the anthropogenic sources
744   of BC AODsources over the Arctic forduring spring and summer seasons. This also
745   supports McCarty et al. (2021)'s BC emission estimate that wildfire emissions account
746   for more than half of all BC yearly emissions north of 60°N yearly (noting(the author's
747   noted much lower wintertime BB emissions during wintertime when anthropogenic BC
748   emission is at its maximum).

749   For Figures 4, 5 and 6 indicate, for both seasons, that dust and sea salt are secondary
750   contributors to the total AOD in the Arctic, except for the: noticeable influences of
751   Saharan and Asian dust in spring ((c.f., for example, Stone et al., 2007; Brieder et al.,
752   2014) and of sea salt in theas well as cyclonic-induced North Atlantic, Greenland Sea,
753   Norwegian Sea, and North Pacific associated with cyclonic activities, especially in
754   springsea salt are observable in Fig. 4. It is also noteworthy that dust AOD in CAMSRA
755   is much lower than the other two models (<0.02) in the spring.

756   From the 10-degree zonal average, it is also seen that monthlyMonthly and
757   regionallatitudinally-segmented mean AOD -AODs were found to gradually
758   decreasesdecrease from lower latitudinal belts to higher latitudinal belts (Fig. 7). Total
759   AOD for the 60°-70°N belt increases, on average, increases from MAM to JJA due to
760   the seasonality of BB activities. However, the total AOD for the 80°-90°N belt decreases
761   slightly from MAM to JJA. This means the decreasing latitudinal gradient of total AOD is
762   characterized by a larger amplitude in JJA than in MAM, which. This is most likely due
763   to moregreater aerosol wet removal of aerosols during transport from source regions to
764   the high Arctic in summer (Garrett et al., 2010, 2011). It is also noted that the CAMSRA
765   latitudinal AOD-gradient of AOD from CAMSRA is larger than those fromof the two other
766   reanalyses, suggesting. This suggests stronger CAMSRA aerosol removal in the Arctic
767   in CAMSRA compared to MERRA-2 and NAAPS-RA.

768
769
770
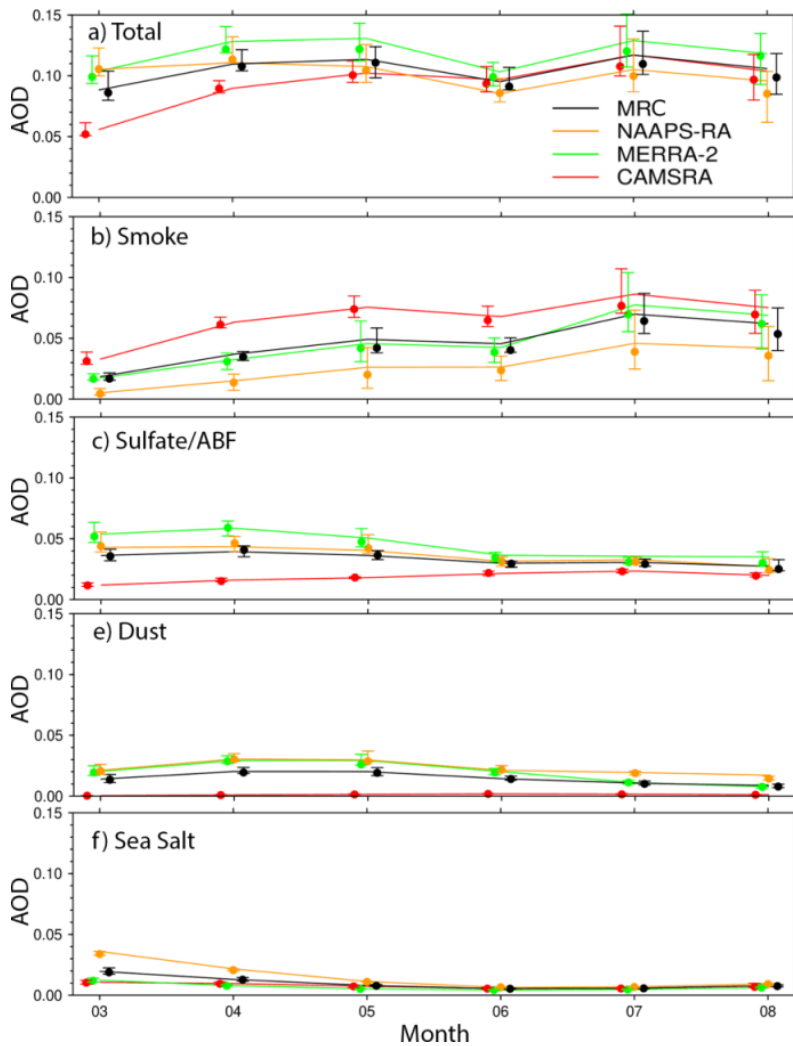
771
772 **Figure 6.** Climatological (2003-2019) seasonal cycle of Arctic (60°-90°N) average total
773 and speciated AODs at 550 nm from the three aerosol reanalyses and the MRC. The
774 top and bottom whiskers and the symbols represent, respectively, the 25% and 75%
775 percentiles and the medians of monthly AODs, and dots represent the median of
776 monthly AODs binned AOD distributions.
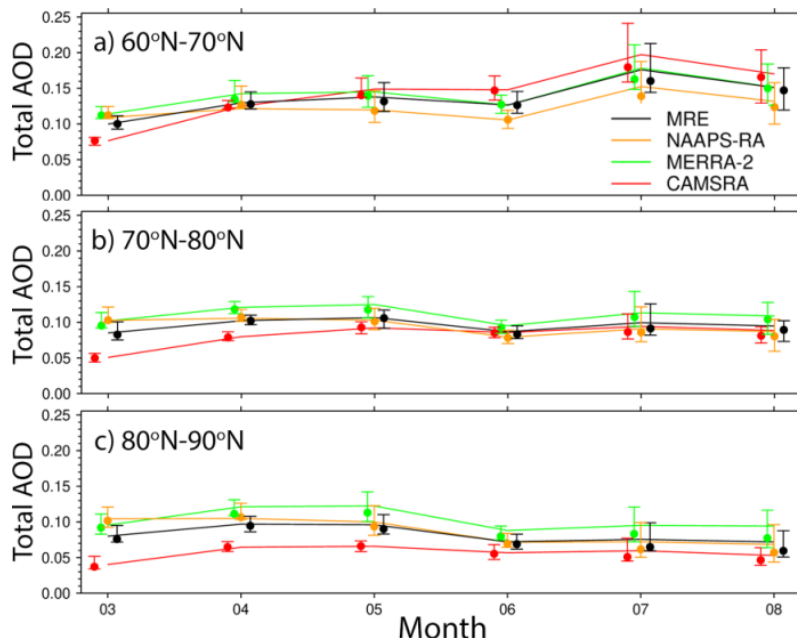
777
778 **Figure 7**. ~~Similar to~~As per Figure 6, but for different latitudinal belts ~~and total AOD~~.
779
780 5.2 Interannual variability of AOD in the Arctic
781 5.2.1 General features of AOD Interannual variability ~~of AOD~~
782 There are, as can be seen in Fig. 2 (and supported by the MAM/JJA discussion in
783 ~~Sect~~Sec. 4), significant interannual AOD variabilities, especially for sites close to boreal
784 fire sources. For example, the summertime peak of the total AERONET AOD at
785 Bonanza Creek, Alaska, is around 0.6 - 0.8 in 2004, 2005, and 2019, while it is <~ 0.1-
786 0.2 for other years ~~between 2003-2019.~~. The year to year ~~difference between~~factor
787 relating high- and low-amplitude summertime peak AOD values at Yakutsk, Siberia, can
788 be 6 fold. The MRC shows that these large interannual variabilities are fairly consistent
789 with AERONET FM AOD variabilities, and are very likely attributable to interannual
790 variabilities in BB smoke.
791
792 For sites far from smoke sources, ~~like~~such as Ittoqqortoormiit on the east coast of
793 Greenland, Hornsund in Svalbard, and Thule on the northwest coast of Greenland, the
794 high-amplitude peak AODs are about 2-3 times the low-amplitude peak AODs. ~~This~~The
795 interannual spring~~to~~/summer variability is ~~also~~ largely associated with BB smoke as
796 suggested by the MRC and the coherent variation of the AERONET FM AOD. (c.f.
797 Figures 6 and 7). Some of the strongest AOD events reported in previous studies have
798 been shown to be associated with the long-range transport of BB smoke. For instance,

799 the strong AOD peak in the summer of 2015 over Hornsund and Andenes was
800 ~~shown~~related to ~~be associated with~~ a series of intense fires that originated in North
801 America (Markowicz et al., 2016). The strong ~~peak AODs~~AOD peaks measured in
802 August 2017 over Resolute Bay, Eureka and Thule were most probably related to
803 intense~~,~~ fire-induced pyroCB events in ~~North America~~British Columbia and the long-
804 range transport of high-altitude smoke (Ranjbar et al., 2019; Das et al., 2021). The high
805 amplitude AOD peak in the spring of 2006 over Hornsund was traced to agricultural fires
806 in Eastern Europe (Stohl et al., 2007). The summer, 2004 boreal fires in North America
807 ~~in the summer 2004~~ led to the maximum-amplitude AOD peaks (~~over the 2003-2019~~
808 ~~period of~~ Fig. 2) for the two Alaskan sites and enhanced AOD on ~~the~~a pan-Arctic scale
809 (Stohl et al., 2004). Some of the high-amplitude AOD peak events were recorded during
810 intensive field campaigns. These included the ARCTAS/ARCPAC multi-platform
811 campaign in the summer of 2008 (Matsui et al., 2011; Saha et al, 2010; McNaughton et
812 al., 2011) and the NETCARE research vessel (Canadian Arctic) campaign in the spring
813 of 2015 (Abbatt et al., 2019). Some of the BB smoke events cause short-term record-
814 high AOD, and some lasted weeks to months, resulting in high monthly mean AOD. The
815 statistics of extreme AOD events, and implications for the impact of regional biomass
816 burning processes are provided in Part 2.

817
818 ~~The MAN measurements and AERONET sites adjacent to the North Atlantic, the~~
819 ~~Greenland Sea, and the Norwegian Sea, notably Ittoqqortoormiit, Hornsund, and~~
820 ~~Andenes have higher CM AODs and higher CM to total AOD ratio compared to other~~
821 ~~sites: this is due to contributions from sea salt aerosols. Sea salt AOD, indicated by the~~
822 ~~MRC, is normally higher in MAM than in JJA.~~

823

824
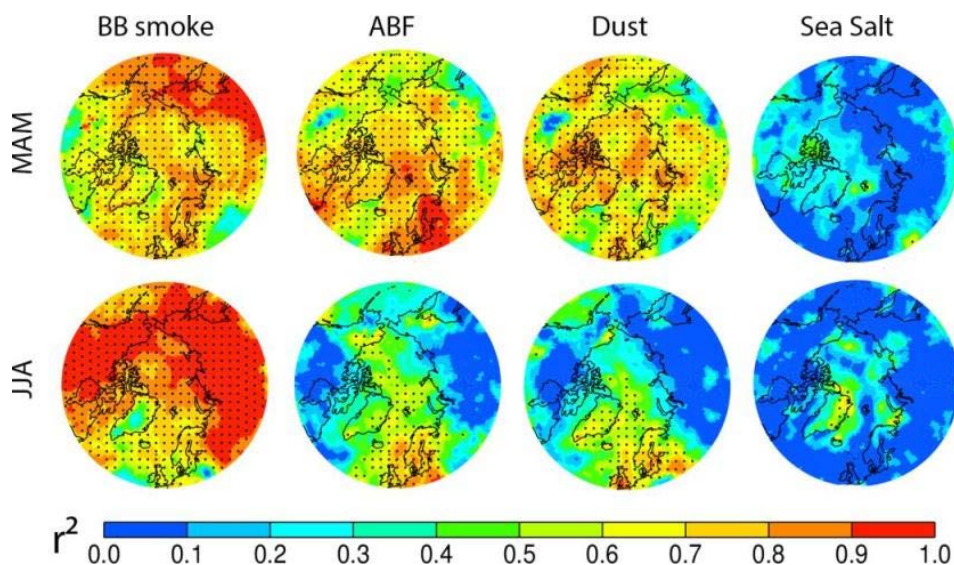
Figure 8. ~~Interannual~~Percentage of interannual MRC variability of ~~MRC~~ MAM (upper
panel) and JJA ~~mean~~ (lower panel) seasonally-binned, total AOD at 550 nm explained
by biomass-burning smoke AOD, ABF, dust, and sea salt aerosols ~~(i.e., the square of
the correlation coefficient between speciated AOD and total AOD)~~ respectively. ~~r²~~Values
in dotted area is statistically significant at the 95% level using a two-tailed Student *t* test.

5.2.2 Attribution of AOD interannual variability

It can be observed in Fig. 6 that the simulated interannual (60-90°N) AOD variability
~~(represented by the Fig. 6 whisker bars)~~ is mostly attributable to the large interannual
variability of smoke AOD (~~especially from May to August~~interannual variability as
measured by the size of the whisker bars). This is consistent across all the reanalysis
products. For March and April, the contribution from sulfate/ABF is as important as BB
smoke, if not larger. The interannual variation of dust AODs, as indicated with MERRA-
2 and NAAPS-RA data, is non-negligible in MAM.

Regarding spatial distribution, Fig. 8 shows the percentage of interannual variabilities of
spring and summer Arctic AOD explained by different aerosol species ~~(i.e., the square
of the correlation coefficient between speciated AOD and total AOD) suggested by~~ as
computed from MRC AODs for 2003-2019. ~~Consistent with the variability of monthly
AOD time series shown in Fig. 2 and 6,~~The fact that both MAM and JJA interannual
variabilities are mostly explained ~~mostly~~ by BB smoke~~, with a higher degree of~~

847 explanation (maximal r² values) is consistent with the correlation of monthly AOD time
848 series shown in Fig. 2 and 6. The JJA r² values for JJABB smoke are generally larger
849 than forthe MAM, values and a lower degree of explanation for over the North Atlantic,
850 the Norwegian Sea and Greenland than over North American and Eurasian sectors
851 overall. For north of 70°N, smoke . Smoke explains 60%-80% of MAM and, with the
852 exception of Greenland, about 80% (except Greenland) of JJA AOD interannual
853 variabilities. Over north of 70°N. JJA values over the North American and Eurasian
854 sectors (>60°N), the number is) represent about 100% for JJA.explained variation. The
855 second-largest contributor is ABF/sulfate and dust for MAM and to a lesser extent for
856 JJA. Contribution from sea salt is the leastweak and is only statistically significant east
857 of Greenland in JJA.
858
859 The contribution fromexplained variation by MAM ABF/sulfate is above 80% over the
860 industry- and -population-concentrated European and northeast North American sectors
861 and their outflow regions ofinto the North Atlantic, Greenland Sea, Norwegian Sea, and
862 the Arctic Ocean in MAM, while this number decreases. Values decrease to above 60%
863 over Europe in general and the European Arctic (including water) and is insignificant
864 over North America in JJA.). Dust, possibly from Asian and high-latitude sources, could
865 explain some of the interannual AOD variabilities over some regions, (e.g., Greenland
866 and the Greenland Sea in JJA and additionally as well as the North Pacific and the
867 Arctic ocean in MAM, however). However, there exist large uncertainties in this
868 evaluation based on the worseweaker verification scorescores of CM compared to FM
869 AOD (Tables 2,3,4). And) and, for example, only the CAMSRA among the three
870 reanalyses considers high-latitude dust. Co-variability of species, e.g., BB smoke,
871 ABF/sulfate, and dust, is discernible in Fig. 8: this is likely due to the same transport
872 pathways being employed from the mid-latitudes to the Arctic. It is also possible that
873 these species covary because of artifacts introduced by intrinsic treatment in AOD data
874 assimilation for low AOD situations (Zhang et al., 2008).
875
876 5.3 Total and speciated AOD trends over 2003-2019
877
878 The total AOD springtime and summertime trends for spring and summer over 2003-
879 2019 derived from MODIS, MISR, and forMISR over 2003-2019 as well 2006-2019 from
880 CALIOP are presented in Fig. 9. Because9. Valid trend analysis is, because of the
881 scarcity of valid Arctic retrievals over the Arctic, the valid trend analysis is, mostly limited
882 to south of 70°N, and the north Atlantic region, and (with less MODIS and MISR
883 coverage in MAM than in JJA from MODIS and MISR and less coverage in JJA than
884 MAM from CALIOP and, for reasons mentioned in Sect. 5.1.1.5.1, less CALIOP
885 coverage in JJA than MAM).
886

5.3.1 AOD springtime trends ~~for springtime~~
~~For MAM, there is a general~~A generally negative ~~trend in~~ total AOD MAM trend over the 50-60°N belt and the North Atlantic~~, with the~~ is shown in Fig. 9. The ~~largest~~amplitude negative trend of ~~-~~Fig. 9 (-0.06 to -0.10 AOD/decade ~~being~~) occurs over Europe~~,~~: this is most ~~probably~~likely due to a decrease in ABF/sulfate from decreased anthropogenic emissions (as ~~indicated by~~we will see in the discussion surrounding the reanalyses ~~(~~of Fig. 10). ~~The~~The CALIOP trend is moderately more negative ~~trend from CALIOP is~~ ~~slightly smaller~~ than ~~those from~~the MODIS and MISR trends. This might, again ~~possibly~~ ~~attributed,~~ be attributable to ~~a~~the shorter length of the data record~~.~~ (where earlier and more polluted years of 2003-2006 for Europe and North America ~~(2003-2006) is~~were not included~~. All~~) and/or the CALIOP daytime signal to noise issues. The Fig. 10 reanalyses ~~also~~all show a negative ~~trend in total AOD~~ pan-Arctic total AOD trend (-0.01 to -0.02 AOD/decade~~),~~) except for a ~~close-to-neutral~~near-zero CAMSRA trend over the Arctic ocean and a very slight positive trend over boreal North America ~~from CAMSRA.~~ ~~All the.~~ The reanalyses collectively suggest that the strong negative trend over the southeast ~~Siberia~~Siberian and East Asian outflow region is associated with a decrease in BB smoke, and ~~a,~~ perhaps, a more moderate decrease in ABF/sulfate from NAAPS-RA and MERRA-2 ~~in tandem~~. Other consistent features ~~found across~~shared by the reanalyses include ~~the~~a negative ABF/sulfate trend over Europe ~~associated with~~ ~~decreasing ABF/sulfate, which is possibly related to~~due to decreased anthropogenic ~~emission decrease over the past two decades~~ emissions (Breider et al., 2017), ~~as well~~ ~~as~~and a weak positive ~~trend of sea salt over the~~ North Atlantic~~, which is~~ sea salt trend due possibly ~~due~~ to ~~the~~an observed increase in cyclonic activities ~~there~~ (Rinke et al., 2017; Waseda et al., 2021; Valkonen et al., 2021). It is ~~worth noting~~notable that NAAPS-RA ~~does~~(and MERRA-2 after 2008) do not ~~include~~incorporate an ABF emission trend ~~for ABF, and MERRA-2 doesn't either after 2008, which~~. This means ~~the~~that their ABF/sulfate trends ~~seen from these two reanalyses~~ are mostly driven by a negative AOD correction applied by the data assimilation systems. This corroborates the negative trend in ABF/sulfate.
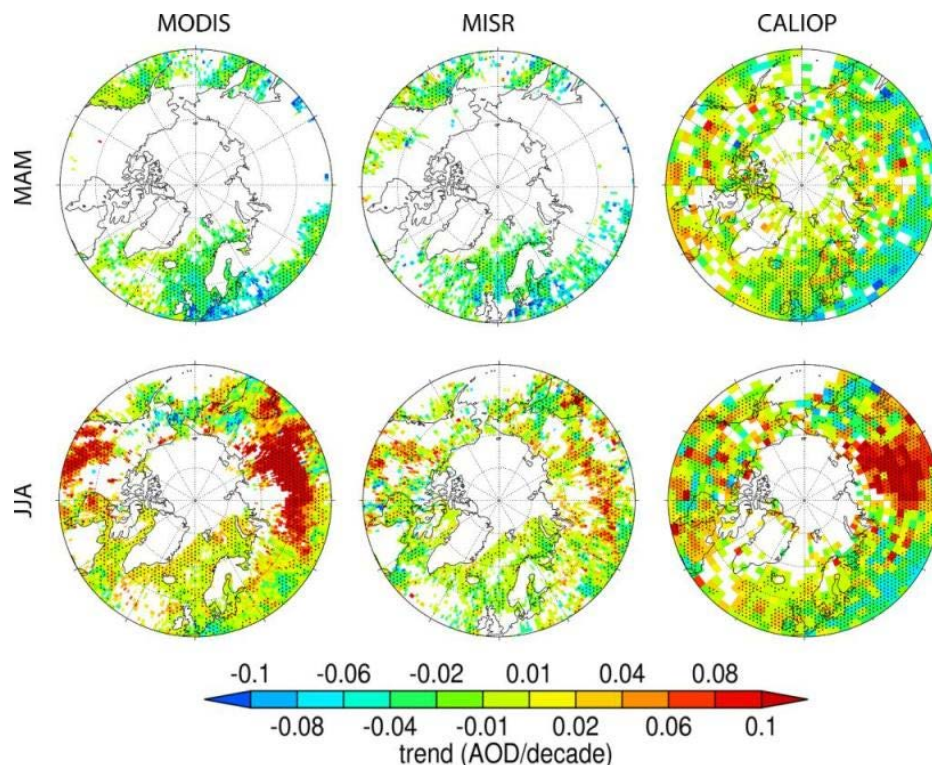
916
917 **Figure 9.** ~~MAM and JJA AOD trends from~~ MODIS, MISR, and CALIOP MAM and JJA
918 AOD trends for the ~~corresponding~~ time periods and AOD wavelengths ~~shown~~given in
919 the Figure 3~~. The trend~~ caption. Trends in the dotted ~~area is~~areas are statistically
920 significant.
921
922 5.3.2 AOD ~~trends for~~ summertime trends
923 ~~For JJA, the~~The most prominent Fig. 9 JJA feature ~~across all three space-borne~~
924 ~~sensors~~ is the strong and positive ~~trend of~~ total AOD trend (> 0.10 AOD/decade) that
925 appears, to a varying, sensor-dependent, spatial extent, over vast regions of Siberia
926 and North America ~~with a magnitude of around or greater than 0.10 AOD/decade.~~. All
927 the reanalyses ~~capture this positive trend and~~ indicate ~~it~~that this trend is
928 ~~attributed~~attributable to a significant increase in BB smoke AOD ~~in these regions over~~
929 ~~2003-2019~~ (Fig. 11). This is ~~in accordance~~coherent with ~~strong~~the FLAMBE-derived,
930 MODIS-hotspot-based emission inventory of Fig. 12 that shows positive regional trends
931 in BB emissions north of 50°N ~~and north of 60°N derived from FLAMBE, a MODIS-fire~~
932 ~~hotspot-based emission inventory (Fig. 12), and from~~ (and with other BB emission
933 inventories~~, e.g.,~~ such as GFED and GFAS ~~(~~ inventories shown in Fig. 2 ~~in McMarty~~of

934 McCarty et al., 2021). At the same time, there are negative trends in total AOD over
935 Alaska, northeast of Russia, and the North Pacific from the reanalyses, which is
936 seemingly consistent with the trend in remote sensing AODs (though for some satellite
937 datasets the coverage is spotty in these regions). These trends are driven by BB smoke
938 and smoke emission trends as suggested by all the reanalyses and FLAMBE. In
939 addition, there is a continued negative trend from MAM to JJA in ABF/sulfate over
940 Europe, which is also reflected in total AOD trend, as shown in the reanalyses. This is
941 consistent with the discernible negative though weak trend from the three sensors. JJA
942 AOD trends in dust and sea salt are neutral from the reanalyses.
943
944 ~~Besides rising surface temperature, climate phenomena such as the El Niño–Southern~~
945 ~~Oscillation (ENSO), Arctic Oscillation (AO), and Pacific Decadal Oscillation (PDO) have~~
946 ~~been reported as affecting fire activity in several key boreal fire source regions (Balzter~~
947 ~~et al., 2007; Macias Fauria and Johnson, 2007; Kim et al., 2020). However rising~~
948 ~~surface temperature, probably contributes more to the observed trend in BB emission in~~
949 ~~the high latitudes. With the rising surface temperature, lightning activity and lightning~~
950 ~~caused wildfires in summertime high latitude regions were observed to increase in the~~
951 ~~past two decades (Zhang et al., 2021; Bieniek et al, 2020; Coogan et al., 2020). In~~
952 ~~addition, agricultural fire activity in Eastern Europe and European Russia (peaking at~~
953 ~~April to May) and central Asia and Asiatic Russian (peaking in August) (Korontzi et al,~~
954 ~~2006; Hall et al., 2016) also affects the seasonality of total BB emissions. The MAM~~
955 ~~negative trend in BB smoke may be relevant to a strengthening of agriculture burning~~
956 ~~regulations in the later part of the 2003-2019 time period. For example, the MAM BB~~
957 ~~emission maxima in 2003, 2006 and 2008 are all associated with wide-spread~~
958 ~~springtime agriculture burnings in high latitudes (Korontzi et al, 2006; Stohl et al., 2007;~~
959 ~~Saha et al., 2010). The aforementioned climate oscillations also modulate interannual~~
960 ~~variations of the transport of pollutants from the mid-latitudes to the Arctic (e.g.,~~
961 ~~Eckhardt et al., 2003; Fisher et al., 2010).~~
962
963 5.3.3 High Arctic AOD trends
964 For the high Arctic ~~(>70°N),~~. AOD trends ~~are~~will hardly be seen with the same color
965 scale as those for the lower latitudes because of lower AOD. Thus, they are shown
966 separately in Fig. 13, where time series of MAM and JJA area-mean total, smoke, and
967 ABF/sulfate AODs are shown individually and for all the reanalyses and the MRC over
968 the 2003-2019 time period. There is a negative trend across models in MAM total AOD
969 with -0.017 AOD/decade (-18%/decade), and a positive trend in JJA total AOD with
970 0.007 AOD/decade (8%decade) based on the MRC. The largest contributor to the MAM
971 negative trend is ABF/sulfate, and the smoke AOD trend is also negative. In the
972 summertime, ABF/sulfate trend continues to be negative; however, ~~the~~ smoke AOD
973 trend turns positive, with a high positive trend of 0.010 AOD/decade (22%/decade). BC

974 AOD trends from MERRA-2 and CAMSRA are dominantly driven by smoke AOD, and
975 have similar trends with smoke AOD in percentage per decade. The negative trend in
976 ABF/sulfate AOD is in line with the decreasing trend in surface sulfate mass
977 concentrations measured over Arctic observational sites (e.g., Breider et al., 2017). The
978 negative trend in MAM and positive trend in JJA for smoke AOD are consistent with the
979 ~~seasonal~~ seasonally-binned and ~~area~~ latitutude-belt-binned mean BB emission trends
980 shown in Fig. 12 (e,f). The trend magnitudes of ~~the trends among~~ the three aerosol
981 reanalyses are different, but the signs are the same, corroborating the trend analysis
982 results based on the MRC. These results are consistent with the trend analysis for lower
983 latitude source regions as shown in Fig. 9-11. All these results also demonstrate that
984 the Arctic aerosol baseline is changing quickly (Schmale et al., 2021), and the
985 estimation here could contribute to the understanding and quantification of this new
986 baseline.

987

988 ### 5.3.4 Possible causes of BB smoke AOD trends

989 Besides rising surface temperature, climate phenomena such as the El Niño–Southern
990 Oscillation (ENSO), Arctic Oscillation (AO), and Pacific Decadal Oscillation (PDO) have
991 been reported as affecting fire activity in several key boreal fire source regions (Balzter
992 et al., 2007; Macias Fauria and Johnson, 2007; Kim et al., 2020). However rising
993 surface temperature, probably contributes more to the observed trend in BB emission in
994 the high latitudes. With the rising surface temperature, lightning activity and lightning-
995 caused wildfires in summertime high latitude regions were observed to increase in the
996 past two decades (Zhang et al., 2021; Bieniek et al, 2020; Coogan et al., 2020). In
997 addition, agricultural fire activity in Eastern Europe and European Russia (peaking at
998 April to May) and central Asia and Asiatic Russian (peaking in August) (Korontzi et al,
999 2006; Hall et al., 2016) also affects the seasonality of total BB emissions. The MAM
1000 negative trend in BB smoke may be relevant to a strengthening of agriculture burning
1001 regulations in the later part of the time period. For example, the MAM BB emission
1002 maxima in 2003, 2006 and 2008 are all associated with wide-spread springtime
1003 agriculture burnings in high latitudes (Korontzi et al, 2006; Stohl et al., 2007; Saha et al.,
1004 2010). The aforementioned climate oscillations also modulate interannual variations of
1005 the transport of pollutants from the mid latitudes to the Arctic (e.g., Eckhardt et al., 2003;
1006 Fisher et al., 2010).

1007

1008 Compared with the BB emission trend, trend in the atmospheric processes, e.g.,
1009 transport and removals, probably plays a secondary role in the Arctic smoke AOD trend.
1010 This is illustrated by the similarity in spatial patterns of smoke AOD and BB emission
1011 trends, and the coincidence of peak years for emissions and the high Arctic area-mean
1012 smoke AODs. For example, 2012 and 2019 are associated with JJA peaks in emission

1013 and high Arctic smoke AOD, while 2003 and 2008 correspond to MAM peaks in both
1014 (Figs. 12 and 13).
1015
1016
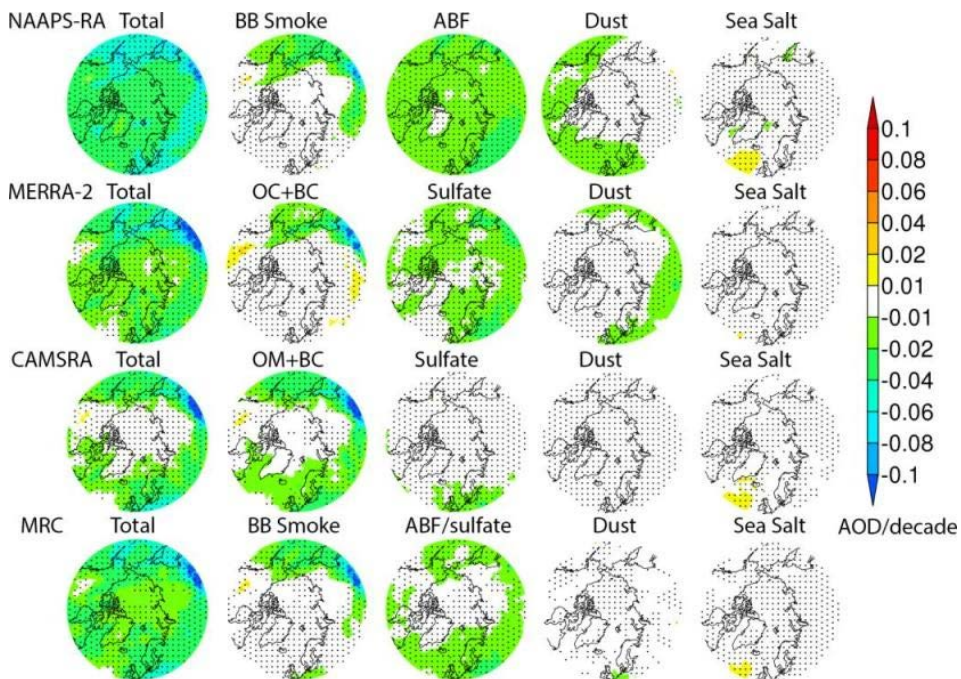
1017
1018 **Figure 10**. Trends of MAM 550 nm total AOD and contributions from BB smoke
1019 /(BC+OC)/(BC+OM),. ABF/Sulfate, dust and sea salt from NAAPS-RA, MERRA-2 and
1020 CAMSRA and the MRC.
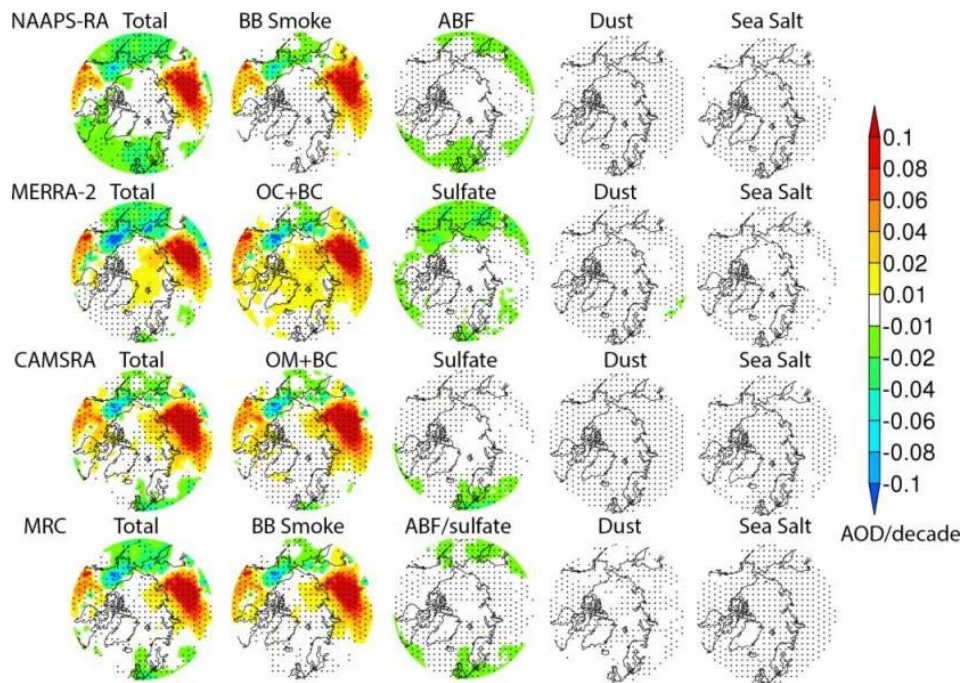
1021
1022 **Figure 11**. Same as Fig. 10, except for JJA.
1023
1024
1025

1026
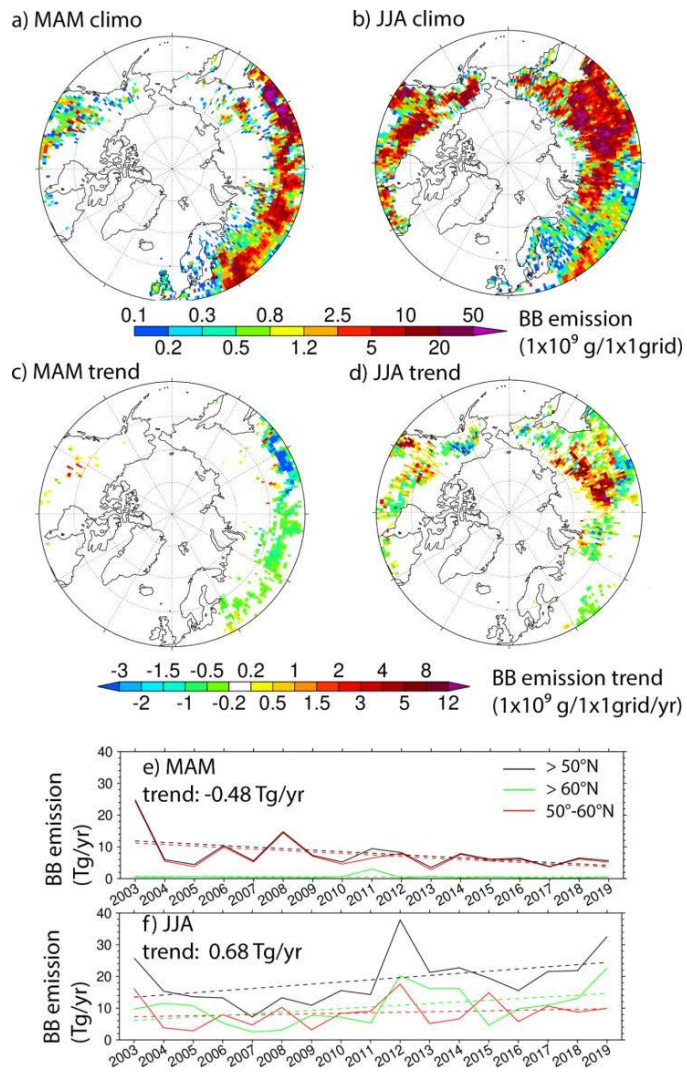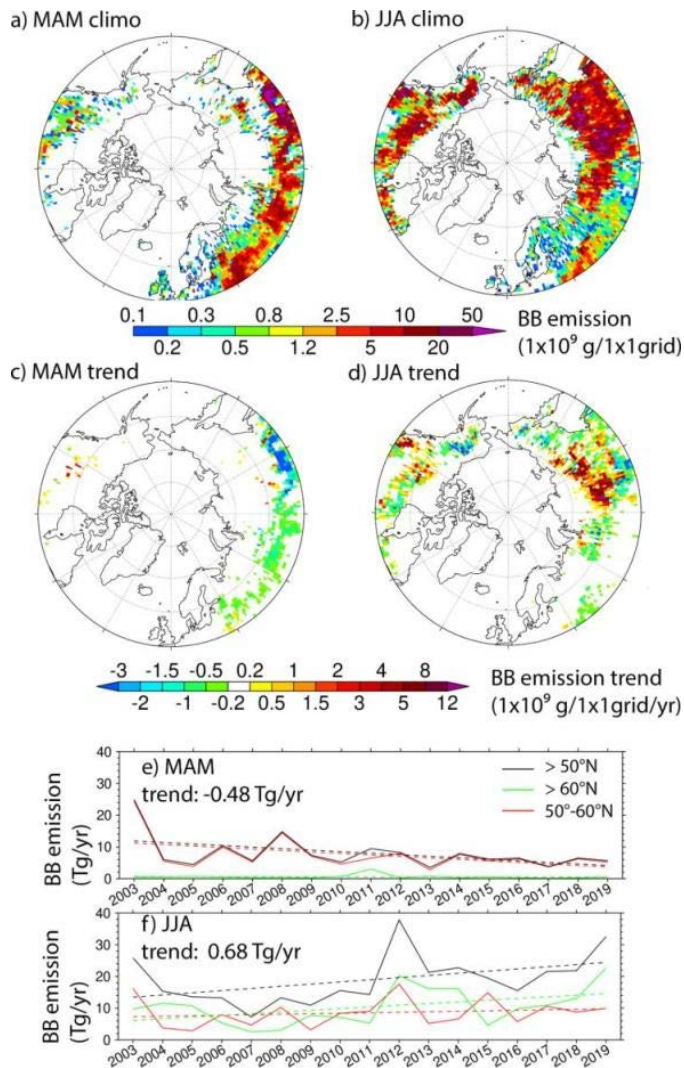
1027
1028
Figure 12. MAM/JJA seasonal total BB smoke particle emission climatology and trend
for 2003-2019 derived from FLAMBE (a-d). e) and f) Time series of seasonally-binned
area-meanmeans (>50°N, >60°N and 50-60°N) BB smoke (PM2.5 particle) emissions
for MAM and JJA respectively. Dashed lines represent linear trends, which are
statistically significant with a confidence level of 95%. The trend for north of 50°N is also
displayed in textsthe legends.
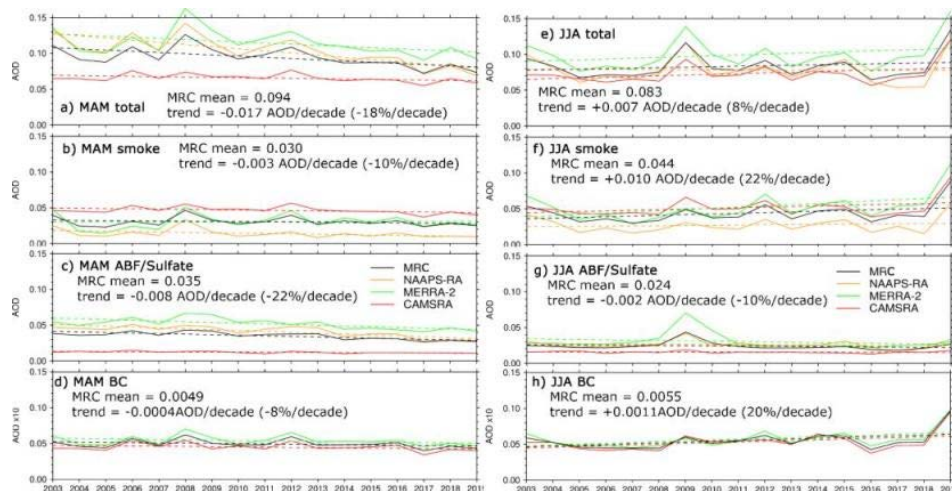
1035
1036
1037 **Figure 13.** Time series of MAM and JJA 70°-90°N area mean total, BB smoke,
1038 ABF/sulfate and BC AODs from the reanalyses and the MRC for 2003-2019 time
1039 period.. Solid lines are AODs, and dashed lines are linear regressions indicating trends.
1040 For easier visualization, BC AOD is multiplied by 10.
1041

1042 **6. Discussion**
1043 The quality control processes applied on the AOD retrievals from MODIS, MISR, and
1044 CALIOP help to generate a consistent AOD climatology and trend near the Arctic. The
1045 cloud-clearing process on the MISR data and QA processes on the MODIS data
1046 removed a good volume of data (about 40% for MISR and MODIS). However, these QA
1047 processes help to retain only the best-quality data, which yield a closer magnitude of
1048 AOD for MODIS and MISR to AERONET AODs near the 70°N latitude circle (around or
1049 less than 0.1), compared to ~0.2 using regular level 3 MODIS and MISR data in Figs 20
1050 and 23 of Tomasi et al., 2015, especially for springtime. The manual QA process on the
1051 AERONET AOD data also reveals more frequent cloud contamination in springtime than
1052 in summertime. Often artificial AOD valuevalues of zero are observed over the Arctic in
1053 CALIOP V4.2 L2 and L3 data, resulted partially from algorithmically setting altitude bins
1054 with retrieval filled values in the aerosol profile to zero, as these represent undetectable
1055 levels of faint aerosol (i.e.,Toth et al., 2016; 2018). With AOD=0 values retained in the
1056 CALIOP V4.2 L2 data analysis (same processing in CALIOP V4.2 L3), the climatological
1057 seasonal mean AOD magnitude is much smaller (about half) than that shown in Fig. 3
1058 and the AOD trends are slightly smaller than those in Fig. 9, although the spatial
1059 patterns of the seasonal AOD and trends are similar to those obtained with AOD data
1060 after removing the AOD=0 values (Fig. S2). After removing the pixels with filled and

1061 zero values, CALIOP AOD seasonal spatial AOD distributions are similar to those from
1062 MODIS and MISR.
1063
1064 The total AOD at 550 nm from the three aerosol reanalyses are much more convergent
1065 in spatial distribution, magnitude, and seasonality in the Arctic compared to the climate
1066 models, and are similar to those from the remote sensors near the Arctic. For example,
1067 for AEROCOM models in Sand et al., 2017, MAM AODs averaged over nine Arctic
1068 AERONET sites (all included in this study) are an order of magnitude different for the
1069 highest and lowest AOD models, and peak AOD season varies among winter, spring
1070 and summer; In the CMIP5 models in Glantz et al., 2014, spring and summertime AODs
1071 over the Svalbard area also show an order of magnitude difference and there are
1072 different seasonality for some of the models. The possible reasons for the convergence
1073 of AOD in the reanalyses include 1) the hourly/daily resolved satellite-hotspot-based BB
1074 emissions used by these reanalyses apply fine-temporal and interannual-variability-
1075 resolved emission constraints; 2) despite that the commonly assimilated satellite AOD
1076 (e.g., MODIS AOD in all three reanalyses) has limited coverage in the Arctic due to
1077 retrieval challenges of dealing with bright surfaces and high cloud coverage, the
1078 observational constraint of model fields through assimilation of AOD in the lower
1079 latitudes is effective in constraining Arctic AOD to a good extent through transport; 3)
1080 more accurate meteorology representations. It is reasonable that the AOD spread
1081 among the three reanalyses increases with latitude, and into the early months (e.g.,
1082 March) when retrieval coverage for lower latitudes is less than summer months.
1083
1084 Except for the chemical processes relevant to conversion of SO_2 to sulfate, the aerosol
1085 reanalysis products (or their underlying aerosol models) don't include other new particle
1086 formation processes that may be important over the Arctic open water/leads in
1087 Springtime or over packed ice during transitional summer to Autumn season (Abbatt et
1088 al., 2019; Baccarini et al., 2021). High latitude dust sources, e.g., glacier dust, which are
1089 present for some areas in the Arctic (Bullard et al., 2016), are only included in
1090 CAMSRA, despite that Arctic dust AOD in CAMSRA is much lower than those in the
1091 other two models (Fig. 6e).
1092
1093 To show the contribution of biomass burning on total AOD in the Arctic, we
1094 approximated BB smoke with the sum of BC and OC/OA from MERRA-2 and CAMSRA.
1095 This approximation is rather arguable. It: it is better suited for JJA than MAM, as the
1096 climatological seasonalseasonally-binned mean of Arctic AOD is dominated by BB
1097 smoke in JJA, which means that BC and OC/OC are mostly from BB sources, while the
1098 contribution of BC and OC/OA from anthropogenic sources is relatively higher in early
1099 spring (Figs. 4, 5). So smoke AOD is overestimated from MERRA-2 and CAMSRA and
1100 more so for MAM. This explains the larger difference in smoke AOD (ratio to total AOD)

1101   in MAM than in JJA between the two reanalyses and NAAPS-RA, which explicitly tracks
1102   aerosol mass from BB sources (Figs. 4, 5, 6). While NAAPS-RA includes BC and OA
1103   from anthropogenic sources and sulfate into ABF, which is an arguably reasonable
1104   configuration for pollution species, as observational studies show a strong correlation
1105   between sulfate and elemental BC surface concentrations at pan-Arctic sites away from
1106   BB sources, indicating the sources contributing to sulfate and BC are similar and that
1107   the aerosols are internally mixed and undergo similar removal (Eckhardt et al., 2015).
1108   BB smoke is expected to have different vertical distributions from anthropogenic
1109   pollution if smoke is emitted above the boundary layer. Some estimates based on
1110   satellite observations near local noon have suggested that the fraction of smoke
1111   escaping the boundary layer is only ~10% (Val Martin et al., 2010), but taking account of
1112   the diurnal cycle of fire activity and potential for pyroconvection, the actual fraction of
1113   elevated smoke could be much larger (Fromm et al., 2010; Peterson et al., 2015;
1114   Peterson et al., 2017).
1115
1116   Stratospheric aerosols from volcanic eruptions can contribute to the total AOD in the
1117   Arctic, especially for the four years after the Mount Pinatubo eruption in 1991 (Herber
1118   2002). For our study period (2003-2019), the eruptions of Kasatochi, Redoubt,
1119   Sarychev, and Eyjafjallajökull in August 2008, March 2009, July 2009, and March 2010,
1120   respectively, would have affected the stratospheric AOD and thus total column AOD.
1121   However, these eruptions are at least one order of magnitude smaller than that of
1122   Pinatubo. The stratospheric AOD contribution to the Arctic background AOD is
1123   estimated to be relatively small at ~0.01 (from Fig. 16 of Thomason et al., 2018; non-
1124   Pinatubo affected years in Fig. 5 of Herber 2002), despite that locally and over a short
1125   period the AOD contribution can be large (e.g., O'Neill et al., 2012). All the reanalyses
1126   have some sort of SO_2 and sulfate representation from volcanic degassing emissions,
1127   but a full representation for explosive volcanic sources is lacking (except that MERRA-2
1128   has time-varying explosive and degassing volcanic SO_2 before December 31, 2010).
1129   The volcanic influence on Arctic AOD, if detectable, would be reflected in the
1130   ABF/sulfate AOD in the reanalyses, but its contribution would be much smaller than the
1131   anthropogenic counterpart for our study period. It is also worth noting that volcanic
1132   activities are not the only influence on the stratospheric aerosol budget: pyroCB-injected
1133   BB smoke can also contribute to stratospheric AOD, as discussed earlier. Stratospheric
1134   BB smoke was also detected over the Arctic with lidar measurements during the
1135   MOSAiC campaign (Engelmann et al., 2021). Stratospheric injection of BB smoke
1136   associated with pyroCB events are not represented in the reanalyses, despite that BB
1137   emission associated with these pyroCB events are included in the emission inventories
1138   with possible large bias in emission amount and height.
1139

1140 Arctic shipping is often brought up as a potentially important source of BC for the Arctic
1141 in the future. All of the reanalyses include shipping emissions, although little interannual
1142 trend is considered especially for the late period in 2003-2019. However "Arctic shipping
1143 is currently only a minor source of black carbon emissions overall" according to the
1144 recent Arctic Monitoring and Assessment Programme (AMAP) report (2021).
1145
1146 **7. Conclusions**
1147
1148 Using remote sensing ~~aerosol optical depth (~~AOD~~)~~ retrievals from ~~the Moderate~~
1149 ~~Resolution Imaging Spectroradiometer (~~MODIS~~), the Multi-angle Imaging~~
1150 ~~SpectroRadiometer (,~~ MISR~~)~~, and ~~Cloud-Aerosol Lidar with Orthogonal Polarization~~
1151 ~~(CALIOP)~~,,, and AODs from three aerosol reanalyses, including ~~the U.S. Naval Aerosol~~
1152 ~~Analysis and Prediction System-ReAnalysis (~~NAAPS-RA~~),the NASA Modern-Era~~
1153 ~~Retrospective Analysis for Research and Applications, version 2 (,~~ MERRA-2~~), and the~~
1154 ~~Copernicus Atmosphere Monitoring Service ReAnalysis (, and~~ CAMSRA~~),,~~ and ground-
1155 based ~~Aerosol Robotic Network (~~AERONET~~)~~ data, we have reported the Arctic/High-
1156 Arctic ~~(defined as 60°-90°N/70°-90°N)~~ AOD climatology, and trend for spring ~~(March-~~
1157 ~~April-May, MAM)~~ and summer ~~(June-July-August, JJA)~~ seasons during 2003-2019.
1158
1159   1) *Arctic AOD climatology*: The total AODs from space-borne remote sensing and
1160   the aerosol reanalyses show quite consistent climatological spatial patterns and
1161   interannual trends for both spring and summer seasons for the lower-Arctic ~~(60-~~
1162   ~~70°N)~~,, where remote sensing data is available. AOD trends for the high Arctic
1163   from the reanalyses have consistent signs too. Climatologically, ~~fine-mode (~~FM~~)~~
1164   AOD dominates ~~coarse-mode (~~CM~~)~~ AOD in the Arctic. Based on the reanalyses,
1165   ~~biomass burning (~~BB~~)~~ smoke AOD increases from March to August associated
1166   with seasonality of BB activities in the boreal region (>50°N);
1167   ~~Sulfate/Anthropogenic and biogenic fine (ABF)~~ABF AOD is slightly higher in
1168   MAM than in JJA; sea salt AOD is highest in March and decreases with time into
1169   later spring and summer; contribution of dust AOD to total AOD is non-negligible
1170   in April and May. The latitudinal gradient of AOD is larger in JJA than in MAM,
1171   consistent with observed more efficient removal in summertime (Garrett et al.,
1172   2011). Among aerosol species, ~~black carbon (~~BC~~)~~ is a very efficient light
1173   absorber, and climate forcing agent (e.g., Bond et al., 2013). We show that over
1174   the Arctic, the contribution of BC AOD from BB source overwhelms
1175   anthropogenic sources in both MAM and JJA, and more so in JJA during 2003-
1176   2019.
1177
1178   2) *Interannual AOD trend*: Total AOD exhibits a general negative trend in the
1179   Arctic in MAM, and strong positive trends in North Americas, Eurasia boreal

1180 regions (except Alaska and northeast Siberia) in JJA. For the high Arctic, the
1181 total AOD trend is -0.017/decade (-18%/decade) for MAM and 0.007/decade
1182 (8%/decade) for JJA based on the ~~multi-reanalysis consensus (MRC).~~ MRC. The
1183 total AOD trends are driven by an overall decrease in sulfate/ABF AOD in both
1184 seasons (-0.008/decade, or -22%/decade for MAM and -0.002/decade or -
1185 10%/decade for JJA), and a negative trend in MAM (-0.003/decade or -
1186 10%/decade) and a strong positive trend in JJA (0.01/decade or 22%/decade)
1187 from biomass burning smoke AOD. The decreasing trend in sulfate in the Arctic
1188 in recent decades is in line with other studies using surface concentration
1189 measurement (e.g., Eckhardt et al., 2015). The smoke AOD trends are
1190 consistent with MODIS fire-hotspot-based BB emission trends over the boreal
1191 continents.

1192

1193 3) ***Impact of BB smoke on AOD interannual variability***: The interannual
1194 variability of total AOD in the Arctic is substantial and predominantly driven by
1195 fine-mode, and specifically BB smoke AOD in both seasons and more so in JJA
1196 than in MAM. For AERONET sites close to BB emission sources, the difference
1197 in monthly total AOD can be 6-fold for high versus low AOD years. For remote
1198 regions away from BB sources, the interannual variability of total AOD can also
1199 be explained mostly by smoke AOD.

1200

1201 4) ***Overall performance of the aerosol reanalyses***: The aerosol reanalyses yield
1202 much more convergent AOD results than the climate models (e.g., AeroCOM
1203 models in Sand et al., 2017; CMIP5 models in Glantz et al., 2014) and verify with
1204 AERONET to some good extent, which corroborates the climatology and trend
1205 analysis. Speciated AODs appear more diverse than the total AOD among the
1206 three reanalyses, and a little more so for MAM than for JJA. NAAPS-RA and
1207 MERRA-2 total and FM AODs verify better in the Arctic than CAMSRA, which
1208 tends to have a high bias in FM overall. The reanalyses generally perform better
1209 in FM than CM. The three reanalyses exhibit different latitudinal AOD gradients,
1210 especially in summertime, indicating different removal efficiencies. The emerging
1211 capability of assimilating OMI Aerosol Index (AI) to constrain absorptive aerosol
1212 amount, could potentially fill in the observational gaps for aerosol data
1213 assimilation in reanalyses over the Arctic (Zhang et al., 2021). With more
1214 advanced retrieval algorithms on the current space-borne sensors for over
1215 snow/ice, new sensors on future satellites, improvements on the underlying
1216 meteorology and aerosol representations in models, improvements in aerosol
1217 reanalysis are expected.

1218 The results presented here provide a baseline of AOD spatiotemporal distribution,
1219 magnitude, and speciation over the Arctic during spring and summer seasons for the

1220 recent two decades. This will help improve aerosol model evaluations and better
1221 constrain aerosol radiative and potentially indirect forcing calculation to evaluate aerosol
1222 impact in the Arctic amplification. For example, the contribution of reduction in sulfate to
1223 Arctic surface warming in recent decades (e.g., Shindell and Faluvegi, 2009; Breider et
1224 al., 2017) could potentially be better quantified, with the caveat that speciated AOD
1225 have larger uncertainties than total AOD in the reanalyses. The AOD statistics could
1226 also provide background information for field campaign data analysis and future field
1227 campaign planning in a larger climate context. It is also recommended that climate
1228 models should take into account BB emissions besides anthropogenic climate forcers
1229 and BB interannual variabilities and trends in Arctic climate change studies.
1230
1231 Appendix A. Summary of data used in the study

Products	Data	resolution	time
MODIS (Moderate Resolution Imaging Spectroradiometer) C6.1L3	550nm AOD	1°x1° monthly	2003-2019
MISR (Multi-angle Imaging SpectroRadiometer) V23	558nm AOD	1°x1°, monthly	2003-2019
CALIOP (Cloud-Aerosol Lidar with Orthogonal Polarisation) V4.2L2	532nm AOD	2°x5°, monthly	2006-2019
AERONET (AErosol RObotic NETwork) V2L3	SDA total, FM, CM AOD at 550nm	6hrly, monthly	2003-2019
MAN (Marine Aerosol Network) Level2	SDA total, FM, CM AOD at 550nm	6hrly	2003-2019
MERRA-2 (Modern-Era Retrospective Analysis for Research and Applications, v2)	Total and speciated AOD at 550nm	0.5°lat x0.63°lon, monthly	2003-2019
CAMSRA (Copernicus Atmosphere Monitoring Service Reanalysis)	Total and speciated AOD at 550nm	0.7°x0.7°, monthly	2003-2019
NAAPS-RA v1 (Navy Aerosol Analysis and Prediction System reanalysis v1)	Total and speciated AOD at 550nm	1°x1°, 6hrly, monthly	2003-2019
MRC (Multi-Reanalysis-Consensus)	Total and speciated AOD at 550nm	1°x1°, monthly	2003-2019
FLAMBE (Fire Locating and Modeling of Burning Emissions) v1.0	BB smoke emission flux	1°x1°, monthly	2003-2019

1232
1233
1234 Note: These are final form of data used in the result section. Some pre-processing and
1235 quality-control were applied to remote sensing data as described in the data section.
1236
1237 **Code and Data Availability:** All data supporting the conclusions of this manuscript are
1238 available either through the links provided below or upon request.
1239 AERONET Version 3 Level 2 data: http://aeronet.gsfc.nasa.gov
1240 MAN data: https://aeronet.gsfc.nasa.gov/new_web/maritime_aerosol_network.html
1241 MODIS DAdata-assimilation-quality AOD: https://nrlgodae1.nrlmry.navy.mil/cgi-
1242 bin/datalist.pl?dset=nrl_modis_l3&summary=Go
1243 Or https://modaps.modaps.eosdis.nasa.gov/services/about/products/c61-
1244 nrt/MCDAODHD.html
1245 MISR AOD: ftp://l5ftl01.larc.nasa.gov/misrl2l3/MISR/MIL2ASAE.003/
1246 CALIOP from NASA Langley Research Center Atmospheric Science Data Center:
1247 https://doi.org/10.5067/CALIOP/CALIPSO/LID_L2_05kmAPro-Standard-V4-20 for the Version
1248 4.2 CALIPSO Level 2 5 km aerosol profile and
1249 https://doi.org/10.5067/CALIOP/CALIPSO/LID_L2_05kmALay-Standard-V4-20 for aerosol layer
1250 products. Further QAed data are available upon request.
1251 NAAPS RA AOD: https://usgodae.org//cgi-
1252 bin/datalist.pl?dset=nrl_naaps_reanalysis&summary=Go

Formatted: Font: 12 pt
Formatted: Font: 12 pt
Formatted: Font: 12 pt
Formatted: Font: 12 pt
Formatted: Font: 12 pt

MERRA-2 AOD;
https://disc.gsfc.nasa.gov/datasets/M2TMNXAER_V5.12.4/summary?keywords=%22MERRA-2%22
CAMSRA AOD: https://www.ecmwf.int/en/research/climate-reanalysis/cams-reanalysis
FLAMBE BB smoke inventory is available upon request from U.S. NRL.

Author contributions: P.X. and J.Z designed this study. P.X. performed most of the data analysis and wrote the initial manuscript. T.T., B.S. and E.H. helped with processing of CALIOP, MISR and MODIS AOD data respectively. All authors contributed to scientific discussion, writing and revision of the manuscript.

Competing interests: The authors declare that they have no conflict of interest.

Acknowledgments
We thank the NASA AERONET and MAN, and Environment and Climate change Canada AEROCAN groups for the sun-photometer data, and NASA MODIS, MISR and CALIOP teams for the AOD data used in the study. We acknowledge NASA GMAO, ECMWF and U.S. ONR and NRL for making the aerosol reanalysis products available. We acknowledge the use of imagery from the NASA Worldview application (https://worldview.earthdata.nasa.gov, last access: Sept 26 2021), part of the NASA Earth Observing System Data and Information System (EOSDIS).

Financial support

The authors acknowledge supports from NASA's Interdisciplinary Science (IDS) program (grant no. 80NSSC20K1260), NASA's Modeling, Analysis and Prediction (MAP) program (NNX17AG52G) and the Office of Naval Research Code 322. N.O. and K.R's work is supported by Canadian Space Agency, SACIA-2 project, Ref. No. 21SUASACOA, ESS-DA program.

References
Abbatt, J. P. D., Leaitch, W. R., Aliabadi, A. A., Bertram, A. K., Blanchet, J.-P., Boivin-Rioux, A., et al. (2019). Overview paper: New insights into aerosol and climate in the Arctic. *Atmospheric Chemistry and Physics*, **19**(4), 2527– 2560. https://doi.org/10.5194/acp-19-2527-2019

AboEl-Fetouh, Y., O'Neill, N. T., Ranjbar, K., Hesaraki, S., Abboud, I., & Sobolewski, P. S. (2020). Climatological-scale analysis of intensive and semi-intensive aerosol parameters derived from AERONET retrievals over the Arctic. *Journal of Geophysical Research: Atmospheres*, *125*, e2019JD031569. https://doi.org/10.1029/2019JD031569
AMAP, 2021. Impacts of Short-lived Climate Forcers on Arctic Climate, Air Quality, and Human Health. Summary for Policy-makers. Arctic Monitoring and Assessment Programme (AMAP), Tromsø, Norway. 20 pp

Baccarini, A., Karlsson, L., Dommen, J. *et al.* Frequent new particle formation over the high Arctic pack ice by enhanced iodine emissions. *Nat Commun* **11,** 4924 (2020). https://doi.org/10.1038/s41467-020-18551-0

Balzter, H., F. F. Gerard, C. T. George, C. S. Rowland, T. E. Jupp, I. McCallum, A. Shvidenko, S. Nilsson, A. Sukhinin, A. Onuchin, C. Schmullius, Impact of the Arctic Oscillation pattern on interannual forest fire variability in central Siberia. *Geophys. Res. Lett.* **32**, L14709 (2005).

Baibakov, K., O'Neill, N. T., Ivanescu, L., Duck, T. J., Perro, C., Herber, A., Schulz, K.-H., and Schrems, O.: Synchronous polar winter starphotometry and lidar measurements at a High Arctic station, AMT, 8, 3789-3809, doi:10.5194/amt-8-3789-2015, 2015.

Bieniek, P. A., Bhatt, U. S., York, A., Walsh, J. E., Lader, R., Strader, H., Ziel, R., Jandt, R. R., & Thoman, R. L. (2020). Lightning Variability in Dynamically Downscaled Simulations of Alaska's Present and Future Summer Climate, *Journal of Applied Meteorology and Climatology*, *59*(6), 1139-1152.

Birch, C. E., Brooks, I. M., Tjernström, M., Shupe, M. D., Mauritsen, T., Sedlar, J., Lock, A. P., Earnshaw, P., Persson, P. O. G., Milton, S. F., and Leck, C.: Modelling atmospheric structure, cloud and their response to CCN in the central Arctic: ASCOS case studies, Atmos. Chem. Phys., 12, 3419–3435, https://doi.org/10.5194/acp-12-3419-2012, 2012.

Boisvert, L.N., A.A. Petty and J.C. Stroeve, 2016: The Impact of the Extreme Winter 2015/16 Arctic Cyclone on the Barents–Kara Seas. Monthly Weather Review, **144** (11), 4279–4287, doi:10.1175/mwr-d-16-0234.1.

Bossioli, E., Sotiropoulou, G., Methymaki, G., & Tombrou, M. (2021). Modeling extreme warm-air advection in the Arctic during summer: The effect of mid-latitude pollution inflow on cloud properties. *Journal of Geophysical Research: Atmospheres*, *126*, e2020JD033291. https://doi.org/10.1029/2020JD033291

Breider, T. J., Mickley, L. J., Jacob, D. J., Wang, Q., Fisher, J. A., Chang, R. Y. W., and Alexander, B.: Annual distributions and sources of Arctic aerosol components, aerosol optical depth, and aerosol absorption, J. Geophys. Res.-Atmos., 119, 4107–4124, https://doi.org/10.1002/2013JD020996, 2014.

Breider, T. J., Mickley, L. J., Jacob, D. J., Ge, C., Wang, J., Payer Sulprizio, M., Croft, B., Ridley, D. A., McConnell, J. R., Sharma, S., Husain, L., Dutkiewicz, V. A., Eleftheriadis, K., Skov, H., and Hopke, P. K.: Multidecadal trends in aerosol radiative forcing over the Arctic: Contribution of changes in anthropogenic aerosol to Arctic warming since 1980, J. Geophys. Res.-Atmos., 122, 3573–3594, https://doi.org/10.1002/2016JD025321, 2017.

1340   Bullard, J. E., et al. (2016), High-latitude dust in the Earth system, Rev. Geophys., 54,
1341   447– 485, doi:10.1002/2016RG000518
1342
1343   Campbell, J. R., Tackett, J. L., Reid, J. S., Zhang, J., Curtis, C. A., Hyer, E. J., ... &
1344   Winker, D. M. (2012). Evaluating nighttime CALIOP 0.532 μm aerosol optical depth and
1345   extinction coefficient retrievals. *Atmospheric Measurement Techniques*, *5*(9), 2143-
1346   2160.
1347
1348   Colarco, P. R., R. A. Kahn, L. A. Remer, and R. C. Levy, 2014: Impact of satellite
1349   viewing-swath width on global and regional aerosol optical thickness statistics and
1350   trends. *Atmospheric Measurement Techniques*, **7,** 2313-2335.
1351
1352   Comiso, J. C., Large Decadal Decline of the Arctic Multiyear Ice Cover (2012). J.
1353   Climate, Vol., 25. 1176-1193. https://doi.org/10.1175/JCLI-D-11-00113.1
1354   Coogan, S. C. P., Cai, X., Jain, P., and Flannigan, M. D. (2020) Seasonality and trends
1355   in human- and lightning-caused wildfires ≥ 2 ha in Canada, 1959–2018. *International*
1356   *Journal of Wildland Fire* **29**, 473-485. https://doi.org/10.1071/WF19129

1357   Coopman, Q., Garrett, T. J., Finch, D. P., & Riedi, J. (2018). High sensitivity of arctic
1358   liquid clouds to long-range anthropogenic aerosol transport. Geo-physical Research
1359   Letters, 45, 372–381. https://doi.org/10.1002/2017GL075795
1360
1361   Dai, A., Luo, D., Song, M., & Liu, J. (2019). Arctic amplification is caused by sea-ice loss
1362   under increasing CO_2. *Nature Communications*, **10**(1),
1363   121. https://doi.org/10.1038/s41467-018-07954-9
1364
1365   Dall´Osto, M., Beddows, D. C. S., Tunved, P., Krejci, R., Ström, J., Hansson, H.-C.,
1366   et al. (2017). Arctic sea ice melt leads to atmospheric new particle formation. *Scientific*
1367   *Reports*, **7**(1), 3318. https://doi.org/10.1038/s41598-017-03328-1
1368
1369   Dang, C., S. G. Warren, Q. Fu, S. J. Doherty, M. Sturm, and J. Su (2017),
1370   Measurements of light-absorbing particles in snow across the Arctic, North America,
1371   and China: Effects on surface albedo, J. Geophys. Res. Atmos., 122, 10,149–10,168,
1372   doi:10.1002/2017JD027070.
1373
1374   Das, S., Colarco, P. R., Oman, L. D., Taha, G., and Torres, O.: The long-term transport
1375   and radiative impacts of the 2017 British Columbia pyrocumulonimbus smoke aerosols
1376   in the stratosphere, Atmos. Chem. Phys., 21, 12069–12090,
1377   https://doi.org/10.5194/acp-21-12069-2021, 2021.
1378
1379   DeRepentigny, P., Jahn, A., Holland, M., Fasullo, J., Lamarque, J.-F., Hannay, C., Mills,
1380   M., Bailey, D., Tilmes, S., and Barrett, A.: Impact of CMIP6 biomass burning emissions
1381   on Arctic sea ice loss, EGU General Assembly 2021, online, 19–30 Apr 2021, EGU21-
1382   9020, https://doi.org/10.5194/egusphere-egu21-9020, 2021.
1383

1384 Eck, T. F., et al. (2009), Optical properties of boreal region biomass burning aerosols in
1385 central Alaska and seasonal variation of aerosol optical depth at an Arctic coastal site,
1386 J. Geophys. Res., 114, D11201, doi:10.1029/2008JD010870.
1387
1388 Eckhardt, S., A. Stohl, S. Beirle, N. Spichtinger, P. James, C. Forster, C. Junker, T.
1389 Wagner, U. Platt, and S. G. Jennings (2003), The North Atlantic Oscillation controls air
1390 pollution transport to the Arctic, Atmos. Chem. Phys., 3(5), 1769–1778,
1391 doi:10.5194/acp-3-1769-2003.
1392
1393 Eckhardt, S., Quennehen, B., Olivié, D. J. L., Berntsen, T. K., Cherian, R., Christensen,
1394 J. H., Collins, W., Crepinsek, S., Daskalakis, N., Flanner, M., Herber, A., Heyes, C.,
1395 Hodnebrog, Ø., Huang, L., Kanakidou, M., Klimont, Z., Langner, J., Law, K. S., Lund, M.
1396 T., Mahmood, R., Massling, A., Myriokefalitakis, S., Nielsen, I. E., Nøjgaard, J. K.,
1397 Quaas, J., Quinn, P. K., Raut, J.-C., Rumbold, S. T., Schulz, M., Sharma, S., Skeie, R.
1398 B., Skov, H., Uttal, T., von Salzen, K., and Stohl, A.: Current model capabilities for
1399 simulating black carbon and sulfate concentrations in the Arctic atmosphere: a multi-
1400 model evaluation using a comprehensive measurement data set, Atmos. Chem. Phys.,
1401 15, 9413–9433, https://doi.org/10.5194/acp-15-9413-2015, 2015.
1402
1403 Engelmann, R., Ansmann, A., Ohneiser, K., Griesche, H., Radenz, M., Hofer, J.,
1404 Althausen, D., Dahlke, S., Maturilli, M., Veselovskii, I., Jimenez, C., Wiesen, R., Baars,
1405 H., Bühl, J., Gebauer, H., Haarig, M., Seifert, P., Wandinger, U., and Macke, A.: Wildfire
1406 smoke, Arctic haze, and aerosol effects on mixed-phase and cirrus clouds over the
1407 North Pole region during MOSAiC: an introduction, Atmos. Chem. Phys., 21, 13397–
1408 13423, https://doi.org/10.5194/acp-21-13397-2021, 2021.
1409
1410 Evangeliou, N., Balkanski, Y., Hao, W. M., Petkov, A., Silverstein, R. P., Corley, R.,
1411 Nordgren, B. L., Urbanski, S. P., Eckhardt, S., Stohl, A., Tunved, P., Crepinsek, S.,
1412 Jefferson, A., Sharma, S., Nøjgaard, J. K., and Skov, H.: Wildfires in northern Eurasia
1413 affect the budget of black carbon in the Arctic – a 12-year retrospective synopsis (2002–
1414 2013), Atmos. Chem. Phys., 16, 7587–7604, https://doi.org/10.5194/acp-16-7587-2016,
1415 2016.
1416
1417 Fisher, J. A. *et al.* Sources, distribution, and acidity of sulfate-ammonium aerosol in the
1418 Arctic in winter-spring. *Atmos Environ* **45**, 7301–7318,
1419 https://doi.org/10.1016/j.atmosenv.2011.08.030 (2011).
1420
1421 Fisher, J. A., et al. (2010), Source attribution and interannual variability of Arctic
1422 pollution in spring constrained by aircraft (ARCTAS, ARCPAC) and satellite (AIRS)
1423 observations of carbon monoxide, Atmos. Chem. Phys., 10(3), 977–996,
1424 doi:10.5194/acp-10-977-2010.
1425 Flanner, M. G., Zender, C. S., Randerson, J. T., & Rasch, P. J. (2007). Present-day
1426 climate forcing and response from black carbon in snow. *Journal of Geophysical*
1427 *Research, 112*(September 2006), D11202. https://doi.org/10.1029/2006JD008003
1428

Formatted: French (Canada)

1429 Flanner, M. G., C. S. Zender, P. G. Hess, N. M. Mahowald, T. H. Painter, V.
1430 Ramanathan, and P. J. Rasch (2009), Springtime warming and
1431 reduced snow cover from carbonaceous particles, Atmos. Chem. Phys., 9(7), 2481–
1432 2497, doi:10.5194/acp-9-2481-2009.
1433
1434 Flannigan, M. D., and J. B. Harrington, 1988: A study of the relation of meteorological
1435 variables to monthly provincial area burned by wildfire in Canada (1953-1980). *J. Appl.*
1436 *Meteorol.*, **27,** 441-452.
1437
1438 Fromm, M., Lindsey, D. T., Servranckx, R., Yue, G., Trickl, T., Sica, R., Doucet, P., &
1439 Godin-Beekmann, S. (2010). The Untold Story of Pyrocumulonimbus, Bulletin of the
1440 American Meteorological Society, 91(9), 1193-1210.
1441
1442 Gabric, A., Matrai, P., Jones, G., & Middleton, J. (2018). The nexus between sea ice
1443 and polar emissions of marine biogenic aerosols. *Bulletin of the American*
1444 *Meteorological Society*, **99**(1), 61– 81. https://doi.org/10.1175/BAMS-D-16-0254.1
1445
1446 Garay, M. J., and Coauthors, 2020: Introducing the 4.4 km spatial resolution Multi-Angle
1447 Imaging SpectroRadiometer (MISR) aerosol product. *Atmospheric Measurement*
1448 *Techniques*, **13,** 593-628.
1449
1450 Garrett, T. J., Zhao, C., and Novelli, P.: Assessing the relative contributions of transport
1451 efficiency and scavenging to seasonal variability in Arctic aerosol, Tellus B, 62, 190–
1452 196, https://doi.org/10.1111/j.1600-0889.2010.00453.x, 2010.
1453
1454 Garrett, T. J., Brattström, S., Sharma, S.,Worthy, D. E., and Novelli, P.: The role of
1455 scavenging in the seasonal transport of black carbon carbon and sulfate to the Arctic,
1456 Geophys. Res. Lett., 38, L16805, https://doi.org/10.1029/2011GL048221, 2011.
1457
1458 Giglio, L., Randerson, J. T., and van der Werf, G. R.: Analysis of daily, monthly, and
1459 annual burned area using the fourthgeneration global fire emissions database (GFED4),
1460 J. Geophys. Res.-Biogeo., 118, 317–328, https://doi.org/10.1002/jgrg.20042, 2013.
1461
1462 Giles, D. M., Sinyuk, A., Sorokin, M. G., Schafer, J. S., Smirnov, A., Slutsker, I., Eck, T.
1463 F., Holben, B. N., Lewis, J. R., Campbell, J. R., Welton, E. J., Korkin, S. V., and
1464 Lyapustin, A. I.: Advancements in the Aerosol Robotic Network (AERONET) Version 3
1465 database – automated near-real-time quality control algorithm with improved cloud
1466 screening for Sun photometer aerosol optical depth (AOD) measurements, Atmos.
1467 Meas. Tech., 12, 169–209, https://doi.org/10.5194/amt-12-169-2019, 2019.
1468
1469 Glantz, P., Bourassa, A., Herber A., Iversen T., Karlsson J., Kirkevag, A., Maturilli, M.,
1470 Seland, O., Stebel, K., Struthers, H., Tesche, M., and Thomason L., (2014), Remote
1471 sensing of aerosols in the Arctic for an evaluation of global climate model simulations, J.
1472 Geophys. Res. Atmos., 119, 8169–8188, doi:10.1002/2013JD021279.
1473

Goosse, H., Kay, J.E., Armour, K.C. *et al.* Quantifying climate feedbacks in polar regions. *Nat Commun* **9,** 1919 (2018). https://doi.org/10.1038/s41467-018-04173-0

Graham, R.M. et al., 2017: Increasing frequency and duration of Arctic winter warming events. Geophysical Research Letters, **44** (13), 6974–6983, doi:10.1002/2017gl073395.

Groot Zwaaftink, C. D., H. Grythe, H. Skov, and A. Stohl (2016), Substantial contribution of northern high-latitude sources to mineral dust in the Arctic, J. Geophys. Res. Atmos., 121, 13,678–13,697, doi:10.1002/ 2016JD025482.

Hall, J. V., Loboda, T. V., Giglio, L., McCarty G. W. (2016), A MODIS-based burned area assessment for Russian croplands: Mapping requirements and challenges. Remote Sensing of Environment, Vol. 184, 506-521. https://doi.org/10.1016/j.rse.2016.07.022

Hansen J. and Nazarenko, L. (2004): Soot climate forcing via snow and ice albedos. PNAS, 101 (2). 423-428.

Hansen, E., Gerland, S., Granskog, M. A., Pavlova, O., Renner, A. H. H., Haapala, J., et al. (2013). Thinning of Arctic sea ice observed in Fram Strait: 1990–2011. Journal of Geophysical Research: Oceans, 118, 5202–5221. https://doi.org/10.1002/jgrc.20393

Herber, A., L. W. Thomason, H. Gernandt, U. Leiterer, D. Nagel, K. Schulz, J. Kaptur, T. Albrecht, and J. Notholt (2002), Continuous day and night aerosol optical depth observations in the Arctic between 1991 and 1999, J. Geophys. Res., 107(D10), 4097, doi:10.1029/2001JD000536.

Hesaraki S, O'Neill NT, Lesins G, Saha A, Martin RV, Fioletov VE, Baibakov K, Abboud I. Comparisons of a chemical transport model with a four-year (April to September) analysis of fine-and coarse-mode aerosol optical depth retrievals over the Canadian Arctic. Atmosphere-Ocean. 2017 Oct 20;55(4-5):213-29.

Hyer, E. J., J. S. Reid, and J. Zhang, 2011: An over-land aerosol optical depth data set for data assimilation by filtering, correction, and aggregation of MODIS Collection 5 optical depth retrievals. *Atmospheric Measurement Techniques*, European Geophysical Union, 379-408.

Hyer, Edward J., Eric S. Kasischke, and Dale J. Allen. "Effects of source temporal resolution on transport simulations of boreal fire emissions." *Journal of Geophysical Research: Atmospheres* 112.D1 (2007). https://doi.org/10.1029/2006JD007234

Hyer EJ, Reid JS, Prins EM, Hoffman JP, Schmidt CC, Miettinen JI, Giglio L. : Patterns of fire activity over Indonesia and Malaysia from polar and geostationary satellite observations Atmospheric Research. 122: 504-519. DOI: 10.1016/J.Atmosres.2012.06.011 , 2013

1520 Inness, A., Ades, M., Agustí-Panareda, A., Barré, J., Benedictow, A., Blechschmidt, A.-
1521 M., Dominguez, J. J., Engelen, R., Eskes, H., Flemming, J., Huijnen, V., Jones, L.,
1522 Kipling, Z., Massart, S., Parrington, M., Peuch, V.-H., Razinger, M., Remy, S., Schulz,
1523 M., and Suttie, M.: The CAMS reanalysis of atmospheric composition, Atmos. Chem.
1524 Phys., 19, 3515–3556, https://doi.org/10.5194/acp-19-3515-2019, 2019.
1525
1526 IPCC 2013 Chapter 8 by Myhre, G., D. Shindell, F.-M. Bréon, W. Collins, J. Fuglestvedt,
1527 J. Huang, D. Koch, J.-F. Lamarque, D. Lee, B. Mendoza, T. Nakajima, A. Robock, G.
1528 Stephens, T. Takemura and H. Zhang, 2013: Anthropogenic and Natural Radiative
1529 Forcing. In: Climate Change 2013: The Physical Science Basis. Contribution of Working
1530 Group I to the Fifth Assessment Report of the Intergovernmental Panel on Climate
1531 Change [Stocker, T.F., D. Qin, G.-K. Plattner, M. Tignor, S.K. Allen, J. Boschung, A.
1532 Nauels, Y. Xia, V. Bex and P.M. Midgley (eds.)]. Cambridge University Press,
1533 Cambridge, United Kingdom and New York, NY, USA.
1534
1535 IPCC. (2021). Climate change 2021: The physical science basis. Contribution of
1536 working group I to the sixth assessment report of the intergovernmental panel on
1537 climate change [Masson-Delmotte. In V. P. Zhai, A. Pirani, S. L. Connors, C. Péan, S.
1538 Berger, N. Caud et al. (Eds.), Cambridge University Press. In Press.
1539
1540 Iziomon, M. G., U. Lohmann, and P. K. Quinn (2006), Summertime pollution events in
1541 the Arctic and potential implications, J. Geophys. Res., 111, D12206,
1542 doi:10.1029/2005JD006223.
1543
1544 Jacob, D. J., J. H. Crawford, H. Maring, A. D. Clarke, J. E. Dibb, L. K. Emmons, R. A.
1545 Ferrare, C. A. Hostetler, P. B. Russell, and H. B. Singh (2010), The arctic research of
1546 the composition of the troposphere from aircraft and satellites (ARCTAS) mission:
1547 Design, execution, and first results, Atmos. Chem. Phys., 10(11), 5191–5212.
1548
1549 Jacobson, M. Z. (2004), Climate response of fossil fuel and biofuel soot, accounting for
1550 soot's feedback to snow and sea ice albedo and emissivity, J. Geophys. Res., 109,
1551 D21201, doi:10.1029/2004JD004945.
1552
1552 Kang S., Y. Zhang, Y. Qian, and H. Wang. 2020. "A review of black carbon in snow
1553 and ice and its impact on the cryosphere." *Earth - Science Reviews* 210. PNNL-SA-
1554 154137. doi:10.1016/j.earscirev.2020.103346
1555
1555 Kapsch, M.-L., R.G. Graversen and M. Tjernström, 2013: Springtime atmospheric
1556 energy transport and the control of Arctic summer sea-ice extent. Nature Climate
1557 Change, **3**, 744, doi:10.1038/nclimate1884.
1558
1559 Khan, A. L., S. Wagner, R. Jaffe, P. Xian, M. Williams, R. Armstrong, and D. McKnight
1560 (2017), Dissolved black carbon in the global cryosphere: Concentrations and chemical
1561 signatures, Geophys. Res. Lett., 44, 6226–6234, doi:10.1002/2017GL073485.
1562

Formatted: A2

Kim, J. S., Kug, J. S., Jeong, S. J., Park, H., and Schaepman-Strub, G.: Extensive fires in southeastern Siberian permafrost linked to preceding Arctic Oscillation, Sci. Adv., 6, eaax3308, https://doi.org/10.1126/sciadv.aax3308, 2020.

Kim, M. H., and Coauthors, 2018: The CALIPSO version 4 automated aerosol classification and lidar ratio selection algorithm. *Atmospheric Measurement Techniques*, **11,** 6107-6135.

Kleidman, R. G., N. T. O'Neill, L. A. Remer, Y. J. Kaufman, T. F. Eck, D. Tanre´, O. Dubovik, and B. N. Holben (2005), Comparison of Moderate Resolution Imaging Spectroradiometer (MODIS) and Aerosol Robotic Network (AERONET) remote-sensing retrievals of aerosol fine mode fraction over ocean, J. Geophys. Res., 110, D22205, doi:10.1029/2005JD005760.

Kokhanovsky, A., and Tomasi, C. (Eds.): Physics and Chemistry of the Arctic Atmosphere. Springer Nature Switzerland AG 2020. https://doi.org/10.1007/978-3-030-33566-3

Köllner, F., Schneider, J., Willis, M. D., Schulz, H., Kunkel, D., Bozem, H., Hoor, P., Klimach, T., Helleis, F., Burkart, J., Leaitch, W. R., Aliabadi, A. A., Abbatt, J. P. D., Herber, A. B., and Borrmann, S.: Chemical composition and source attribution of sub-micrometre aerosol particles in the summertime Arctic lower troposphere, Atmos. Chem. Phys., 21, 6509–6539, https://doi.org/10.5194/acp-21-6509-2021, 2021.

Kondo, Y., et al. (2011), Emissions of black carbon, organic, and inorganic aerosols from biomass burning in North America and Asia in 2008, J. Geophys. Res., 116, D08204, doi:10.1029/2010JD015152.

Korontzi, S., J. McCarty, T. Loboda, S. Kumar, and C. Justice (2006), Global distribution of agricultural fires in croplands from 3 years of Moderate Resolution Imaging Spectroradiometer (MODIS) data, Global Biogeochem. Cycles, 20, GB2021, doi:10.1029/2005GB002529.

Kwok, R. and Rothrock D. A. (2009) Decline in Arctic sea ice thickness from submarine and ICESate records: 1958-2008. Geophys. Res. Lett. 36 L15501.

Law, K. S. and A. Stohl, 2007: Arctic air pollution: Origins and impacts. *Science*, **315**, 1537–1540, doi:10.1126/science.1137695.

Lubin, D., and Vogelmann, A. M. (2006). A climatologically significant aerosol longwave indirect effect in the Arctic. *Nature*, *439*, 453–456. https://doi.org/10.1038/nature04449

Lynch, P., J. S. Reid, D. L. Westphal, J. Zhang, T. Hogan, E. J. Hyer, C. A. Curtis, D. Hegg, Y. Shi, J. R. Campbell, J. Rubin, W. Sessions, J. Turk and A. Walker: An 11-year Global Gridded Aerosol Optical Thickness Reanalysis (v1.0) for Atmospheric and Climate Sciences. Geosci. Model Dev., 9, 1489-1522, doi:10.5194/gmd-9-1489-2016, 2016.

1609
1610 Macias Fauria, M, E. A. Johnson, Large-scale climatic patterns control large lightning
1611 fire occurrence in Canada and Alaska forest regions. *J. Geophys. Res.* **111**, G04008
1612 (2006).
1613
1614 Markowicz, K. M., et al. (2016), Impact of North American intense fires on aerosol
1615 optical properties measured over the European Arctic in July 2015, J. Geophys. Res.
1616 Atmos., 121, 14,487–14,512, doi:10.1002/2016JD025310.
1617
1618 Markowicz, K.M., Lisok, J., Xian, P., Simulation of long-term direct aerosol radiative
1619 forcing over the arctic within the framework of the iAREA project, Atmospheric
1620 Environment (2021), doi: https://doi.org/10.1016/j.atmosenv.2020.117882.
1621
1622 Mauritsen, T., Sedlar, J., Tjernström, M., Leck, C., Martin, M., Shupe, M., Sjogren, S.,
1623 Sierau, B., Persson, P. O. G., Brooks, I. M., and Swietlicki, E.: An Arctic CCN-limited
1624 cloud-aerosol regime, Atmos. Chem. Phys., 11, 165–173, https://doi.org/10.5194/acp-
1625 11-165-2011, 2011.
1626
1627 McCarty, J. L., Aalto, J., Paunu, V.-V., Arnold, S. R., Eckhardt, S., Klimont, Z., Fain, J.
1628 J., Evangeliou, N., Venäläinen, A., Tchebakova, N. M., Parfenova, E. I., Kupiainen, K.,
1629 Soja, A. J., Huang, L., and Wilson, S.: Reviews and syntheses: Arctic fire regimes and
1630 emissions in the 21st century, Biogeosciences, 18, 5053–5083,
1631 https://doi.org/10.5194/bg-18-5053-2021, 2021.
1632
1633 McNaughton, C. S., Clarke, A. D., Freitag, S., Kapustin, V. N., Kondo, Y., Moteki, N.,
1634 Sahu, L., Takegawa, N., Schwarz, J. P., Spackman, J. R., Watts, L., Diskin, G.,
1635 Podolske, J., Holloway, J. S., Wisthaler, A., Mikoviny, T., de Gouw, J., Warneke, C.,
1636 Jimenez, J., Cubison, M., Howell, S. G., Middlebrook, A., Bahreini, R., Anderson, B. E.,
1637 Winstead, E., Thornhill, K. L., Lack, D., Cozic, J., and Brock, C. A.: Absorbing aerosol in
1638 the troposphere of the Western Arctic during the 2008 ARCTAS/ARCPAC airborne field
1639 campaigns, Atmos. Chem. Phys., 11, 7561–7582, https://doi.org/10.5194/acp-11-7561-
1640 2011, 2011.
1641
1642 Meier, W. N., Hovelsrud, G. K., van Oort, B. E. H., Key, J. R., Kovacs, K. M., Michel, C.,
1643 et al. (2014). Arctic sea ice in transformation: A review of recent observed changes and
1644 impacts on biology and human activity. *Reviews of*
1645 *Geophysics*, **52**, 185– 217. https://doi.org/10.1002/2013RG000431
1646
1647 Morrison, A.L. et al., 2018: Isolating the Liquid Cloud Response to Recent Arctic Sea
1648 Ice Variability Using Spaceborne Lidar Observations. Journal of Geophysical Research:
1649 Atmospheres, **123** (1), 473–490, doi:10.1002/2017jd027248.
1650
1651 Notz D. and Stroeve, J. Observed Arctic sea-ice loss directly follows anthropogenic
1652 CO_2 emission (2016) *Science.* Vol. 354, Issue 6313, pp. 747-750 DOI:
1653 10.1126/science.aag2345
1654

1655 Nummelin, A., C. Li and P.J. Hezel, 2017: Connecting ocean heat transport changes
1656 from the midlatitudes to the Arctic Ocean. Geophysical Research Letters, **44** (4), 1899–
1657 1908, doi:10.1002/2016GL071333.

1659 O'Neill, N.T., T.F.Eck, B.N.Holben, A.Smirnov, O.Dubovik, and A.Royer (2001) Bimodal
1660 size distribution influences on the variation of Angstrom derivatives in spectral and
1661 optical depth space, J. Geophys. Res., 106, 9787-9806.

1663 O'Neill, N. T., Perro, C., Saha, A., Lesins, G., Duck, T. J., Eloranta, E. W., Nott, G. J.,
1664 Hoffman, A., Karumudi, M. L., Ritter, C., Bourassa, A., Abboud, I., Carn S., A.,
1665 Savastiouk, V. (2012) Properties of Sarycheve Sulphate aerosols over the Arctic. J.
1666 Geophys. Res. Atmos. Vol. 117, D04203, https://doi.org/10.1029/2011JD016838

1668 O'Neill, N. T., Perro, C., Saha, A., Lesin, G., Duck, T., Eloranta, E., Hoffman, M. L.
1669 Karumudi, A., Ritter, C., A. Bourassa, I. Aboud, S. Carn, V. Savastiouk, Impact of
1670 Sarychev sulphate aerosols over the Arctic, *Jour. Geophys. Res.*, VOL. 117, D04203,
1671 doi:10.1029/2011JD016838, 2012.

1673 O'Neill, N. T., Eck, T. F., Smirnov, A., Holben, B. N., and Thulasiraman S. (2003)
1674 Spectral discrimination of coarse and fine mode optical depth. J. Geophys. Res., 108,
1675 D05212, doi:10.1029/2002JD002975.

1677 Peterson, D. A., Fromm, M. D., Solbrig, J. E., Hyer, E. J., Surratt, M. L., & Campbell, J.
1678 R. (2017). Detection and Inventory of Intense Pyroconvection in Western North America
1679 using GOES-15 Daytime Infrared Data, Journal of Applied Meteorology and
1680 Climatology, 56(2), 471-493.

1682 Peterson, D. A., Hyer, E. J., Campbell, J. R., Fromm, M. D., Hair, J. W., Butler, C. F., &
1683 Fenn, M. A. (2015). The 2013 Rim Fire: Implications for Predicting Extreme Fire Spread,
1684 Pyroconvection, and Smoke Emissions, Bulletin of the American Meteorological
1685 Society, 96(2), 229-247.

1687 Perovich, D. K., and C. Polashenski (2012), Albedo evolution of seasonal Arctic sea ice,
1688 Geophys. Res. Lett., 39, L08501, doi:10.1029/2012GL051432

1690 Prenni, A. J., Harrington, J. Y., Tjernstöm, M., DeMott, P. J., Avramov, A., Long, C. N.,
1691 Kreidenweis, S. M., Olsson, P. Q., and Verlinde, J.: Can ice-nucleating aerosols affect
1692 arctic seasonal climate?, B. Am. Meteorol. Soc., 88, 541–550,
1693 https://doi.org/10.1175/BAMS-88-4-541, 2007.

1695 Quinn, P. K., et al. (2008), Short-lived pollutants in the Arctic: Their climate impact and
1696 possible mitigation strategies, Atmos. Chem. Phys., 8(6), 1723–1735, doi:10.5194/acp-
1697 8-1723-2008.

1699 Randles, C. A., daSilva, A. M., Buchard, V., Colarco, P. R., Darmenov, A., Govindaraju,
1700 R., et al.: The MERRA-2 aerosol reanalysis, 1980 onward. Part I: System description

Formatted: Hyperlink, Font color: Custom Color(RGB(0,82,116))

Formatted: Normal

Formatted: French (Canada)

1701 and data assimilation evaluation. Journal of Climate, 30(17), 6823-6850.
1702 https://doi.org/10.1175/JCLI-D-16-0609.1, 2017.

1703
1704 Randerson, J. T., and Coauthors, 2006: The impact of boreal forest fire on climate
1705 warming. Science, 314, 1130–1132, doi:10.1126/science.1132075.

1706
1707 Ranjbar, K., O'Neill, N. T., Lutsch, E., McCullough, E. M., AboEl-Fetouh, Y., Xian, P., et
1708 al. (2019). Extreme smoke event over the high Arctic. *Atmospheric Environment*, *218*,
1709 117002. https://doi.org/10.1016/j.atmosenv.2019.117002

1710
1711 Reid, J. S., Hyer, E. J., Prins, E. M., Westphal, D. L., Zhang, J., Wang, J., Christopher,
1712 S. A., Curtis, C. A., Schmidt, C. C., Eleuterio, D. P., Richardson, K. A., and Hoffman, J.
1713 P.: Global Monitoring and Forecasting of Biomass-Burning Smoke: Description of and
1714 Lessons from the Fire Locating and Modeling of Burning Emissions (FLAMBE)
1715 Program, IEEE J. Sel. Top. Appl., 2, 144–162, JSTARS-2009-00034, 2009.

1716
1717 Reid, J. S., Koppmann, R., Eck, T. F., and Eleuterio, D. P.: A review of biomass burning
1718 emissions part II: intensive physical properties of biomass burning particles, Atmos.
1719 Chem. Phys., 5, 799–825, https://doi.org/10.5194/acp-5-799-2005, 2005.

1720
1721 Rinke, A., Maturilli, M., Graham, R. M., Hatthes, H., Handorf, D., Cohen, L., Hudson, S.
1722 R. and Moore, J. C., (2017), Extreme cyclone events in the Arctic: Wintertime variability
1723 and trends. *Environ. Res. Lett.* **12** 094006

1724
1725 Rosel, A., Itkin, P., King, J., Divine, D., Wang, C., Granskog, M. A., Krumpen, T., and
1726 Gerland, S. (2018). Thin sea ice, thick snow and widespread negative freeboard
1727 observed during N-ICE2015 north of Svalbard. J. Geophys. Res: Oceans, 123, 1156–
1728 1176. https://doi.org/10.1002/2017JC012865

1729
1730 Saha, A., et al. (2010), Pan-Arctic sunphotometry during the ARCTAS-A campaign of
1731 April 2008, Geophys. Res. Lett., 37, L05803, doi:10.1029/2009GL041375.

1732
1733 Sand, M., T. K. Berntsen, Ø. Seland, and J. E. Kristjánsson (2013), Arctic surface
1734 temperature change to emissions of black carbon within Arctic or midlatitudes, J.
1735 Geophys. Res. Atmos., 118, 7788–7798, doi:10.1002/jgrd.50613.

1736
1737 Sand, M., Berntsen, T., Von Salzen, K., Flanner, M., Langner, J., and Victor, D.:
1738 Response of Arctic temperature to changes in emissions of short-lived climate forcers,
1739 Nat. Clim. Change, 6, 286–289, https://doi.org/10.1038/nclimate2880, 2016.

1740
1741 Sand, M., Samset, B. H., Balkanski, Y., Bauer, S., Bellouin, N., Berntsen, T. K., Bian,
1742 H., Chin, M., Diehl, T., Easter, R., Ghan, S. J., Iversen, T., Kirkevåg, A., Lamarque, J.-
1743 F., Lin, G., Liu, X., Luo, G., Myhre, G., Noije, T. V., Penner, J. E., Schulz, M., Seland,
1744 Ø., Skeie, R. B., Stier, P., Takemura, T., Tsigaridis, K., Yu, F., Zhang, K., and Zhang,
1745 H.: Aerosols at the poles: an AeroCom Phase II multi-model evaluation, Atmos. Chem.
1746 Phys., 17, 12197–12218, https://doi.org/10.5194/acp-17-12197-2017, 2017.

1747
1748 Sayer, A. M. and Knobelspiesse, K. D.: How should we aggregate data? Methods
1749 accounting for the numerical distributions, with an assessment of aerosol optical depth,
1750 Atmos. Chem. Phys., 19, 15023–15048, https://doi.org/10.5194/acp-19-15023-2019,
1751 2019.
1752
1753 Serreze, M.C. and R.G. Barry, 2011: Processes and impacts of Arctic amplification: A
1754 research synthesis. Global and Planetary Change, **77** (1– 2), 85–96,
1755 doi:10.1016/j.gloplacha.2011.03.004.
1756
1757 Serreze, M.C., Francis, J.A. The Arctic Amplification Debate. *Climatic Change* **76,** 241–
1758 264 (2006). https://doi.org/10.1007/s10584-005-9017-y
1759
1760 Sharma, S., M. Ishizawa, D. Chan, D. Lavoué, E. Andrews, K. Eleftheriadis, and S.
1761 Maksyutov (2013), 16-year simulation of Arctic black carbon: Transport, source
1762 contribution, and sensitivity analysis on deposition, J. Geophys. Res. Atmos., 118, 943–
1763 964, doi:10.1029/2012JD017774.
1764
1765 Shi, Y., J. Zhang, J. S. Reid, E. J. Hyer, and N. C. Hsu, 2013: Critical evaluation of the
1766 MODIS Deep Blue aerosol optical depth product for data assimilation over North Africa.
1767 *Atmospheric Measurement Techniques*, **6,** 949-969.
1768
1769 Shi, Y., J. Zhang, J. S. Reid, B. Holben, E. J. Hyer, and C. Curtis, 2011: An analysis of
1770 the collection 5 MODIS over-ocean aerosol optical depth product for its implication in
1771 aerosol assimilation. *Atmos. Chem. Phys.*, **11,** 557-565.
1772
1773 Shindell, D. and Faluvegi, G.: Climate response to regional radiative forcing during the
1774 twentieth century, Nat. Geosci., 2, 294–300, https://doi.org/10.1038/ngeo473, 2009.
1775
1776 Schlosser, J. S., R. A. Braun, T. Bradley, H. Dadashazar, A. B. MacDonald, A. A.
1777 Aldhaif, M. A. Aghdam, A. H. Mardi, P. Xian, and A. Sorooshian (2017), Analysis of
1778 aerosol composition data for western United States wildfires between 2005 and 2015:
1779 Dust emissions, chloride depletion, and most enhanced aerosol constituents, J.
1780 Geophys. Res. Atmos., 122, 8951–8966, doi:10.1002/2017JD026547.
1781
1782 Skiles S. M., Flanner, M., Cook, J. M., Dumont, M. and Painter, T. (2018) Radiative
1783 forcing by light-absorbing particles in snow. Nature Climate Change, 8, 964-971.
1784 https://doi.org/10.1038/s41558-018-0296-5
1785
1786 Skinner, W. R., B. J. Stocks, D. L. Martell, B. Bonsal, and A. Shabbar, 1999: The
1787 association between circulation anomalies in the mid- troposphere and area burned by
1788 wildland fire in Canada. *Theoretical and Applied Climatology*, **63,** 89-105.
1789
1790 Stohl, A., et al. (2006), Pan-Arctic enhancements of light absorbing aerosol
1791 concentrations due to North American boreal forest fires during summer 2004, J.
1792 Geophys. Res., 111, D22214, doi:10.1029/2006JD007216.

Stohl, A., et al. (2007), Arctic smoke—Record high air pollution levels in the European Arctic due to agricultural fires in eastern Europe in spring 2006, Atmos. Chem. Phys., 7(2), 511–534, doi:10.5194/acp-7-511-2007.

Stone, R. S., G. P. Anderson, E. Andrews, E. G. Dutton, E. P. Shettle, and A. Berk (2007), Incursions and radiative impact of Asian dust in northern Alaska, Geophys. Res. Lett., 34, L14815, doi:10.1029/2007GL029878.

Taylor, P., B. Hegyi, R. Boeke and L. Boisvert, 2018: On the Increasing Importance of Air-Sea Exchanges in a Thawing Arctic: A Review. Atmosphere, **9** (2), doi:10.3390/atmos9020041.

Tomasi, C., Kokhanovsky, A. A., Lupi, A., Ritter, C., Smirnov, A., O'Neill, N. T., Stone, R. S., Holben, B. N., Nyeki, S., Wehrli, C., Stohl, A., Mazzola, M., Lanconelli, C., Vitale, V., Stebel, K., Aaltonen, V., de Leeuw, G., Rodriguez, E., Herber, A. B., Radionov, V. F., Zielinski, T., Petelski, T., Sakerin, S. M., Kabanov, D. M., Xue, Y., Mei, L., Istomina, L., Wagener, R., McArthur, B., Sobolewski, P. S., Kivi, R., Courcoux, Y., Larouche, P., Broccardo, S., & Piketh, S. J. (2015). Aerosol remote sensing in polar regions. *Earth-Science Reviews, 140*, 108–157. https://doi.org/10.1016/j.earscirev.2014.11.001.

Tomasi, C., Vitale, V., Lupi, A., Di Carmine, C., Campanelli, M., Herber, A., Treffeisen, R., Stone, R. S., Andrews, E., Sharma, S., Radionov, V., von Hoyningen-Huene, W., Stebel, K., Hansen, G. H., Myhre, C. L.,Wehrli, C., Aaltonen, V., Lihavainen, H., Virkkula, A., Hillamo, R., Ström, J., Toledano, C., Cachorro, V. E., Ortiz, P., de Frutos, A. M., Blindheim, S., Frioud, M., Gausa, M., Zielinski, T., Petelski, T., & Yamanouchi, T. (2007). Aerosols in polar regions: a historical overview based on optical depth and in situ observations. *Journal of Geophysical Research, Atmospheres, 112*, D16. https://doi.org/10.1029/2007JD008432.

Thomason, L. W., Ernest, N., Luis, M. L., Rieger, L., Bourassa, A., Vernier, J.-P., Manney, G., Luo, B., Arfeuille, F., & Peter, T. (2018). A global space-based stratospheric aerosol climatology: 1979–2016. *Earth System Science Data, 10*, 469–492. https://doi.org/10.5194/essd-10-469-2018.

Torres, O., Bhartia, P. K., Taha, G., Jethva, H., Das, S., Colarco, P., Krotkov, N., Omar, A., and Ahn, C.: Stratospheric Injection of Massive Smoke Plume From Canadian Boreal Fires in 2017 as Seen by DSCOVR-EPIC, CALIOP, and OMPS-LP Observations, J. Geophys. Res.-Atmos., 125, e2020JD032579, https://doi.org/10.1029/2020JD032579, 2020.

Toth, T. D., Campbell, J. R., Reid, J. S., Tackett, J. L., Vaughan, M. A., Zhang, J., & Marquis, J. W. (2018). Minimum aerosol layer detection sensitivities and their subsequent impacts on aerosol optical thickness retrievals in CALIPSO level 2 data products. *Atmospheric Measurement Techniques, 11*(1), 499-514.

1838 Toth, T. D., Zhang, J., Campbell, J. R., Reid, J. S., & Vaughan, M. A. (2016). Temporal
1839 variability of aerosol optical thickness vertical distribution observed from
1840 CALIOP. *Journal of Geophysical Research: Atmospheres*, *121*(15), 9117-9139.
1841
1842 Valkonen, E., Cassano, J., & Cassano, E. (2021). Arctic cyclones and their interactions
1843 with the declining sea ice: A recent climatology. Journal of Geophysical Research:
1844 Atmospheres, 126, e2020JD034366. https://doi.org/10.1029/2020JD034366
1845
1846 van der Werf, G. R., J. T. Randerson, L. Giglio, G. J. Collatz, P. S. Kasibhatla, and A. F.
1847 Arellano Jr., 2006: Interannual variability in global biomass burning emissions from 1997
1848 to 2004. Atmos. Chem. Phys., 6, 3423–3441, doi:10.5194/acp-6-3423-2006.
1849
1850 Warneke, C., Froyd, K. D., Brioude, J., Bahreini, R., Brock, C. A., Cozic, J., et al.
1851 (2010). An important contribution to springtime Arctic aerosol from biomass burning in
1852 Russia. *Geophysical Research Letters*, *37*, L01801.
1853 https://doi.org/10.1029/2009GL041816
1854
1855 Waseda, T., Nose, T., Kodaira, T, Sasmal, K and Webb, A. (2021) Climatic trends of
1856 extreme wave events caused by Arctic cyclones in the western Arctic Ocean. Polar
1857 Science. Vol 27, 100625, doi:10.1016/j.polar.2020.100625
1858
1859 Wendisch, M., Macke, A., Ehrlich, A., Lupkes, C., Mech, M., Chechin, D., et al. (2019).
1860 The Arctic cloud puzzle: Using ACLOUD/PASCAL multiplatform observations to unravel
1861 the role of clouds and aerosol particles in Arctic amplification. *Bulletin of the American
1862 Meteorological Society*, *100*, 841–871. https://doi.org/10.1175/BAMS-D-18-0072.1
1863
1864 Wex, H., Huang, L., Zhang, W., Hung, H., Traversi, R., Becagli, S., Sheesley, R. J.,
1865 Moffett, C. E., Barrett, T. E., Bossi, R., Skov, H., Hünerbein, A., Lubitz, J., Löffler, M.,
1866 Linke, O., Hartmann, M., Herenz, P., and Stratmann, F.: Annual variability of ice-
1867 nucleating particle concentrations at different Arctic locations, Atmos. Chem. Phys., 19,
1868 5293–5311, https://doi.org/10.5194/acp-19-5293-2019, 2019.
1869
1870 Winker, D. M., Pelon, J. R., & McCormick, M. P. (2003, March). CALIPSO mission:
1871 spaceborne lidar for observation of aerosols and clouds. In *Lidar Remote Sensing for
1872 Industry and Environment Monitoring III* (Vol. 4893, pp. 1-11). International Society for
1873 Optics and Photonics.
1874
1875 Winker, D. M., Vaughan, M. A., Omar, A., Hu, Y., Powell, K. A., Liu, Z., Hunt, W. H., and
1876 Young, S. A. (2009). Overview of the CALIPSO Mission and CALIOP Data Processing
1877 Algorithms. J. of Atmos. Oceanic Tech. Vol 26., 2310-2323,
1878 https://doi.org/10.1175/2009JTECHA1281.1
1879
1880 Woods, C., & Caballero, R. (2016). The role of moist intrusions in Winter Arctic warming
1881 and sea ice decline. *Journal of Climate*, *29*, 4473–4485. https://doi.org/10.1175/JCLI-D-
1882 15-0773.1
1883

1884 Xian, P., Klotzbach, P. J., Dunion, J. P., Janiga, M. A., Reid, J. S., Colarco, P. R., and
1885 Kipling, Z.: Revisiting the relationship between Atlantic dust and tropical cyclone activity
1886 using aerosol optical depth reanalyses: 2003–2018, Atmos. Chem. Phys., 20, 15357–
1887 15378, https://doi.org/10.5194/acp-20-15357-2020, 2020.
1888
1889 Xian, P., Reid J. S., Hyer, E., Sampson, C.R., Rubin,J., Ades M., et. al., Current state of
1890 the global operational aerosol multi-model ensemble: an update from the International
1891 Cooperative for Aerosol Prediction (ICAP), 2019, Quarterly J. of the Royal Met. Soc.
1892 https://doi.org/10.1002/qj.3497
1893
1894 Xian, P., J. S. Reid, J. F. Turk, E. J. Hyer and D. L. Westphal: Impact of models versus
1895 satellite measured tropical precipitation on regional smoke optical thickness in an
1896 aerosol transport model, *Geophys. Res. Lett.*, 36, L16805, doi:10.1029/2009GL038823,
1897 2009.
1898
1899 Yang, Y., Wang, H., Smith, S. J., Easter, R. C., and Rasch, P. J.: Sulfate Aerosol in the
1900 Arctic: Source Attribution and Radiative Forcing, J. Geophys. Res.-Atmos., 123, 1899–
1901 1918, https://doi.org/10.1002/2017JD027298, 2018.
1902
1903 Zamora, L. M., Kahn, R. A., Cubison, M. J., Diskin, G. S., Jimenez, J. L., Kondo, Y.,
1904 McFarquhar, G. M., Nenes, A., Thornhill, K. L., Wisthaler, A., Zelenyuk, A., and Ziemba,
1905 L. D.: Aircraftmeasured indirect cloud effects from biomass burning smoke in the Arctic
1906 and subarctic, Atmos. Chem. Phys., 16, 715–738, https://doi.org/10.5194/acp-16-715-
1907 2016, 2016.
1908
1909 Zhang, J. L., and J. S. Reid, 2006: MODIS aerosol product analysis for data
1910 assimilation: Assessment of over-ocean level 2 aerosol optical thickness retrievals. *J.
1911 Geophys. Res.-Atmos.*, **111**.
1912
1913 Zhang, J. L., and J. S. Reid, D. L. Westphal, N. L. Baker, and E. J. Hyer, 2008: A
1914 system for operational aerosol optical depth data assimilation over global oceans. J.
1915 Geophys. Res., 113, D10208, doi:10.1029/2007JD009065.
1916
1917 Zhang, J. and Reid, J. S.: A decadal regional and global trend analysis of the aerosol
1918 optical depth using a data-assimilation grade over-water MODIS and Level 2 MISR
1919 aerosol products, Atmos. Chem. Phys., 10, 18879-18917, doi:10.5194/acpd-10-18879-
1920 2010, 2010.
1921
1922 Zhang J., Reid, J. S., Alfaro-Contreras, R., Xian P., Has China been exporting less
1923 particulate air pollution over the past decade?, *Geophysical Research Letters*,
1924 10.1002/2017GL072617, 2017.
1925
1926 Zhang, J., Spurr, R. J. D., Reid, J. S., Xian, P., Colarco, P. R., Campbell, J. R., Hyer, E.
1927 J., and Baker, N. L.: Development of an Ozone Monitoring Instrument (OMI) aerosol
1928 index (AI) data assimilation scheme for aerosol modeling over bright surfaces – a step

1929 toward direct radiance assimilation in the UV spectrum, Geosci. Model Dev., 14, 27–42,
1930 https://doi.org/10.5194/gmd-14-27-2021, 2021.
1931
1932 Zhao, C., & Garrett, T. J. (2015). Effects of Arctic haze on surface cloud radiative
1933 forcing. *Geophysical Research Letters*, *42*, 557–564.
1934 https://doi.org/10.1002/2014GL062015
1935
1936 Zhang, Z.; Wang, L.; Xue, N.; Du, Z. Spatiotemporal Analysis of Active Fires in the
1937 Arctic Region during 2001–2019 and a Fire Risk Assessment Model. *Fire* **2021**, *4*, 57.
1938 https://doi.org/10.3390/fire4030057

Arctic spring and summertime aerosol optical depth baseline from long-term observations and model reanalyses - Part 2: Statistics of extreme AOD events, and implications for the impact of regional biomass burning processes

Peng Xian[1], Jianglong Zhang[2], Norm T. O'Neill[3], Jeffrey S. Reid[1], Travis D. Toth[4], Blake Sorenson[2], Edward J. Hyer[1], James R. Campbell[1], and Keyvan Ranjbar[3, a]

[1]Naval Research Laboratory, Monterey, CA, USA.
[2]Department of Atmospheric Sciences, University of North Dakota, Grand Forks, ND
[3]Département de géomatique appliqué, Université de Sherbrooke, Sherbrooke, Québec, Canada
[4]NASA Langley Research Center, Hampton, Virginia, USA.
[a]now at: Flight Research Laboratory, National Research Council Canada, Ottawa, ON, Canada

Correspondence: Peng Xian (peng.xian@nrlmry.navy.mil)

Abstract

~~We~~In a companion paper (Part I of the study), we present an Arctic aerosol optical depth (AOD) climatology and trend analysis for 2003-2019 spring and summertime periods derived from a combination of aerosol reanalyses, remote sensing retrievals, and ground observations ~~in a companion paper (Part 1). In this paper~~. Continued from the previous discussion and as the second part of the study, we report the statistics and trends of Arctic AOD extreme events using the U.S. Navy Aerosol Analysis and Prediction System ReAnalysis version 1 (NAAPS-RA v1), the sun photometer data from the Aerosol Robotic Network (AERONET) sites, and the oceanic Maritime Aerosol Network (MAN) measurements. ~~The AERONET and MAN median for 6 hr total AOD at 550 nm in the Arctic is ~0.06-0.07 while the 95th percentile value is ~0.23, with a dominant contribution from fine-mode aerosols. Extreme AOD events~~ Here, extreme AOD events are defined as events with AOD exceeding the 95th percentile (denoted "AOD_{95}") ~~6 hr or daily~~of AOD ~~data and histogram~~ distributions ~~representing specific~~ for given locations ~~or across a given region (the region north of 70° N for example). The occurrence and magnitude of extreme AOD events in the Arctic~~ using 6 hourly or daily AOD data. While AERONET and MAN data estimate that the Arctic median 550 nm AOD value to be 0.07, the 95th percentile value is 0.23. Such extreme events are dominant by fine-mode aerosol particles, largely attributable to biomass burning (BB) smoke events for the North American Arctic, the Asian Arctic, and most areas of the Arctic Ocean. ~~Regionally, the occurrence of~~However, extreme AOD events for the lower European Arctic is more attributable to anthropogenic ~~and /~~biogenic ~~fine aerosols in the lower European Arctic~~particles. The extreme-event occurrence dominance of sea salt ~~aerosols~~ is largely limited to the North Atlantic and Norwegian Seas. The extreme AOD amplitudes of ~~ABF~~anthropogenic and biogenic fine mode and sea-salt AOD are, however, significantly lower than those regions where extreme smoke AOD is dominant. Even for sites distant from BB source regions, BB smoke is the principle driver of AOD variation above the AOD_{95} threshold. ~~Extreme total AOD Arctic events also show large seasonal and interannual variabilities, with the interannual AOD variability largely modulated by BB smoke.~~

~~There is an overall increase in the maximum~~Maximum AOD values in the high Arctic in 2010-2019 have increased compared to 2003-2009, indicating stronger extreme BB smoke influence in more recent years. The occurrence of extreme smoke events tended to be more equally distributed over all months (April-August) during the 2003-2009 period while being more concentrated in the late season (July-August) during the 2010-2019 period. ~~The extreme smoke and total AOD trends resembled the extreme-smoke occurrence trends: more seasonally balanced during the 2003-2009 period and summertime dominance during the 2010-2019 period.~~ The temporal shift of the occurrence of AOD extreme events is ~~associated with the shift in extreme smoke AOD~~

55 ~~events which is, in turn,~~ likely due to improved control of early-season agriculture
56 burning, ~~increased~~ climate change related increases in summertime lightning
57 frequencies ~~with climate change in the northern hemisphere high latitudes~~, and a
58 reduction in anthropogenic pollution ~~aerosols~~ over the 2010-2019 period. ~~The shift in~~
59 ~~extreme smoke events is consistent with a general multi-year decreasing springtime~~
60 ~~trend and an increasing summertime trend of BB emissions north of 50° N (Part 1).~~

62   1.   Introduction

63   Warming faster than the rest of the world, the Arctic is a focal point for global warming
64   (Serreze and Francis 2006; Serreze and Barry 2011). Interactions between the
65   atmosphere, ocean, land surface, and sea ice, compounded by numerous human
66   factors make the Arctic climate system challenging to predict, with large diversity
67   between current numerical model outcomes (IPCC 2013). Arctic aerosol2021). Aerosol
68   particles from anthropogenic and natural sources affect regional energy balance
69   through direct radiative processes and indirect cloud processes (Quinn et al., 2008;
70   Engvall et al., 2009; Flanner, 2013; Sand et al., 2013; Markowicz et al., 2021; Yang et
71   al., 2018). When deposited on the surface of snow and ice, light-absorbing aerosol
72   particles, including dust and black/brown carbon from biomass burning and
73   anthropogenic emissions, can trigger albedo feedbacks and accelerate melting (Hansen
74   & Nazarenko, 2004; Jacobson, 2004; Flanner et al., 2007; Skiles et al., 2018; Dang et
75   al., 2017; Kang et al., 2020).

76   Arctic aerosol concentrations are in general relatively weaklow, with spring and
77   summertime median/mean 550 nm aerosol optical depths (AOD) of 0.06 - 0.07 (e.g.,
78   Tomasi et al., 2007; Saha et al., 2010; AboEl-Fetouh et al., 2020) as compared to a
79   global mean of roughly 0.20 over land and 0.12 over water (e.g., Levy et al., 2010;
80   XianLynch et al., 2016; Shutgers et al., 2020; Sogacheva et al., 2020). Extreme AOD
81   events do occur within the Arctic, mostly associated with large-scale transport from
82   lower latitudes. Biomass burning (BB) smoke from boreal wildfires, for example, can
83   episodically result in record-high Arctic AOD (Myhre et al. 2007; Stohl et al., 2007;
84   Markowicz et al., 2016; Ranjbar et al., 2019). Some strong smoke events were recorded
85   during intensive field campaigns, including the ARCTAS/ARCPAC campaign in the
86   summer of 2008 (Matsui et al., 2011; Saha et al, 2010; McNaughton et al., 2011) and
87   the NETCARE research vessel (Canadian Arctic) campaign in the spring of 2015
88   (Abbatt et al., 2019). More extreme BB smoke cases in the Arctic can be found in Sec.
89   3.3.

90   Extreme AOD events cause large perturbations in regional energy balance (e.g., Myhre
91   et al., 2007; Stone et al., 2008; Lisok et al., 2018). For example, a BB smoke transport
92   event from North America to the High Arctic region of Svalbard in early July 2015 led to
93   500 nm AOD exceeding 1.2 at Spitsbergen (Markowicz et al., 2016). The two-day mean
94   aerosol direct radiative forcing was estimated to cause overall cooling (-79 W/m^2 at the
95   surface and -47 W/m^2 at the top of the atmosphere TOA). However, a corresponding
96   atmospheric heating rate profile was solved of up to 1.8 K/day within the BB plume
97   (Lisok et al., 2018). Over bright snow and ice surfaces, or above clouds, top of the
98   atmosphere (TOA) BB smoke forcing can turn from negative to positive (i.e., warming)
99   by reducing columnar albedo (Yoon et al., 2019; Markowicz et al., 2021).

100 Although the microphysical impacts of aerosol particles on Arctic clouds and
101 precipitation processes are generally more difficult to measure and quantify, Arctic
102 clouds are generally believed more sensitive to changes in the relatively low
103 concentration of aerosols compared with the lower latitudes (Prenni et al., 2007;
104 Mauritsen et al. 2011; Birch et al., 2012; Coopman et al., 2018; Wex et al., 2019).
105 Extreme aerosol events correspond with an influx of relatively large concentrations of
106 potential cloud condensation nuclei (CCN) and/or ice ~~nuclei (IN~~nucleating particles
107 (INP), in what is otherwise a comparatively pristine background environment (Mauritsen
108 et al. 2011; Leck et al., 2015). Such extreme events will accordingly have observable
109 impacts on cloud albedo, lifetime, phase, and probability of precipitation (e.g., Lance et
110 al., 2011; Zhao and Garrett 2015; Zamora et al, 2016; ~~Zamora et al., 2016;~~ Bossioli et
111 al., 2021) and further influence the regional energy budget. Dry deposition (and blowing
112 snow processes), as well as wet deposition of BB smoke particles, can also trigger
113 sustained surface radiative forcing by inducing surface snow discoloration and attendant
114 surface albedo reduction (Warren and Wiscombe, 1980; Stohl et al., 2007; Hadley and
115 Kirchstetter, 2012).

116 Extreme aerosol events, especially BB smoke events, often modulate the interannual
117 variability of Arctic AOD (Part 1 of this study; Xian et al., 2022), as well as to the total
118 annual aerosol budget in the Arctic. The modeling study by DeRepentigny et al. (2021)
119 shows, in comparison with BB emissions characterized by a fixed annual cycle, that the
120 inclusion of interannually varying BB emissions leads to larger Arctic climate variability
121 and enhanced sea-ice loss. Their finding illustrates the unique sensitivity of climate-
122 relevant processes to regional aerosol interannual variability, and further suggests that
123 extreme aerosol events play an important Arctic climate role. It is accordingly important
124 to understand how extreme aerosol-event statistics change with the changing Arctic
125 climate to better inform climate simulations and our baseline understanding of how the
126 region is poised to evolve.

127 This is the second of two papers examining spring and summertime Arctic AOD
128 climatologies and their trends. In Part 1 (Xian et al., 2022), we report a baseline Arctic
129 AOD climatology from AERONET, MAN, and satellite AOD data for those two seasons
130 and the skill of three reanalysis AOD products in simulating those climatologies. The
131 reanalyses and space-borne retrievals show consistent climatological spatial patterns
132 and trends. Overall, AOD exhibits a multi-year negative trend for springtime and a
133 positive trend for summertime during 2003-2019, due to an overall decrease in
134 sulfate/anthropogenic pollution and a significant summertime increase in BB smoke.
135 This second paper focuses on ~~reporting~~the statistics and trends of extreme Arctic- AOD
136 events. ~~We define such events as those corresponding with AOD exceeding the 95th~~
137 ~~percentile mark in 6 hr or daily AOD~~The data ~~relative to climatological means at a~~
138 ~~specific location or across a given region (the region north of 70°N for example). The~~

139 ~~data~~and methods we employ are described in Sec. 2, while results are provided in Sec.
140 3. Conclusions are presented in Sec. 4.

2. Data

142 ~~We employ 6 hr AERONET AODs as well as speciated daily~~ and ~~6 hr NAAPS-RA AOD~~
143 ~~to depict the frequency and magnitude of the large fine-mode (FM) AOD events. The~~
144 ~~companion paper made use of three independent aerosol reanalysis products. For this~~
145 ~~study, the NAAPS-RA reanalysis was chosen given its slightly better (AERONET-~~
146 ~~referenced; Part 1) performance in terms of FM and total AOD bias, RMSE, and r²~~
147 ~~scores, as well as its capability of separating BB smoke from other aerosol species. To~~
148 ~~simplify some of the discussion below, we frequently employed the symbol "AODₙ" to~~
149 ~~represent the AOD associated with the n% percentile of its cumulative (histogram)~~
150 ~~distribution.~~ One important application of this AODₙ formulation was to employ a
151 ~~particular value (AOD₉₅) as a threshold for the definition of extreme events (see Section~~
152 ~~3.1 below).~~ Methods

2.1 AERONET

154 The AErosol RObotic NETwork (AERONET) is a federated ground-based sun
155 photometer network with over 600 active sites across the globe. AERONET's Cimel
156 photometers measure sun and sky radiance at several wavelengths, ranging from the
157 near-ultraviolet to the near-infrared. While the exact set of bands depend on the model,
158 all Cimel configurations include 440, 670, 870 and 1020 nm bands. All the sites used
159 here also included 380 and 500 nm bands. The network has been providing high-
160 accuracy daytime measurements of aerosol optical properties since the 1990s (Holben
161 et al., 1998; Holben et al., 2001). Cloud-screened and quality-assured Version 3 Level 2
162 AERONET data (Giles et al., 2019~~),~~) are used in this study.

163 Fine mode (FM) and Coarse mode (CM) AOD at 550 nm are derived based on the
164 Spectral Deconvolution Method (SDA) of O'Neill et al. (2003) and averaged over 6 hr
165 time bins. The same ten AERONET sites employed in Part 1, were selected (Fig. 1) for
166 this study. Those sites had been chosen based on their regional representativeness as
167 well as the availability of data records between Jan 2003 and Dec 2019 ~~(our~~
168 ~~primary~~period of study ~~period).~~.

169 Optically thin clouds, mostly cirrus, occasionally contaminate CM aerosol retrievals in
170 Level 2, Version 3 AERONET data (~~Chew et al., 2012;~~ Ranjbar et al., 2022). Data were
171 manually inspected, and retrievals screened, using ~~Terra and Aqua~~MODIS imagery at
172 visible wavelengths from ~~NASA Worldview~~ NASA Worldview
173 (https://worldview.earthdata.nasa.gov/ last accessed 15 May 2022) and by comparing 6-
174 hrly NAAPS-RA with AERONET AODs. This step is likely an incomplete one, given the

175 likely lesser sensitivity of MODIS imagers to thin clouds (Marquis et al., 2017). As such,
176 CM AODs that deviate by more than the 3-sigma level from the background
177 climatological mean were also removed (as per AboEl-Fetouh et al., 2020).

178 2.2 AERONET Marine Aerosol Network AOD Datasets

179 The Marine Aerosol Network (MAN) is part of the broader AERONET global network: in
180 this case however, it is limited to AODs collected over open water. Hand-held
181 Microtops sun photometers are deployed during research cruises of opportunity
182 (Smirnov et al., 2009, 2011). Data processing is similar to that of AERONET with
183 product nomenclature similar to AERONET. Level 2 data acquired above 70°N in the
184 2003-2019 period are used in this study. FM and CM AOD at 550 nm are derived using
185 the SDA and averaged over 6 hr time bins.

186 2.3 NAAPS AOD reanalysis v1

187 The Navy Aerosol Analysis and Prediction System (NAAPS) AOD reanalysis (NAAPS-
188 RA) v1 was developed at the U.S. Naval Research Laboratory. It provides 550 nm
189 speciated AOD and concentrations at a global scale with 1°x1° degree latitude/longitude
190 and 6 hr resolution for the years 2003-2019 (Lynch et al., 2016). This reanalysisNAAPS-
191 RA is driven by the Navy Operational Global Analysis and Prediction System
192 (NOGAPS; Hogan and Rosmond, 1991), with satellite precipitation applied within the
193 tropics to mitigate model precipitation errors (Xian et al., 2009). NAAPS-RA features
194 assimilation of quality-controlled and quality-assured AOD retrievals from MODIS and
195 MISR (Zhang et al., 2006; Hyer et al., 2011; Shi et al., 2011). A first-order approximation
196 of secondary organic aerosol (SOA) processes is adopted. Production of SOA from its
197 precursors is assumed to be instantaneous and is included with the original
198 anthropogenic species to form a combined anthropogenic and biogenic fine (ABF)
199 species (. In other words, ABF is a mixture of sulfate, BC, organic aerosols and
200 secondary organic aerosols from non-BB sources).. Monthly anthropogenic emissions
201 come from a 2000-2010 average of the ECMWF MACC inventory (e.g., Granier et al.,
202 2011). BB smoke is derived from Fire Locating and Modeling of Burning Emissions
203 inventory (FLAMBE, Reid et al., 2009). This version of FLAMBE uses MODIS, near-
204 real-time satellite-based thermal anomaly data to initialize the smoke source where
205 corrections that minimize the impact of inter-orbit variations are applied to the MODIS
206 data (Lynch et al., 2016). FLAMBE processing is applied consistently through the
207 reanalysis time period while a smoke-particle emission climatology and its spring and
208 summertime trends (both north of 50°N and 60°N) are provided in Fig. 12 of Part 1. Dust
209 is emitted dynamically and is a function of modeled friction velocity to the fourth power,
210 surface wetness, and surface erodibility. In this model run, erodibility is adopted from

211 Ginoux, et al., (2001) with regional tuning)-,. Sea-salt modeling is the same as Witek et
212 al. (2007) and sea-salt emission is driven dynamically by sea surface wind.

213 Verification of monthly-binned NAAPS-RA modal and total AODs at 550 nm using
214 monthly-binned AERONET data from 10 Arctic sites (Table 1 and Fig. 2 of Part 1)
215 shows (coupled with the bias and rmse results of Figure 2 in Part 1) that NAAPS-RA is
216 able to capture the AOD interannual variability. The spatial distributions and magnitudes
217 of climatological and seasonal AOD averages and their trends for 2003-2019 are also
218 consistent with those derived from MODIS, MISR, and CALIOP (Part 1).

219 2.4 Data analysis methods

220 Our study period is Jan 2003 to Dec 2019, the same principal study period as used in
221 Part 1. We define extreme events as those corresponding to AOD exceeding the 95th
222 percentile mark in 6 hr or daily AOD data at a specific location or across a given region
223 (the region north of 70°N for example). We employ 6 hr AERONET AODs as well as
224 speciated daily and 6 hr NAAPS-RA AOD to depict the frequency and magnitude of the
225 large FM AOD events. Pair-wised data are used for verification. "Pairwise" refers to
226 those NAAPS-RA AODs that correspond to a resampled AERONET or MAN AOD
227 whose $\pm$ 3hr bin contains at least one AERONET/MAN retrieval. Three independent
228 aerosol reanalysis products were used in the Part 1 of the study. For this study, the
229 NAAPS-RA reanalysis was chosen given its slightly better performance in terms of FM
230 and total AOD bias, RMSE, and r^2 scores (Part 1), as well as its capability of separating
231 BB smoke from other aerosol species. To simplify some of the discussion below, we
232 frequently employed the symbol "AOD_n" to represent the AOD associated with the n%
233 percentile of its cumulative (histogram) distribution. One important application of this
234 AOD_n formulation is to employ a particular value (AOD_{95}) as a threshold for the
235 definition of extreme events (see Section 3.1 below). AOD_{75}, AOD_{90}, AOD_{99}, $AOD_{99.5}$
236 and maximum AOD are also calculated to show AOD gradients for high AODs. A local
237 extreme total AOD event for the NAAPS-RA means AOD > AOD_{95} for the model grid
238 cell of 1° x 1° (Latitude/Longitude). Again, we define the Arctic and the high-Arctic as
239 regions north of 60°N and 70°N respectively. To reference source influences from
240 lower-latitude, the area of 50°N-90°N is included for context.

241 3. Results

242 Seasonal AOD averages and trends derived from remote sensing measurements for the
243 2003-2019 sampling period are provided in Part 1. The interannual Arctic AOD
244 variability is, as discussed in Part I, considerable and driven mostly by FM aerosol
245 events (notably BB transport events). Regional statistics and trends of extreme AOD
246 events are presented in this section: 6-hr AERONET AOD as well as speciated daily

247   and 6-hr NAAPS-RA AOD are employed to characterize the frequency and magnitude
248   of strong FM AOD events.

249   3.1 Verification of NAAPS-RA AOD over the Arctic

250   The reanalysis performance for 6-hr time bins was evaluated in order to study extreme
251   events. Our choice of AOD_{95} as an extreme event threshold was influenced by the fact
252   that it was an upper-limit cumulative probability indicator that was robust. We reasoned,
253   at the same time, that it should be comparable with the analog parameter derived from
254   NAAPS-RA. Figure 1 displays NAAPS-RA AOD_{95} overplotted with those from the ten
255   selected AERONET sites for spring and summertime 2003-2019. NAAPS-RA appears
256   to successfully capture the AOD_{95} amplitude and spatial pattern, as well as those of FM
257   AOD_{95} and CM AOD_{95}. It also shows that FM is the main contributor to AOD_{95} in the
258   Arctic.
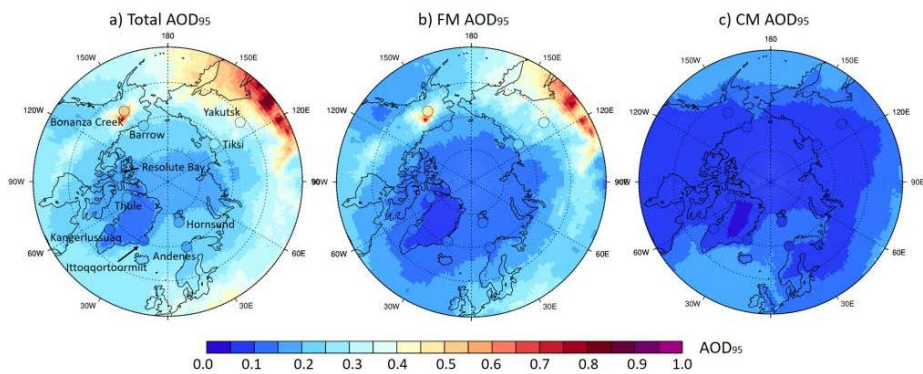
259

260   **Figure 1.** Total, FM and CM AOD at the 95th percentile (AOD_{95}) for the March-August
261   time frame from the NAAPS-RA and the ten AERONET sites (based on 6hrly data
262   between 2003-2019).

263   Table 1 provides detailedDetailed geographical coordinates of the ten AERONET sites
264   employed in our study are included in Table 1, as well as the simulation performance
265   indicators of NAAPS-RA 550 nm total, FM and CM AOD. These AERONET parameters
266   are an analogue to Part 1parameters used in the first part of the study and its Table 1
267   statistics, except that the averaging period extends across both the spring and summer
268   seasons (meaning in practice that, as the averaging period is mostly confined to the
269   April-August time frame). Scatter plots of NAAPS-RA vs AERONET AODs at all sites
270   north of 60°N are shown in Fig. 2. NAAPS-RA performance indicators relative to MAN
271   data are shown in Fig. S1 and S2.

NAAPS-RA performance for this large averaging period is reasonable for FM and total AOD, though it is less skillful at predicting CM AOD. The FM AOD exhibits an average (Table 1) bias over all stations of -0.01, a root mean square error (RMSE) of 0.08 and a coefficient of determination (r^2) of 0.66. RMSE values for total and FM AOD are generally large for sites vulnerable to strong smoke influence ~~(~~, e.g. Bonanza Creek, Barrow, Tiksi and Yakutsk~~).~~. Total AOD r^2 values are mostly between 0.5-0.7, except for Hornsund, Kangerlussuaq and Ittoqqortoormiit. FM AOD r^2 values exceed those of the total AOD for all sites except Kangerlussuaq. The ~~monthly~~6-hr-binned Table 1 total AOD bias ~~(where the Table 1 averaging over the spring and summer is the simple average of the spring and summer averages)~~ is similar to the monthly-binned NAAPS-RA bias results of Table 2, Part 1~~).~~. This is due to the numerous ~~(~~6-hr~~)~~ samples included in the ~~(signed)~~ AERONET bias averaging. In contrast, the Table 1 RMSE values are roughly doubled, and the r^2 values drop by about 30% relative to those of Tables 3 and 4 of Part 1. This suggests Table 1 model shortcomings in capturing finer temporal-scale ~~(higher frequency)~~ AERONET-AOD variations. This is also consistent with model performance for regions other than the Arctic, and is generally a common result for numerical aerosol models (Lynch et al., 2016; Yumimoto et al., 2017)

The lesser CM vs FM skill of the NAAPS-RA might be a reflection of AERONET limitations as one approaches typical instrumental errors ~ 0.01 in total AOD or they could be a reflection of simulation and / or reanalysis limitations as one approaches very small values of CM AOD. The lack of model representation of CM smoke and possible soil particles associated with severe burning events may also contribute. At the same time, it must be recognized that residual cloud contamination in AERONET ~~(and MAN)~~ data cannot be ruled out as a "false" indicator of poor simulation skill. Cloud screening issues aside, a lesser CM vs FM correlation skill is a common feature of both the Table 1 and Table 4 (Part 1) reanalyses. However, modeled monthly CM AOD correlation is slightly more skillful than the averages derived from 6 hr data (Table 4 in Part 1 vs Table 1) inasmuch as the seasonal CM signal associated with dust and sea salt aerosols are apparently better resolved in the former case ~~(~~. The better model skill in seasonal CM simulation is likely due to the relative insensitivity of ~~the~~ the model to the higher frequency components of the reference data in the latter case~~).~~. It is also noted that the NAAPS-RA is generally less skillful in the Arctic region relative to global reanalyses (c.f Fig. 7 in Lynch et al., 2016). This is understandable given that ~~(compared with lower latitudes)~~ there is little satellite-based ~~Arctic~~ AOD data available to constrain the model through assimilation in the Arctic compared to lower latitudes. We note however that Zhang et al. (2021) attempted to address this problem with assimilation of Ozone Monitoring Instrument (OMI) Aerosol Index. To date, no remedy for aerosol data assimilation has yet been implemented in a larger RA-quality study.

Table 1. Geographical coordinates along with the total, FM and CM AOD statistics (2003-2019 depending on availability) for AERONET and 6-hrly NAAPS-RA 550 nm performance indicators versus AERONET ~~(mean bias, root mean square error (rmse) and coefficient of determination (r²))~~. The last row shows the same statistics for MAN AODs acquired north of 70°N as the bias reference. These numbers are given as information: as indicated above the table statistics in Part 1 were explicitly computed using monthly binned data (which were, in turn, derived from the 6 hr data).

sites	latitude	longitude	elevation (m)	region	AEORNET mean total | FM | CM	total | FM | CM AOD Bias	rmse	r²	n
Hornsund	77.0°N	15.6°E	12	Svalbard	0.09|0.06|0.03	-0.01|-0.02|0.01	0.04|0.04|0.03	0.55|0.62|0.06	1,817
Thule	76.5°N	68.8°W	225	Greenland	0.07|0.06|0.02	0.00|-0.01|0.01	0.04|0.03|0.03	0.52|0.60|0.07	2,518
Kangerlussuaq	67.0°N	50.6°W	320	Greenland	0.07|0.05|0.02	0.02|0.00|0.01	0.05|0.04|0.03	0.32|0.30|0.03	2,725
Ittoqqortoormiit	70.5°N	21.0°W	68	Greenland	0.06|0.05|0.02	0.01|-0.00|0.01	0.04|0.03|0.03	0.41|0.49|0.04	1,825
Andenes	69.3°N	16.0°E	379	Norway	0.08|0.05|0.02	0.01|-0.01|0.01	0.04|0.03|0.03	0.54|0.56|0.16	1,829
Resolute_Bay	74.7°N	94.9°W	35	Nunavut	0.08|0.05|0.02	0.01|-0.01|0.01	0.06|0.05|0.03	0.55|0.62|0.02	1,698
Barrow	71.3°N	156.7°W	8	Alaska	0.10|0.08|0.02	-0.00|-0.02|0.01	0.09|0.08|0.04	0.53|0.61|0.07	1,760
Bonanza_Creek	64.7°N	148.3°W	353	Alaska	0.16|0.12|0.03	-0.02|-0.02|-0.00	0.16|0.15|0.04	0.69|0.70|0.07	2,670
Tiksi	71.6°N	129.0°E	17	Siberia	0.12|0.10|0.02	-0.01|-0.02|0.01	0.09|0.08|0.03	0.69|0.73|0.01	488
Yakutsk	61.7°N	129.4°E	119	Siberia	0.16|0.12|0.03	-0.01|-0.02|0.01	0.13|0.12|0.04	0.61|0.62|0.15	4,095
MAN	>70°N	-	-	Arctic Ocean	0.07|0.05|0.02	-0.00|-0.01|0.00	0.04|0.03|0.02	0.51|0.32|0.07	520
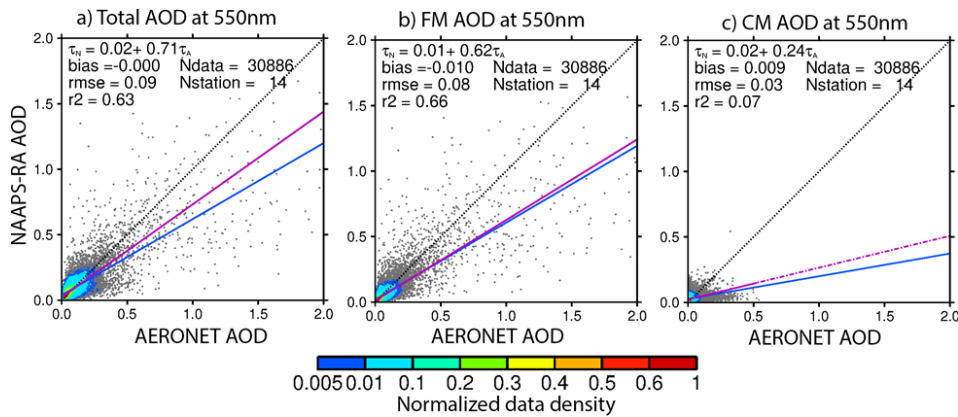
~~Figure 2.~~ ~~Pairwise comparison of the NAAPS-RA 6-hr AOD and AERONET AOD with respect to total (left), fine (middle) and coarse (right) modes at 550 nm for all sites north of 60° N for 2003–2019. The normalized data density is shown in color. The solid magenta line represents a Theil–Sen linear regression: the corresponding linear equation and bias statistics are shown in the top left hand corner of each graph (where τ_N and τ_A are the NAAPS-RA and AERONET AODs respectively. The solid blue line is a least-squares linear regression (corresponding equation is not shown). Also shown are the bias, root mean square error (rmse), coefficient of determination (r²), total number of stations (Nstation) and total number of 6-hr AERONET data (Ndata). AODs greater than 2.0 are not shown but were incorporated in the statistics calculations.~~

sites	latitude	longitude	elevation (m)	region	AEORNET mean total | FM | CM	total | FM | CM AOD Bias	rmse	r²	n
Hornsund	77.0°N	15.6°E	12	Svalbard	0.09|0.06|0.03	-0.01|-0.02|0.01	0.04|0.04|0.03	0.55|0.62|0.06	1,975
Thule	76.5°N	68.8°W	225	Greenland	0.07|0.06|0.02	0.00|-0.01|0.01	0.04|0.03|0.03	0.52|0.60|0.07	2,934
Kangerlussuaq	67.0°N	50.6°W	320	Greenland	0.07|0.05|0.02	0.02|0.00|0.01	0.05|0.04|0.03	0.32|0.30|0.03	3,066
Ittoqqortoormiit	70.5°N	21.0°W	68	Greenland	0.06|0.05|0.02	0.01|-0.00|0.01	0.04|0.03|0.03	0.41|0.49|0.04	2,041
Andenes	69.3°N	16.0°E	379	Norway	0.08|0.05|0.02	0.01|-0.01|0.01	0.04|0.03|0.03	0.54|0.56|0.16	2,222
Resolute_Bay	74.7°N	94.9°W	35	Nunavut	0.08|0.05|0.02	0.01|-0.01|0.01	0.06|0.05|0.03	0.55|0.62|0.02	1,876
Barrow	71.3°N	156.7°W	8	Alaska	0.10|0.08|0.02	-0.00|-0.02|0.01	0.09|0.08|0.04	0.53|0.61|0.07	1,920
Bonanza_Creek	64.7°N	148.3°W	353	Alaska	0.16|0.12|0.03	-0.02|-0.02|-0.00	0.16|0.15|0.04	0.69|0.70|0.07	3,177
Tiksi	71.6°N	129.0°E	17	Siberia	0.12|0.10|0.02	-0.01|-0.02|0.01	0.09|0.08|0.03	0.69|0.73|0.01	631
Yakutsk	61.7°N	129.4°E	119	Siberia	0.16|0.12|0.03	-0.01|-0.02|0.01	0.13|0.12|0.04	0.61|0.62|0.15	4,797
MAN	>70°N	-	-	Arctic Ocean	0.07|0.05|0.02	-0.00|-0.01|0.00	0.04|0.03|0.02	0.51|0.32|0.07	520
All AERONET sites	total|FM|CM median: 0.07|0.05|0.01					0.10|0.08|0.02	-0.00|-0.01|0.01	0.09|0.08|0.03	0.63|0.66|0.07	24,639

329

330   3.2 General statistics of extreme events

331   Fig. Shown in Figure 1 showsand Table 2 are NAAPS-RA and AERONET AOD_{95} values
332   for the March-August time frame and the 2003-2019 period (see also Table 2).. The
333   values of AOD_{95} are high (0.4~0.55) over Siberia and Alaska (and over the Yakutsk and
334   Bonanza Creek AERONET stations) due to strong BB smoke influence. North of 70°N,
335   the values are mostly between 0.15 to 0.25, with the exception of Greenland where they
336   are largely below 0.15 (weak values that are attributable to the high terrain). It is also
337   shown that $(FM\ AOD)_{95}$ has similar spatial distribution and magnitude as $AOD_{95,}$
338   suggesting the dominant contribution of FM to $AOD_{95.}$ Contribution of CM is relatively
339   larger over the North Atlantic and European Arctic, though $(CM\ AOD)_{95}$ and $(FM\ AOD)_{95}$
340   are comparable in these regions.

341   Fig. 3 shows the The site-by-site, total, and FM AOD ranges are also shown in Fig. 2
342   from the 6-hr AERONET data for all 550 nm retrievals (in black) acquired between
343   2003-2019. The 6-hr pairwise NAAPS-RA AOD ranges (in red) facilitate model skill
344   evaluation (see the caption of Fig. 3 for "pairwise" details). In general, the NAAPS-RA
345   largely captures the AERONET FM and total AOD range. This includes, for example,
346   the AERONET AOD_5 to AOD_{95} values ((0.02 to > ≥ 0.10 for most sites), and the
347   larger 0.02 to 0.4-0.6 range of sites with known strong BB influence (notably Bonanza
348   Creek, Tiksi, and Yakutsk). Mean and median AODs are also comparable to AERONET
349   values. Maximum AERONET FM AODs vary between 0.5 (Ittoqqortoormiit) to < 2.0
350   for most sites and around 3.0 for sites with strong BB smoke influence (see also Table
351   2). Maximum NAAPS-RA AOD values are often biased low, which is a common
352   challenge for global aerosol models (e.g. Sessions et al., 2015; Xian et al., 2019).

353

354
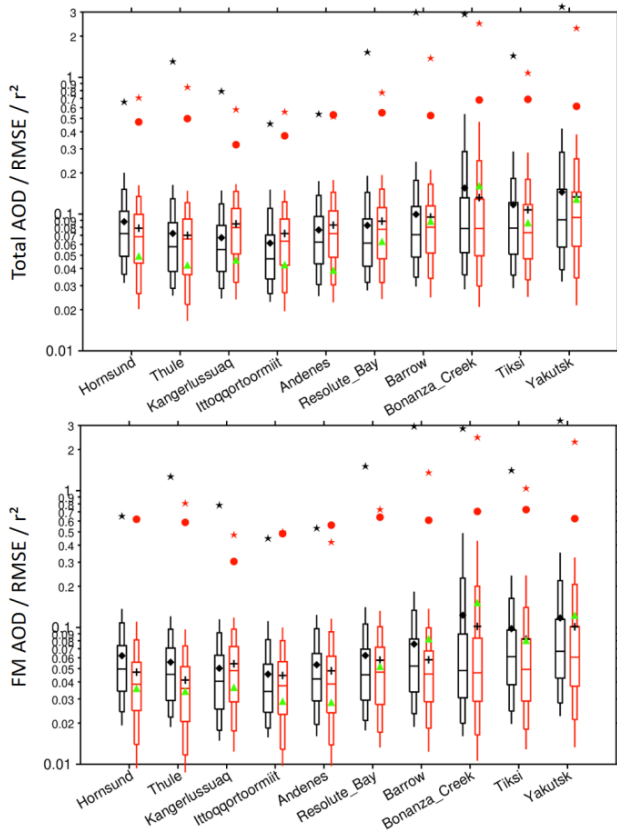
Figure 2. Comparison of the 6-hrly (550 nm) total (top) and FM AOD (bottom) of the
NAAPS-RA (red) at 95, 90, 75, 50, 25, 10, and 5% percentiles (respective, sequential
features of the doubled spear-like symbols from the top tip to the bottom tip) with
pairwise AERONET V3L2 data (black) for the ten AERONET sites of Table 1 and
~~Figure~~Fig. 1 for the 2003-2019 time period ~~("pairwise" refers to those NAAPS-RA AODs~~
~~that correspond to a resampled AERONET AOD whose ± 3hr bin contains at least one~~
~~AERONET retrieval).~~ Also shown are the site means of the NAAPS-RA and AERONET
AODs ("+" and "♦" symbols respectively) and the NAAPS-RA RMSE ("▲"), the
coefficient of determination (r^2) between the NAAPS-RA and AERONET ("●") and the
maximum AERONET and NAAPS-RA AODs ("★" and "★" respectively). Note that
values greater than 3.0 are not shown.

366
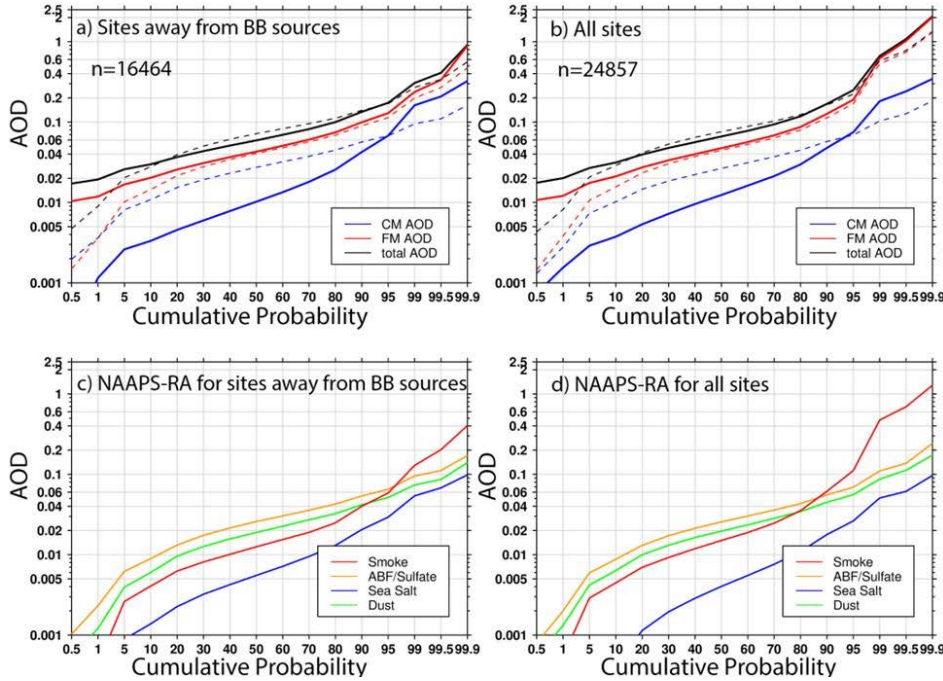
Figure 43. Upper panes (a, b): cumulative probability distributions of 2003-2019, 6-hr total, FM and CM AOD at 550 nm for AERONET V3 L2 data (solid curves) and pair-wise NAAPS-RA (dashed curves). Lower panes (c,d): cumulative probability distributions for the corresponding speciated AOD from the NAAPS-RA. Left hand panes (a,c): AOD for sites that are distant from BB source regions, including Barrow, Resolute Bay, Kangerlussuaq, Thule, Andenes, Hornsund and Ittoqqootoormiit (see the discussion of Table 2 for emission considerations with respect to the particular site of Barrow). Right-hand panels (b,d) are all sites ~~north of 60°N.~~ "n" represents the total number of 6-hrly data points over the 2003-2019 period~~.~~, including a small amount of AERONET data from September besides the March-August time frame.

~~Figure 4 shows the~~ The cumulative probability ~~distribution~~distributions of 6-hr total, FM and CM AODs are shown in Fig. 3 for AERONET and pair-wise NAAPS-RA total and modal AODs ~~(Figures 3a and b)~~ and speciated AODs ~~(Figures 3c and d).~~. The median ~~(50%)~~ AOD for all AERONET sites in the Arctic (all sites north of 60°-N) for 2003-2019 is ~0.~~06~~07, while the AOD_{95} extreme-event threshold is ~0.23 with a dominant FM contribution. The CM AOD median for all measurements is ~0.01, with a $(CM\ AOD)_{95}$ threshold of only ~0.07. NAAPS-RA total AOD bias is, due to a relatively large positive

 bias in CM AOD of —0.01 below the 95% threshold, slightly positive (<0.01) for all sites
north of 60°-N, and for the 20%-80% cumulative probability range (a positive bias that is
generally evident in Table 1).

It is common for models to bias low for extreme events (e.g. Sessions et al. 2015; Xian et al., 2019). The negative bias found at the largest CM AOD values could conceivably
be associated with an underestimation of the CM AOD generated by sea-salt aerosols
in the presence of strong winds or CM smoke and soil particles associated with severe
burnings. We should, however, reemphasize this caveat: despite the quality-control
measures taken to filter out cloud-contaminated AERONET data, the impact of CM
residual clouds may still influence estimates of CM AOD.

It worth noting that BB smoke plays a dominant role compared to other aerosol species
above our AOD$_{95}$ extreme-event threshold (see Fig. 3c, d in particular and note that Fig.
3a, b shows the expected dominance of FM AOD). Even for sites distant from BB
source regions, including Resolute Bay, Kangerlussuaq, Thule, Andenes, Hornsund,
Ittoqqortoormiit, BB smoke is the principal driver of AOD variations above the AOD$_{95}$
threshold. To some extent, Barrow can be categorized as being a site that is distant
from BB emissions. However, it is also relatively close to the region of Alaska fires,
depending on dominant upstream winds and trajectories (see Eck et al., 2009 for
details).

Table 2. AERONET V2L3 FM, CM, and total AOD at 550nm at different percentiles for the listed
Arctic sites along with maximum AOD values in the third last column. "N" represents the total
number of 6-hr AODs for 2003-2019. The percentage of extreme FM events relative to the number
of extreme total AOD events (using our AOD$_{95}$ extreme-event threshold) is also shown in the last
column. The 2nd to last row shows MAN statistics for data acquired north of 70° N70°N.

	Total | FM | CM AOD at 550nm								FM
	Median	75%	90%	95%	99%	99.9%	maximum	N	event
Hornsund	0.072|0.049|0.014	0.103|0.074|0.028	0.145|0.108|0.048	0.184|0.135|0.077	0.320|0.300|0.155	0.663|0.654|0.222	0.663|0.654|0.222	1975	67%
Thule	0.055|0.043|0.006	0.083|0.067|0.014	0.121|0.092|0.034	0.156|0.116|0.057	0.294|0.198|0.164	0.914|0.913|0.315	1.310|1.272|0.315	2934	59%
Kangerlussuaq	0.055|0.040|0.009	0.082|0.063|0.020	0.118|0.091|0.037	0.149|0.115|0.059	0.234|0.198|0.109	0.510|0.461|0.203	0.794|0.786|0.222	3066	75%
Ittoqqortoormiit	0.046|0.033|0.006	0.069|0.053|0.014	0.108|0.083|0.031	0.144|0.112|0.054	0.238|0.215|0.121	0.456|0.446|0.232	0.459|0.450|0.233	2041	73%
Andenes	0.062|0.042|0.014	0.096|0.064|0.027	0.136|0.098|0.049	0.172|0.123|0.072	0.274|0.210|0.148	0.451|0.432|0.249	0.541|0.534|0.258	2222	69%
Resolute_Bay	0.061|0.045|0.011	0.092|0.069|0.021	0.143|0.106|0.039	0.187|0.140|0.059	0.409|0.389|0.152	1.530|1.516|0.379	1.530|1.516|0.379	1876	72%
Barrow	0.071|0.053|0.013	0.114|0.082|0.024	0.175|0.134|0.047	0.232|0.183|0.076	0.455|0.415|0.174	2.999|2.962|0.328	2.999|2.962|0.328	1920	81%
Bonanza_Creek	0.078|0.048|0.022	0.130|0.089|0.036	0.280|0.230|0.057	0.532|0.497|0.083	1.713|1.643|0.186	2.619|2.591|0.341	2.908|2.857|0.345	3177	99%
Tiksi	0.079|0.061|0.011	0.121|0.096|0.021	0.182|0.163|0.040	0.286|0.239|0.060	0.936|0.915|0.123	1.442|1.413|0.238	1.442|1.413|0.238	631	97%
Yakutsk	0.094|0.069|0.014	0.153|0.119|0.027	0.272|0.221|0.053	0.400|0.345|0.089	0.980|0.963|0.201	3.018|2.972|0.317	3.296|3.259|0.340	4797	96%
MAN	0.052|0.029|0.021	0.090|0.062|0.031	0.126|0.097|0.042	0.164|0.118|0.052	0.281|0.253|0.085	0.777|0.761|0.234	0.777|0.761|0.234	520	92%

BB smoke plays a dominant role compared with other aerosol species above our AOD$_{95}$
extreme-event threshold (see Fig. 4b in particular and note that Fig. 4d shows the
expected dominance of FM AOD). Even for sites distant from BB source regions
(including Resolute Bay, Kangerlussuaq, Thule, Andenes, Hornsund, Ittoqqortoormiit)
BB smoke is the principal driver of AOD variations above the AOD$_{95}$ threshold (see Fig.

	Total | FM | CM AOD at 550nm							N	FM event
	Median	75%	90%	95%	99%	99.9%	maximum		
Hornsund	0.072|0.049|0.014	0.103|0.074|0.028	0.145|0.108|0.048	0.184|0.135|0.077	0.320|0.300|0.155	0.663|0.654|0.222	0.663|0.654|0.222	1975	67%
Thule	0.055|0.043|0.006	0.083|0.067|0.014	0.121|0.092|0.034	0.156|0.116|0.057	0.294|0.198|0.164	0.914|0.913|0.315	1.310|1.272|0.315	2934	59%
Kangerlussuaq	0.055|0.040|0.009	0.082|0.063|0.020	0.118|0.091|0.037	0.149|0.115|0.059	0.234|0.198|0.109	0.510|0.461|0.203	0.794|0.786|0.222	3066	75%
Ittoqqortoormiit	0.046|0.033|0.006	0.069|0.053|0.014	0.108|0.083|0.031	0.144|0.112|0.054	0.238|0.215|0.121	0.456|0.446|0.232	0.459|0.450|0.233	2041	73%
Andenes	0.062|0.042|0.014	0.096|0.064|0.027	0.136|0.098|0.049	0.172|0.123|0.072	0.274|0.210|0.148	0.451|0.432|0.249	0.541|0.534|0.258	2222	69%
Resolute_Bay	0.061|0.045|0.011	0.092|0.069|0.021	0.143|0.106|0.039	0.187|0.140|0.059	0.409|0.389|0.152	1.530|1.516|0.379	1.530|1.516|0.379	1876	72%
Barrow	0.071|0.053|0.013	0.114|0.082|0.024	0.175|0.134|0.047	0.232|0.183|0.076	0.455|0.415|0.174	2.999|2.962|0.328	2.999|2.962|0.328	1920	81%
Bonanza_Creek	0.078|0.048|0.022	0.130|0.089|0.036	0.280|0.230|0.057	0.532|0.497|0.083	1.713|1.643|0.186	2.619|2.591|0.341	2.908|2.857|0.345	3177	99%
Tiksi	0.079|0.061|0.011	0.121|0.096|0.021	0.182|0.163|0.040	0.286|0.239|0.060	0.936|0.915|0.123	1.442|1.413|0.238	1.442|1.413|0.238	631	97%
Yakutsk	0.094|0.069|0.014	0.153|0.119|0.027	0.272|0.221|0.053	0.400|0.345|0.089	0.980|0.963|0.201	3.018|2.972|0.317	3.296|3.259|0.340	4797	96%
MAN	0.052|0.029|0.021	0.090|0.062|0.031	0.126|0.097|0.042	0.164|0.118|0.052	0.281|0.253|0.085	0.777|0.761|0.234	0.777|0.761|0.234	520	92%
All AERONET sites	0.066|0.047|0.012	0.104|0.077|0.024	0.166|0.128|0.046	0.243|0.193|0.070	0.661|0.619|0.158	2.073|2.030|0.290	3.296|3.259|0.379	24639	86%

418

419 ~~To some extent, Barrow can be categorized as being a site that is distant from BB~~
420 ~~emissions. However, it is also relatively close to the region of Alaska fires, depending on~~
421 ~~dominant upstream winds and trajectories (see Eck et al., 2009 for details).~~

422 The modal and total AOD values at different percentile levels for the AERONET sites
423 and MAN data collected north of 70° N are provided in Table 2. For sites closer to BB
424 sources, including Bonanza Creek, Yakutsk, and Tiksi, the AOD_{99} and $(FM\ AOD)_{99}$
425 values are ~~>~~ larger than 1.0 while the maximum values are between 1.4-3.3. For the
426 more distant sites, the AOD_{99} and $(FM\ AOD)_{99}$ values vary between 0.23-0.46 while the
427 maximum values are between 0.45-3.0 (1.5 for Resolute Bay and 3.0 for Barrow). FM
428 event occurrences for the extreme total AOD events, range from 60-99~~%~~%, with an
429 average of 86%, and accordingly dominate CM events statistically. Sites closer to the
430 BB source regions show relative occurrences over 95%.

431 Large particles like ash and soil components emitted from vigorous burning during
432 extreme BB smoke events (Reid et al., 2005; Schlosser et al., 2017) can likely be
433 detected as AERONET CM AOD (see, for example, the correlation between the FM and
434 "weak" CM particle size distributions for Bonanza Creek in Fig. 9a of Eck et al. [2009]).
435 The extreme AOD events described above ~~((~~ are likely dominated by smoke. For
436 example, (FM AOD)$_{99}$ ~~of~~ is 1.~~643~~64 at Bonanza Creek and 0.~~936~~94 at Tiksi in Table 2~~,~~
437 ~~for example) are likely dominated by smoke. The~~. For events with FM AOD greater than
438 (FM AOD)$_{99}$~~,~~ the associated CM AOD means ~~for those~~ at the two ~~cases~~ sites showed
439 significantly larger values of 0.~~049~~05 and 0.~~033~~03, respectively (significantly larger
440 relative to, for example, the CM AOD means in Table 1). The coherency of the
441 associated CM AOD mean increase with the FM AOD mean increase suggests the
442 presence of detectable CM smoke and/or soil particles induced by severe burning. The
443 inability of the model to simulate potential CM smoke or soil components associated
444 with severe burning could be a contributing reason as to why it performs less well in
445 predicting CM AOD near BB sites.

446 3.3. Extreme biomass burning smoke AOD cases

447 A distinct class of extreme smoke cases comes from pyrocumulonimbus (pyroCb)
448 events induced by intense biomass burning sources: these events inject smoke high
449 into the troposphere or even well into the stratosphere (Fromm et al., 2010; Peterson et
450 al., 2017). A significant pyroCb smoke event that occurred over British Columbia (BC) in
451 August 2017 led to ~~significant~~substantial increases in various optical measures of
452 aerosol concentration in the lower Canadian and European Arctic (Peterson et al., 2018;
453 Torres et al., 2020; Das et al., 2021). Ranjbar et al. (2019) showed that a specific Aug.
454 19, 2017 smoke event over the high Arctic PEARL observatory at Eureka, Nunavut was
455 induced by the BC pyroCb fires and that it was a statistically significant extreme FM
456 AOD event. More recent eastern Siberian fires in June - August 2021, induced more
457 than a dozen cases of elevated smoke intrusion into the high Arctic with some smoke
458 plumes reaching the North Pole and/or its vicinity. For example, on the 5th of August,
459 2021, operational NAAPS (common chemistry, physics, and BB emission sources with
460 the NAAPS-RA) resolved a smoke plume north of 80°N (Fig. ~~5~~4) with AOD values of 2-
461 3. Smoke AOD over the source region was also 2 to >3 with a similar amplitude to
462 AODs measured at Yakutsk. CALIOP data suggested a 1-6 km high smoke layer in the
463 source region.

464 Other extreme or near-extreme smoke events in the Arctic have been reported. A series
465 of intense fires originating in North America led to strong AOD peaks in the summer of
466 2015 over Svalbard (Markowicz et al., 2016; Lisok et al., 2018). Agricultural fires in
467 Eastern Europe in the spring of 2006 caused record-high AODs and pollution levels in
468 the European Arctic (Stohl et al., 2007). The North American boreal fires in the summer
469 of 2004 led to large-amplitude AOD peaks in Alaska and enhanced AODs on a pan-
470 Arctic scale (Stohl et al., 2004). ~~Strong smoke events were also~~
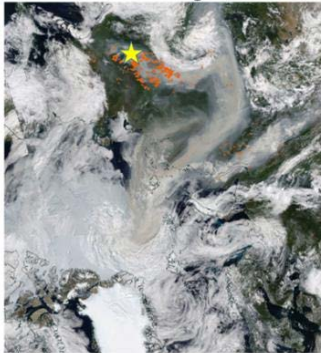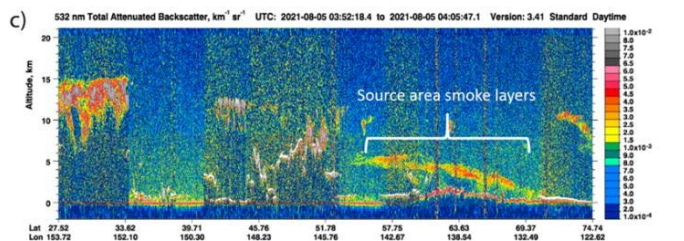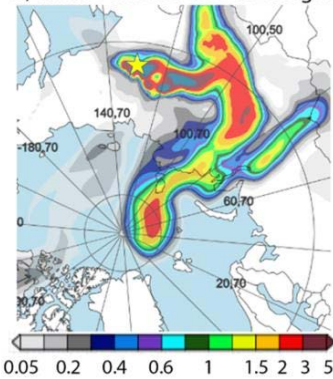
recorded during intensive field campaigns, including the ARCTAS/ARCPAC campaign in the summer of 2008 (Matsui et al., 2011; Saha et al, 2010; McNaughton et al., 2011) and the NETCARE research vessel (Canadian Arctic) campaign in the spring of 2015 (Abbatt et al., 2019).

476
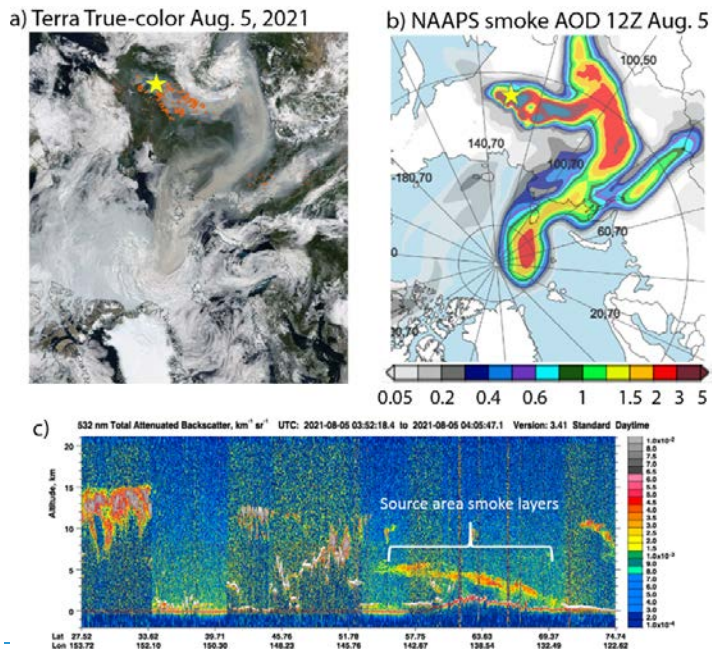
Figure 5̶4. An August 5, 2021 example of BB smoke intrusion into the high Arctic from
fires originating in eastern Siberia. a) Composite true-color Terra satellite imagery. The
red dots represent satellite-detected fire hotspots. b) Operational NAAPS smoke AOD
analysis at 12Z. c) CALIOP 532 nm attenuated backscatter coefficient showing the
smoke layers around the source area. The yellow stars on a) and b) represent the
location of Yakutsk, which experienced a daily mean total AOD (500 nm) of 2.0 (FM
AOD ~1.9) and an intra-day peak around 2.5 (̶based on AERONET V3L1.5 data)̶.̲
Sources: MODIS-Terra true-color satellite imagery and CALIOP-CALIPSO 532 nm
attenuated backscatter coefficient profile (respectively
https://worldview.earthdata.nasa.gov/ and https://www-calipso.larc.nasa.gov/).

3.4 Geographic distribution of extreme AODs

~~Having demonstrated that the NAAPS-RA simulations approximately reproduce the
statistics of the Arctic AERONET and MAN data over the 2003-2019 period we allow
ourselves the opportunity to exploit the spatial, temporal, and species-dependent model
capabilities to investigate Arctic wide variations and trends in terms of AOD and AOD
extremes.~~

493   The NAAPS-RA total-AOD map at different percentile levels locally for March-August
494   2003-2019 is shown in Fig. 6 (projection north of 50°N).5. We separated the entire
495   2003-2019study period into early (2003-2009) and late (2010-2019) subperiods. The
496   end-year of the first period was chosen as 2009 given the drop in ABF/sulfate emissions
497   due to the civil Clean Air Acts enacted across the U.S. (e.g., Tosca et al., 2017; Kaku et
498   al., 2018) as well as Europe and China, and the attendant decrease in ABF/sulfate AOD
499   in these countries/regions (Lynch et al., 2016; Zhang et al., 2017). This ABF/sulfate
500   AOD decrease was also observed in the Arctic, as shown in Fig. 13 of Part 1. The
501   median Arctic AOD (<(less than 0.1 as compared with ~0.0607 for the AERONET sites
502   from Fig. 43 and Table 2) are an order of magnitude smaller than the maximum AODs.
503   Clear BB smoke features in the North American and Asian boreal burning regions start
504   to emerge in the AOD$_{95}$ maps (see also Fig. 1). The maximum AOD is high (greater
505   than 2.0) while being relatively low over the Arctic Ocean (~ 0.3 - 1.0) and the North
506   Atlantic (, with the lowest values over the generally high-elevation Greenland
507   landmass).. The maximum AOD is associated with peak burning activities and generally
508   occurs in July and August (except for. The exception is the Norwegian Sea area, where
509   the maximum AODs occurs in March-May; this, as can be seen in Fig. 7,. This is
510   possibly associated with a combined high AOD level from anthropogenic pollutions,
511   marine aerosols and springtime agriculture fires)..

512
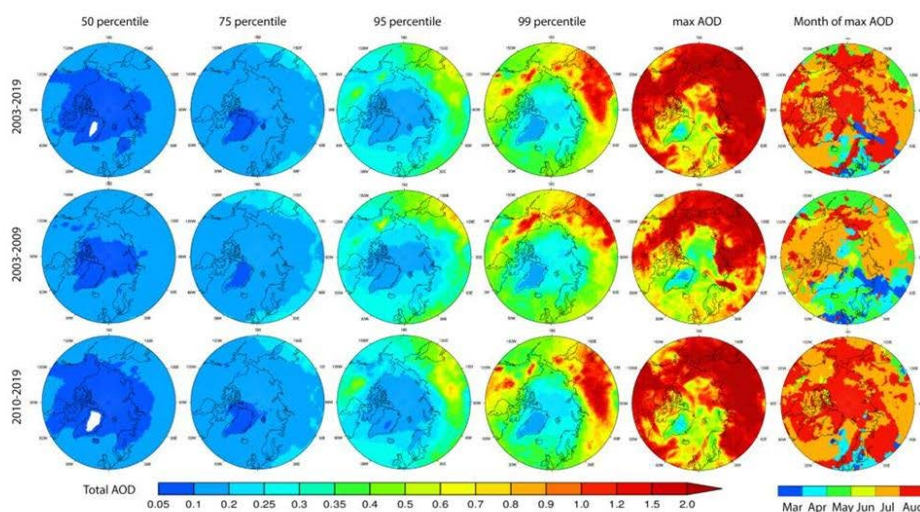
513   **Figure 65.** NAAPS-RA daily (550 nm) total-AOD maps (north of 50° latitude) at different
514   percentile levels for the March-August time frame, the maximum AOD and (rightmost
515   column) the month that the maximum AOD occurred. The three rows represent

516 respectively, the sampling periods of 2003-2019, 2003-2009, and 2010-2019. The
517 AOD_{95} value for 2003-2019 is the same as that of Fig. 1 (aside from adespite of different
518 color scales)..

519 The occurrence of different aerosol species (%) relative to the occurrence of total AOD
520 for total AOD extreme events (March-August time frame) are shown in Fig. 7. Recall
521 that an extreme total AOD event means total AOD > AOD_{95} locally (the AOD_{95} values
522 can be inferred from the 95th percentile column of Fig. 6 and "locally" refers to the
523 NAAPS-RA grid cell of 1° × 1°). 6. The occurrence maps accordingly indicate which
524 aerosol species are numerically dominant for extreme AOD events. As expected, BB
525 smoke is the prevailing extreme event contributor over the North American and Asian
526 Arctic (, especially near the boreal source regions and associated transport pathways),
527 as well as most of the Arctic ocean (except the Barents Sea and the Norwegian Sea).
528 ABF occurrence dominates the low European Arctic. Sea-salt particles and, to a lesser
529 extent, ABF are the most significant occurrence contributors, in the North Atlantic and
530 the Norwegian Sea. Dust occurrences to extreme AOD events are very small (0-10%)
531 except over the predominantly high-elevation region of Greenland where the relative
532 occurrence of high-altitude African dust dominates the relative occurrence of the other
533 species.

534 In terms of AOD amplitudes for total AOD extreme events (Fig. 87), BB smoke AOD
535 shows dominant contributions, especially in the areas near the boreal source regions
536 and transport pathways (, including most areas of the high Arctic)... ABF and sea salt
537 show slightly higher extreme-event AODs than BB smoke over the North Atlantic and
538 European Arctic. The regional extreme AODs are not, however, as large as the extreme
539 AODs in the BB smoke-dominant regions.

540

541
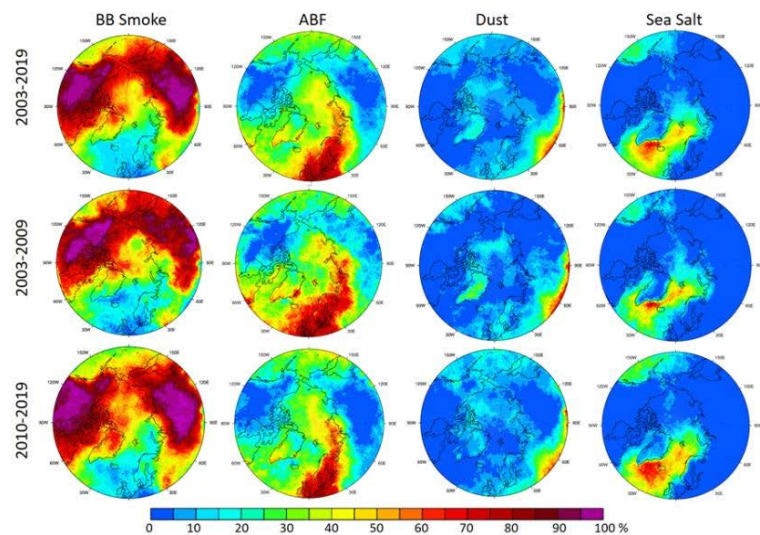
Figure ~~7~~6. Occurrence ~~~of different aerosol species (expressed as a percent)~~~ relative to the occurrence of total AOD extreme events (daily total AOD > AOD_{95} locally) for the March-August time frame ~~(sampling periods, from top to bottom of 2003-2019, 2003-2009, and 2010-2019). The qualifier "locally" refers to a NAAPS-RA grid cell of 1° x 1°~~. The sampling periods are the same as in Fig. 5.

547

AOD

548
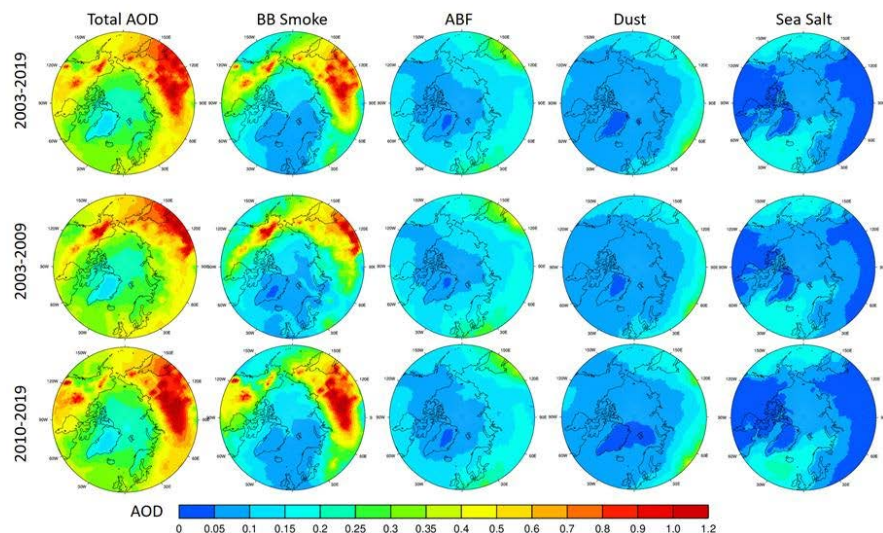
Figure 87. Mean speciated and total AODs averaged for days with speciated AOD or total AOD > AOD$_{95}$ (i.e. the mean value of the top 5% AOD data) for the March-August time frame (. The sampling periods~~, from top to bottom, of 2003-2019, 2003-2009,~~ are the same as in Figs. 5 and ~~2010-2019).~~6.

3.5 Seasonality of extreme AOD events

~~Figure 9 depicts the~~The NAAPS-RA seasonal cycle of total and speciated AOD are shown in Figure 8 for daily averages across the area north of 70° N (a latitude limit which largely excludes BB source regions). The seasonal cycle of monthly mean total AOD ~~(black solid circles in Fig. 9)~~ shows relatively higher values in Mar-Apr-May (MAM) compared with the lower AODs in Jun-Jul-Aug (JJA), and a minimum in June. The spread of the ABF AOD seasonal values is moderately stable, with a relatively higher mean/median in MAM than JJA (see the Figure 9 caption for a definition of spread). Sea-salt AOD and its spread are relatively higher in the earlier months (March and April). Dust AOD and spread are generally stable through the season, with a visibly higher mean/median in April and May. Smoke AOD amplitude and spread exhibit the greatest inter-species seasonal variations with the lowest mean and spread in March, increased means and spreads in April, and significantly higher mean and spread in later months. July and August appear to have the largest mean, spread and maximum smoke AODs (a smoke importance statement that is generally consistent with the results of Fig.~~7~~6). These smoke features significantly contribute to the seasonality of

569 total AOD extremes. It is also noted that the MAM total and smoke AOD means
570 approximately equal their medians, but that the JJA means are greater than their
571 medians (and that this is especially true for August). The greater number of smoke AOD
572 extremes in the later season and the attendant consequence of greater positive
573 histogram skewness would explain those relative increases in the mean.

574

575
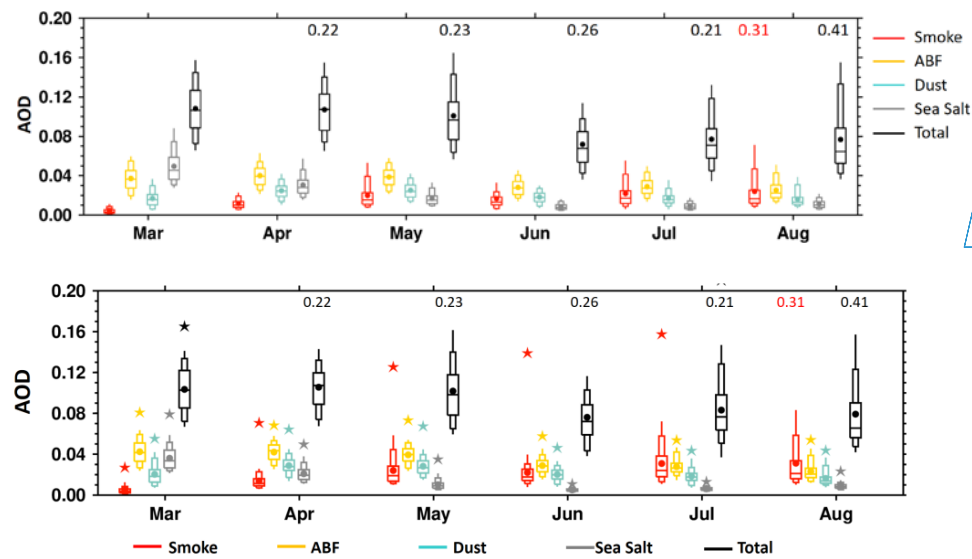
576 **Figure 98.** Box and whisker plot of daily and area-averaged (70°N-90°N) speciated
577 AOD at 550 nm from NAAPS-RA (2003-2019) for different months. The box and ~~whisker~~
578 ~~details are explained in the Figure 3 caption~~whiskers represent AOD at 95, 90, 75, 50,
579 25, 10, and 5 percentiles. Mean total AODs are shown as solid black circles and
580 maximum AODs as stars. Maximum AOD values appear as appropriately colored
581 numerical values if they extend beyond the 0.2 plot maximum. ~~The "spread" alluded to~~
582 ~~in the text refers to the spread of the boxes and whiskers where "whiskers" includes the~~
583 ~~vertical spread of the boxes as well as the maximum value.~~

584   3.5 Trends of extreme AOD events

585 There is, as shown in ~~Figure 12 of~~ Part 1 of the study, a multi-year decreasing MAM
586 trend and an increasing JJA trend for total AOD in the Arctic over the 2003-2019
587 sampling period. This was attributed to an overall decrease in ~~MMA~~MAM and JJA
588 sulfate/ABF AOD coupled with a negative trend in MAM, and a strong positive trend in
589 JJA for biomass-burning smoke AOD. In terms of extreme event trends, AOD_{95} (Fig. ~~6~~5)
590 and the average AOD above AOD_{95} (Fig. ~~7~~6) generally increased over the boreal

591 continents from the 2003-2009 to ~~2019~~2010-2019 period (with the notable exception of
592 Alaska and northeastern Siberia in 2010-2019). This is consistent with the ~~(Part 1)~~
593 positive BB emission trends in JJA north of 50°N and 60°N (for which the JJA trend
594 dominated the MAM trend inasmuch as JJA was associated with much higher BB
595 emissions; Part 1).

596 The negligible or slight decrease in high Arctic ~~(>70°N)~~ AOD_{50}, AOD_{75} and AOD_{95}
597 values from the 2003-2009 to the 2010-2019 period (Figure ~~6~~5), is likely associated with
598 the generally weak ABF decrease seen in Figure ~~8~~7. However, the increase in the
599 maximum AOD value (Fig. ~~6~~5) and the contribution of BB smoke to AOD extreme
600 events (Fig. ~~8~~7) in the latter period is an indication of stronger extreme BB smoke
601 influence in more recent years. It is also noted that the maximum high-Arctic AOD
602 occurred later in the season (mostly August) in 2010-2019 compared with the more
603 balanced variation occurring in March through August in 2003-2009.This is likely
604 attributable to overall lower ABF levels in the 2010-2019 period (especially in MAM),
605 and a shift in extreme smoke events to later in the season (~~Table 3, Fig. 10).~~Fig. 9).
606 Specific counts of extreme BB smoke days for different months and years and yearly
607 cumulative extreme AODs also support the seasonal shift of extreme smoke events
608 (Table S1).

609
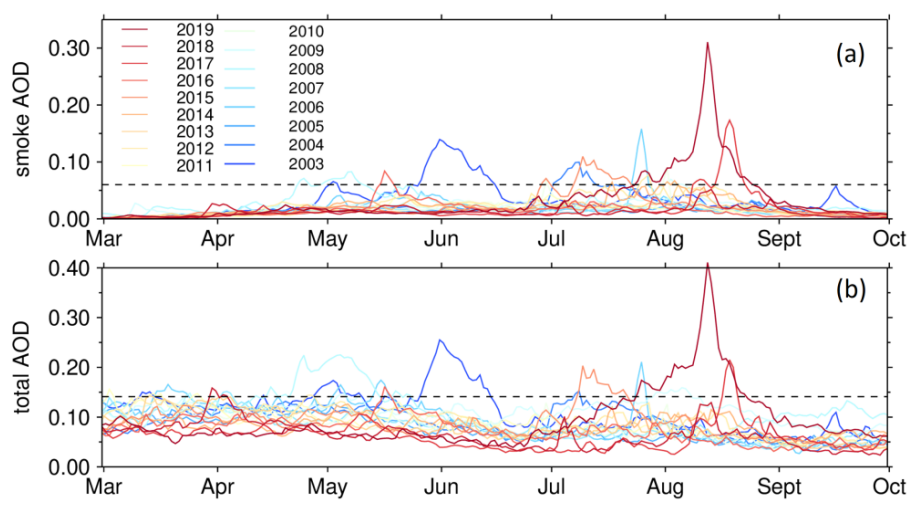
610 **Figure ~~10~~9.** Seasonal (March to September) time series of daily-mean AODs averaged
611 over the (70°N-90°N) high-Arctic area for each individual year of the 2003-~~201~~2019
612 period: (a) BB smoke AOD, and (b) total AOD. The years before 2010 are shown as
613 cold colors, and years after 2010 are shown as warm colors. The dashed horizontal

614 lines show the smoke AOD_{95} value of 0.06 and the total AOD_{95} value of 0.14
615 respectively during the study period.

616 The time series of high-Arctic-averaged daily-mean BB smoke and total AOD from
617 March to September for all years between 2003-2019 is shown in Fig. ~~10~~9. The extreme
618 total AOD variation is largely dictated by ~~extreme~~ BB smoke ~~AOD~~. There is also a
619 discernible 2003-2009 to 2010-2019 springtime reduction in extreme total AOD: this, as
620 discussed in the previous paragraph, is likely due to an overall reduction in ABF AOD~~.~~.
621 The occurrence of extreme smoke events tended to be more equally distributed over all
622 months (April-August) during the 2003-2009 period while being more concentrated in
623 the late season (July-August) during the 2010-2019 period. The extreme smoke and
624 total AOD trends resembled the extreme-smoke occurrence trends: more seasonally
625 balanced during the 2003-2009 period and summertime dominance during the 2010-
626 2019 period.

627 The occurrence of extreme high-Arctic smoke events thus demonstrates a clear smoke
628 and total AOD shift from a more balanced spring and summer to the late season
629 (notably the months of July and August; see also Table ~~3~~S1). This is consistent with the
630 temporal shift of fire activity to a later time in Siberia over 2003-2018 (Liu et al., 2020),
631 and the projection of emerging pan-Arctic fire regimes marked by increases in the
632 likelihood of extreme fires later in the growing season (McCarty et al., 2021). An earlier
633 fire season in the boreal region normally suggests a better-managed forest/land with
634 fewer large and destructive fires, while a later fire season indicates the opposite.

635 The shift of boreal fire activity, and the resulting BB smoke AOD extremes in the Arctic
636 from early season to late season, is probably related to early-season strengthening of
637 agriculture burning regulations and increased summertime lightning frequencies with
638 climate change in the latter decade. For example, the springtime BB smoke AOD peak
639 values in 2003, 2006 and 2008 are all associated with agricultural activity (resulting in
640 fires burning out of control) and widespread high-latitude burning (Korontzi et al, 2006;
641 Stohl et al., 2007; Saha et al., 2010). At the same time, with climate change, lightning
642 activity and lightning-caused wildfires in summertime high-~~-~~latitude regions were
643 observed to increase in the past two decades (Zhang et al., 2021; Bieniek et al, 2020;
644 Coogan et al., 2020). Also noted is a lengthening of growing season in boreal regions,
645 which infers lengthening of fire season as well (Park et al., 2016). These factors aside,
646 climate oscillations, including the Arctic Oscillation, ENSO and Pacific Decadal
647 Oscillation, also affect boreal fire activities (Balzter et al., 2007; Macias Fauria and
648 Johnson, 2007; Kim et al., 2020). These climate factors ~~also~~ modulate interannual
649 variations and possibly the transport dynamics of pollutants from the mid-latitudes to the
650 Arctic region (e.g. Eckhardt et al., 2003; Fisher et al., 2010).

651 The dominant contributor (, ABF), to regional extreme AOD occurrence and magnitude
652 in the lower European Arctic decreased slightly from 2003-2009 to 2010-2019 (Fig. ~~7~~6
653 and ~~8~~7): This observation is generally coherent with the Part 1 results showing a pan-
654 Arctic ABF AOD decrease in the 2003-2019 period and Fig. ~~10~~9. Extreme total-AOD
655 events dominated by sea-salt contributions in the North Atlantic and Norwegian Sea
656 increased slightly in 2010-2019. This was possibly due to the observed increase in
657 cyclonic activities (Rinke et al., 2017; Waseda et al., 2021; Valkonen et al., 2021).
658 Although the model simulation of CM AOD is not as skillful as that of FM, trend analysis
659 of CM AOD which is based on relative change is arguably significant.

660 ~~Table 3. Occurrence statistics of high-Arctic daily area-mean (>70°N) BB smoke AOD extreme~~
661 ~~event. These are defined as days with smoke AOD > smoke AOD₉₅ (~ 0.06) based on 2003-~~
662 ~~2019 NAAPS-RA data. Years without an extreme smoke event are omitted but are counted in~~
663 ~~the period average calculation. Cumulative extreme AOD is calculated as the sum of extreme~~
664 ~~BB smoke AOD.~~

	Extreme BB smoke days						max smoke	cumulative
year	APR	MAY	JUN	JUL	AUG	Annual total	AOD	extreme AOD
2003	0	9	16	0	0	25	0.14	2.4
2004	0	0	0	12	0	12	0.10	0.95
2006	0	0	0	4	0	4	0.16	0.49
2008	4	11	0	0	0	15	0.08	1.04
2009	0	0	0	0	5	5	0.07	0.32
2003-2009 ave	0.6	2.9	2.3	2.3	0.7	8.7	0.08	0.74
2010	0	0	1	0	2	3	0.09	0.22
2012	0	0	0	3	0	3	0.08	0.22
2014	0	0	0	1	2	3	0.07	0.2
2015	0	0	2	17	0	19	0.11	1.51
2016	0	4	0	0	0	4	0.08	0.29
2017	0	0	0	0	13	13	0.17	1.27
2019	0	0	0	7	25	32	0.31	3.75
2010-2019 ave	0	0.4	0.3	2.8	4.2	7.7	0.09	0.75

665

666 **4. ~~Conclusions~~ Summary**

667 ~~Aerosol optical depth~~ (AOD) data from the ~~U.S. Naval Aerosol Analysis and Prediction~~
668 ~~System-ReAnalysis (NAAPS-RA),~~ NAAPS-RA, the ground-based ~~Aerosol Robotic~~
669 ~~Network~~ (AERONET), and ~~Marine Aerosol Network~~ (MAN) were employed in analyzing
670 the 2003-2019 statistics and trends of extreme Arctic-AOD events for spring and
671 summer seasons ~~(March-August).~~ Extreme AODs are defined as any AOD greater than
672 the 95th percentile (AOD₉₅) for any given distribution of AODs (, whether that
673 distribution is generated by the ensemble of AODs representing the time series of a
674 specific location or of a regional average). Total, ~~fine mode~~ (FM) and ~~coarse mode~~

675 (CM) AODs at 550 nm from 6-hr resolution NAAPS-RA were first validated against
676 AERONET and MAN AOD data. NAAPS-RA was shown to be capable of largely
677 capturing FM and total AOD ranges and variability. The NAAPS-RA performance in
678 simulating CM AOD was significantly better if the temporal resolution of the all-season
679 statistics was less sensitive to high frequency dust and sea-salt events (i.e. the use of
680 temporal resolution bins of a month rather than 6 hr). Statistics of the 6-hr Arctic AOD
681 and extreme AOD events were analyzed. Finally, trends of extreme AOD in the Arctic
682 were presented and analyzed.

683 ***Baseline statistics for 6hrly AOD***: The median of 6-hr total AODs at 550 nm for all
684 Arctic AERONET sites and MAN retrievals over the 2003-2019 period is ~~0.06~~ 0.07
685 while ~~the 95th percentile value~~ (AOD_{95}) is ~0.23. Both the median and AOD_{95} values
686 show a dominant FM AOD contribution. The CM AOD median is ~0.01 while AOD_{95} is
687 ~0.07. The maximum AOD over the 2003-2019 period varies between 0.5-3.0 for
688 measurements made away from BB source regions, and 1.5 to greater than 3.0 for
689 measurements made closer to BB source regions. The seasonal~~,~~ NAAPS-RA spread of
690 smoke AOD is much higher than other speciated AODs ~~(~~, including ~~anthropogenic and~~
691 ~~biogenic fine (~~ABF~~)~~, dust, and sea salt AODs~~)~~, for all months between May and August:
692 the spread is especially large in July and August. These late-season smoke features
693 significantly contribute to the seasonality and interannual variabilities of extremes in
694 total AOD.

695 ***Extreme AOD events:*** Extreme AOD events using the Arctic spring and summer data
696 are largely attributable to FM AOD events ~~(~~, and notably BB smoke transport events in
697 general~~)~~. Extreme Arctic AOD events show large seasonal and interannual variability,
698 with the interannual AOD variability largely modulated by BB smoke. Extreme AOD
699 occurrences in the North American Arctic, the Asian Arctic, and the high Arctic ~~(>70°N)~~
700 are dominated by BB smoke events ~~(the lower European Arctic being the exception to~~
701 ~~this affirmation).~~ The occurrence of regionally extreme AOD events is attributed more to
702 ABF in the lower European Arctic. The extreme-event occurrence dominance of sea salt
703 aerosols is largely limited to the North Atlantic and Norwegian Seas. The extreme AOD
704 amplitudes of ABF and sea-salt AOD are, however, significantly lower than those
705 regions where extreme-AOD smoke AOD is dominant. Even for sites distant from BB
706 source regions, BB smoke is the principal driver of AOD variation above the AOD_{95}
707 threshold.

708 ***Shift of extreme AOD events from spring-summer to summer season***: There is an
709 overall increase in the maximum AOD values in the high Arctic in 2010-2019 compared
710 to 2003-2009, suggesting stronger extreme BB smoke influence for more recent years.
711 Extreme AOD events are observed to occur in a more balanced fashion over the entire
712 April-August season during 2003-2009 while being more concentrated in the latter part

713 of the season (i.e., July and August) during 2010-2019. The seasonal shift in extreme
714 smoke AOD events is consistent with the multi-year negative MAM trend and positive
715 JJA trend in BB emissions (north of 50°N, Part 1). These trends are likely attributable to
716 early season agricultural burning controls, and increased lightning activity and lightning-
717 caused wildfires in summertime in the boreal high-latitude regions on top of the overall
718 lower level, especially in spring, of 2010-2019 vs 2003-2009 anthropogenic aerosols.
719 The shift in extreme smoke events is consistent with a general multi-year decreasing
720 springtime trend and an increasing summertime trend of BB emissions north of 50°-N
721 (Part 1).

722 Global warming is expected to continue generating drier conditions and increased
723 wildfire activities in the high latitudes (McCarty et al., 2021) and thus render the Arctic
724 more susceptible to extreme smoke events. These events can significantly change the
725 regional aerosol budget by bringing large amounts of smoke aerosols into the Arctic.
726 These extreme smoke events will likely play an increasingly important Arctic aerosol
727 budget role given the decreasing (Part 1) baseline in anthropogenic pollution aerosols
728 over the 2003-2019 period. Smoke aerosols are, notably, much more light-absorbing
729 than anthropogenic sulfate. As well, their different physical and chemical properties
730 relative to anthropogenic aerosols will translate into different efficiencies in their role as
731 CCN and ININP. When deposited on surface snow and ice, they impact the surface
732 radiative forcing budget by reducing surface albedo. The climate impacts of BB smoke
733 would, accordingly, differ and possibly counteract the dynamics of anthropogenic
734 aerosols. Therefore, the baseline AOD trends reported in Part 1 and the trends in
735 extreme AOD events reported here are important in terms of implications for the
736 changing Arctic climate. The greater sensitivity of Arctic climate to aerosol forcings
737 relative to other regions of the globe (e.g. Wang et al., 2018), the impact of the extreme
738 BB smoke events and their interannual variability and trends on Arctic climate warrants
739 further exploration. The statistics of extreme AODs reported here are expected to help
740 in the formulation of climate sensitivity experiments and improve our knowledge of the
741 relative importance of aerosol processes compared to other factors of the changing
742 Arctic climate.

743 **Code and Data Availability:** All data supporting the conclusions of this manuscript are
744 available through the links provided below.

745 AERONET Version 3 Level 2 data: http://aeronet.gsfc.nasa.gov

746 MAN data: https://aeronet.gsfc.nasa.gov/new_web/maritime_aerosol_network.html

747 NAAPS RA AOD: https://usgodae.org//cgi-
748 bin/datalist.pl?dset=nrl_naaps_reanalysis&summary=Go

Author contributions: P.X. designed this study, performed most of the data analysis and wrote the initial manuscript. All authors contributed to scientific discussion, revision and editing of the manuscript.

Competing interests: The authors declare that they have no conflict of interest.

Acknowledgments

We thank the NASA AERONET, and MAN, and Environment and Climate change Canada (ECCC) AEROCAN group for the sun-photometer data. We acknowledge the use of imagery from the NASA Worldview application (https://worldview.earthdata.nasa.gov, last access: Mar 11, 2022), and NASA CALIPSO website (https://www-calipso.larc.nasa.gov/).

Financial support

The authors acknowledge support from NASA's Interdisciplinary Science (IDS) program (grant no. 80NSSC20K1260), NASA's Modeling, Analysis and Prediction (MAP) program (NNX17AG52G) and the Office of Naval Research Code 322. N.O. and K.R's work was supported by the Canadian Space Agency, SACIA-2 project, Ref. No. 21SUASACOA, ESS-DA program.

References

AboEl-Fetouh, Y., O'Neill, N. T., Ranjbar, K., Hesaraki, S., Abboud, I., & Sobolewski, P. S. (2020). Climatological-scale analysis of intensive and semi-intensive aerosol parameters derived from AERONET retrievals over the Arctic. *Journal of Geophysical Research: Atmospheres*, *125*, e2019JD031569. https://doi.org/10.1029/2019JD031569

Balzter, H., F. F. Gerard, C. T. George, C. S. Rowland, T. E. Jupp, I. McCallum, A. Shvidenko, S. Nilsson, A. Sukhinin, A. Onuchin, C. Schmullius, Impact of the Arctic Oscillation pattern on interannual forest fire variability in central Siberia. *Geophys. Res. Lett.* **32**, L14709 (2005).

Baibakov, K., O'Neill, N. T., Ivanescu, L., Duck, T. J., Perro, C., Herber, A., Schulz, K.-H., and Schrems, O.: Synchronous polar winter starphotometry and lidar measurements at a High Arctic station, AMT, 8, 3789-3809, doi:10.5194/amt-8-3789-2015, 2015.

Bieniek, P. A., Bhatt, U. S., York, A., Walsh, J. E., Lader, R., Strader, H., Ziel, R., Jandt, R. R., & Thoman, R. L. (2020). Lightning Variability in Dynamically Downscaled Simulations of Alaska's Present and Future Summer Climate, Journal of Applied Meteorology and Climatology, 59(6), 1139-1152.

784

785 Birch, C. E., Brooks, I. M., Tjernström, M., Shupe, M. D., Mauritsen, T., Sedlar, J., Lock,
786 A. P., Earnshaw, P., Persson, P. O. G., Milton, S. F., and Leck, C.: Modelling
787 atmospheric structure, cloud and their response to CCN in the central Arctic: ASCOS
788 case studies, Atmos. Chem. Phys., 12, 3419–3435, https://doi.org/10.5194/acp-12-
789 3419-2012, 2012.
790

791 Boisvert, L.N., A.A. Petty and J.C. Stroeve, 2016: The Impact of the Extreme Winter
792 2015/16 Arctic Cyclone on the Barents–Kara Seas. Monthly Weather Review, **144** (11),
793 4279–4287, doi:10.1175/mwr-d-16-0234.1.
794

795 Bossioli, E., Sotiropoulou, G., Methymaki, G., & Tombrou, M. (2021). Modeling extreme
796 warm-air advection in the Arctic during summer: The effect of mid-latitude pollution
797 inflow on cloud properties. *Journal of Geophysical Research: Atmospheres*, *126*,
798 e2020JD033291. https://doi.org/10.1029/2020JD033291

799 Coogan, S. C. P., Cai, X., Jain, P., and Flannigan, M. D. (2020) Seasonality and trends
800 in human- and lightning-caused wildfires ≥ 2 ha in Canada, 1959–2018. *International*
801 *Journal of Wildland Fire* **29**, 473-485. https://doi.org/10.1071/WF19129

802 Coopman, Q., Garrett, T. J., Finch, D. P., & Riedi, J. (2018). High sensitivity of arctic
803 liquid clouds to long-range anthropogenic aerosol transport. Geo-physical Research
804 Letters, 45, 372–381. https://doi.org/10.1002/2017GL075795
805

806 Dang, C., S. G. Warren, Q. Fu, S. J. Doherty, M. Sturm, and J. Su (2017),
807 Measurements of light-absorbing particles in snow across the Arctic, North America,
808 and China: Effects on surface albedo, J. Geophys. Res. Atmos., 122, 10,149–10,168,
809 doi:10.1002/2017JD027070.
810

811 Das, S., Colarco, P. R., Oman, L. D., Taha, G., and Torres, O.: The long-term transport
812 and radiative impacts of the 2017 British Columbia pyrocumulonimbus smoke aerosols
813 in the stratosphere, Atmos. Chem. Phys., 21, 12069–12090,
814 https://doi.org/10.5194/acp-21-12069-2021, 2021.
815

816 DeRepentigny, P., Jahn, A., Holland, M., Fasullo, J., Lamarque, J.-F., Hannay, C., Mills,
817 M., Bailey, D., Tilmes, S., and Barrett, A.: Impact of CMIP6 biomass burning emissions
818 on Arctic sea ice loss, EGU General Assembly 2021, online, 19–30 Apr 2021, EGU21-
819 9020, https://doi.org/10.5194/egusphere-egu21-9020, 2021.
820

821   Eck, T. F., et al. (2009), Optical properties of boreal region biomass burning aerosols in
822   central Alaska and seasonal variation of aerosol optical depth at an Arctic coastal site,
823   J. Geophys. Res., 114, D11201, doi:10.1029/2008JD010870.
824
825   Eckhardt, S., A. Stohl, S. Beirle, N. Spichtinger, P. James, C. Forster, C. Junker, T.
826   Wagner, U. Platt, and S. G. Jennings (2003), The North Atlantic Oscillation controls air
827   pollution transport to the Arctic, Atmos. Chem. Phys., 3(5), 1769–1778,
828   doi:10.5194/acp-3-1769-2003.
829
830   Engelmann, R., Ansmann, A., Ohneiser, K., Griesche, H., Radenz, M., Hofer, J.,
831   Althausen, D., Dahlke, S., Maturilli, M., Veselovskii, I., Jimenez, C., Wiesen, R., Baars,
832   H., Bühl, J., Gebauer, H., Haarig, M., Seifert, P., Wandinger, U., and Macke, A.: Wildfire
833   smoke, Arctic haze, and aerosol effects on mixed-phase and cirrus clouds over the
834   North Pole region during MOSAiC: an introduction, Atmos. Chem. Phys., 21, 13397–
835   13423, https://doi.org/10.5194/acp-21-13397-2021, 2021.
836
837   Evangeliou, N., Balkanski, Y., Hao, W. M., Petkov, A., Silverstein, R. P., Corley, R.,
838   Nordgren, B. L., Urbanski, S. P., Eckhardt, S., Stohl, A., Tunved, P., Crepinsek, S.,
839   Jefferson, A., Sharma, S., Nøjgaard, J. K., and Skov, H.: Wildfires in northern Eurasia
840   affect the budget of black carbon in the Arctic – a 12-year retrospective synopsis (2002–
841   2013), Atmos. Chem. Phys., 16, 7587–7604, https://doi.org/10.5194/acp-16-7587-2016,
842   2016.
843
844   Fisher, J. A., et al. (2010), Source attribution and interannual variability of Arctic
845   pollution in spring constrained by aircraft (ARCTAS, ARCPAC) and satellite (AIRS)
846   observations of carbon monoxide, Atmos. Chem. Phys., 10(3), 977–996,
847   doi:10.5194/acp-10-977-2010.
848
849   Flanner, M. G., Zender, C. S., Randerson, J. T., & Rasch, P. J. (2007). Present-day
850   climate forcing and response from black carbon in snow. *Journal of Geophysical
851   Research*, *112*(September 2006), D11202. https://doi.org/10.1029/2006JD008003
852
853   Garrett, T. J., Zhao, C., and Novelli, P.: Assessing the relative contributions of transport
854   efficiency and scavenging to seasonal variability in Arctic aerosol, Tellus B, 62, 190–
855   196, https://doi.org/10.1111/j.1600-0889.2010.00453.x, 2010.
856
857   Giles, D. M., Sinyuk, A., Sorokin, M. G., Schafer, J. S., Smirnov, A., Slutsker, I., Eck, T.
858   F., Holben, B. N., Lewis, J. R., Campbell, J. R., Welton, E. J., Korkin, S. V., and
859   Lyapustin, A. I.: Advancements in the Aerosol Robotic Network (AERONET) Version 3
860   database – automated near-real-time quality control algorithm with improved cloud

861 screening for Sun photometer aerosol optical depth (AOD) measurements, Atmos.
862 Meas. Tech., 12, 169–209, https://doi.org/10.5194/amt-12-169-2019, 2019.
863
864 Hall, J. V., Loboda, T. V., Giglio, L., McCarty G. W. (2016), A MODIS-based burned
865 area assessment for Russian croplands: Mapping requirements and challenges.
866 Remote Sensing of Environment, Vol. 184, 506-521.
867 https://doi.org/10.1016/j.rse.2016.07.022
868
869 Hesaraki S, O'Neill NT, Lesins G, Saha A, Martin RV, Fioletov VE, Baibakov K, Abboud
870 I. Comparisons of a chemical transport model with a four-year (April to September)
871 analysis of fine-and coarse-mode aerosol optical depth retrievals over the Canadian
872 Arctic. Atmosphere-Ocean. 2017 Oct 20;55(4-5):213-29.
873
874 Hogan, T.F. and T.E. Rosmond: The description of the Navy Operational Global
875 Atmospheric Prediction System's spectral forecast model. Mon. Wea. Rev., 119, 1786-
876 1815, 1991.
877
878 Hyer, E. J., J. S. Reid, and J. Zhang, 2011: An over-land aerosol optical depth data set
879 for data assimilation by filtering, correction, and aggregation of MODIS Collection 5
880 optical depth retrievals. *Atmospheric Measurement Techniques*, European Geophysical
881 Union, 379-408.
882
883 IPCC Chapter 6, Szopa, S., V. Naik, B. Adhikary, P. Artaxo, T. Berntsen, W.D. Collins, S. Fuzzi,
884 L. Gallardo, A. Kiendler-Scharr, Z. Klimont, H. Liao, N. Unger, and P. Zanis, 2021: Short-Lived
885 Climate Forcers. In Climate Change 2021: The Physical Science Basis. Contribution of Working
886 Group I to the Sixth Assessment Report of the Intergovernmental Panel on Climate Change
887 [Masson-Delmotte, V., P. Zhai, A. Pirani, S.L. Connors, C. Péan, S. Berger, N. Caud,
888 Y. Chen, L. Goldfarb, M.I. Gomis, M. Huang, K. Leitzell, E. Lonnoy, J.B.R. Matthews,
889 T.K. Maycock, T. Waterfield, O. Yelekçi, R. Yu, and B. Zhou (eds.)]. Cambridge University
890 Press, Cambridge, United Kingdom and New York, NY, USA, pp. 817–922,
891 doi:10.1017/9781009157896.008.
892
893 Jacob, D. J., J. H. Crawford, H. Maring, A. D. Clarke, J. E. Dibb, L. K. Emmons, R. A.
894 Ferrare, C. A. Hostetler, P. B. Russell, and H. B. Singh (2010), The arctic research of
895 the composition of the troposphere from aircraft and satellites (ARCTAS) mission:
896 Design, execution, and first results, Atmos. Chem. Phys., 10(11), 5191–5212.
897
898 Kang S., Y. Zhang, Y. Qian, and H. Wang. 2020. "A review of black carbon in snow and
899 ice and its impact on the cryosphere." *Earth - Science Reviews* 210. PNNL-SA-154137.
900 doi:10.1016/j.earscirev.2020.103346
901

902 Khan, A. L., S. Wagner, R. Jaffe, P. Xian, M. Williams, R. Armstrong, and D. McKnight
903 (2017), Dissolved black carbon in the global cryosphere: Concentrations and chemical
904 signatures, Geophys. Res. Lett., 44, 6226–6234, doi:10.1002/2017GL073485.
905
906 Kaku, K. C., Reid, J. S., Hand, J. L., Edgerton, E. S., Holben, B. N., Zhang, J., & Holz, R. E.:
907 Assessing the challenges of surface-level aerosol mass estimates from remote sensing during the
908 SEAC⁴RS and SEARCH campaigns: Baseline surface observations and remote sensing in the
909 southeastern United States. *Journal of Geophysical Research:*
910 *Atmospheres*, 123, 7530– 7562. https://doi.org/10.1029/2017JD028074, 2018.
911
912 Korontzi, S., J. McCarty, T. Loboda, S. Kumar, and C. Justice (2006), Global distribution
913 of agricultural fires in croplands from 3 years of Moderate Resolution Imaging
914 Spectroradiometer (MODIS) data, Global Biogeochem. Cycles, 20, GB2021,
915 doi:10.1029/2005GB002529.
916
917 Leck, C. and Svensson, E.: Importance of aerosol composition and mixing state for cloud
918 droplet activation over the Arctic pack ice in summer, Atmos. Chem. Phys., 15, 2545–2568,
919 https://doi.org/10.5194/acp-15-2545-2015, 2015.
920
921 Levy, R. C., Remer, L. A., Kleidman, R. G., Mattoo, S., Ichoku, C., Kahn, R., and Eck, T. F.:
922 Global evaluation of the Collection 5 MODIS dark-target aerosol products over land, Atmos.
923 Chem. Phys., 10, 10399–10420, https://doi.org/10.5194/acp-10-10399-2010, 2010.
924
925 Lund Myhre, C., Toledano, C., Myhre, G., Stebel, K., Yttri, K. E., Aaltonen, V., Johnsrud, M.,
926 Frioud, M., Cachorro, V., de Frutos, A., Lihavainen, H., Campbell, J. R., Chaikovsky, A. P.,
927 Shiobara, M., Welton, E. J., and Tørseth, K.: Regional aerosol optical properties and
928 radiative impact of the extreme smoke event in the European Arctic in spring 2006, Atmos.
929 Chem. Phys., 7, 5899–5915, https://doi.org/10.5194/acp-7-5899-2007, 2007.
930
931 Lynch, P., J. S. Reid, D. L. Westphal, J. Zhang, T. Hogan, E. J. Hyer, C. A. Curtis, D.
932 Hegg, Y. Shi, J. R. Campbell, J. Rubin, W. Sessions, J. Turk and A. Walker: An 11-year
933 Global Gridded Aerosol Optical Thickness Reanalysis (v1.0) for Atmospheric and
934 Climate Sciences. Geosci. Model Dev., 9, 1489-1522, doi:10.5194/gmd-9-1489-2016,
935 2016.
936
937 Macias Fauria, M, E. A. Johnson, Large-scale climatic patterns control large lightning
938 fire occurrence in Canada and Alaska forest regions. *J. Geophys. Res.* **111**, G04008
939 (2006).
940
941 Markowicz, K. M., et al. (2016), Impact of North American intense fires on aerosol
942 optical properties measured over the European Arctic in July 2015, J. Geophys. Res.
943 Atmos., 121, 14,487–14,512, doi:10.1002/2016JD025310.

944   Markowicz, K.M., Lisok, J., Xian, P., Simulation of long-term direct aerosol radiative
945   forcing over the arctic within the framework of the iAREA project, Atmospheric
946   Environment (2021), doi: https://doi.org/10.1016/j.atmosenv.2020.117882.

948   Mauritsen, T., Sedlar, J., Tjernström, M., Leck, C., Martin, M., Shupe, M., Sjogren, S.,
949   Sierau, B., Persson, P. O. G., Brooks, I. M., and Swietlicki, E.: An Arctic CCN-limited
950   cloud-aerosol regime, Atmos. Chem. Phys., 11, 165–173, https://doi.org/10.5194/acp-
951   11-165-2011, 2011.

953   McCarty, J. L., Aalto, J., Paunu, V.-V., Arnold, S. R., Eckhardt, S., Klimont, Z., Fain, J.
954   J., Evangeliou, N., Venäläinen, A., Tchebakova, N. M., Parfenova, E. I., Kupiainen, K.,
955   Soja, A. J., Huang, L., and Wilson, S.: Reviews & Syntheses: Arctic Fire Regimes and
956   Emissions in the 21st Century, Biogeosciences Discuss. [preprint],
957   https://doi.org/10.5194/bg-2021-83, in review, 2021.

959   O'Neill, N.T., T.F.Eck, B.N.Holben, A.Smirnov, O.Dubovik, and A.Royer (2001) Bimodal
960   size distribution influences on the variation of Angstrom derivatives in spectral and
961   optical depth space, J. Geophys. Res., 106, 9787-9806.

963   O'Neill, N. T., Eck, T. F., Smirnov, A., Holben, B. N., and Thulasiraman S. (2003)
964   Spectral discrimination of coarse and fine mode optical depth. J. Geophys. Res., 108,
965   D05212, doi:10.1029/2002JD002975.

967   Peterson, D. A., E. J. Hyer, J. R. Campbell, J. E. Solbrig and M. D. Fromm (2017), A
968   conceptual model for development of intense pyroconvection in western North America.
969   *Mon. Wea. Rev*., **145,** 2235-2255, DOI: 10.1175/MWR-D-16-0232.1.

970   Peterson, D. A., J. R. Campbell, E. J. Hyer, M. D. Fromm, G. P. Kablick, J. H. Cossuth,
971   and M. T. Deland (2018), Wildfire-driven thunderstorms cause a volcano-like
972   stratospheric injection of smoke. *NPJ Clim. and Atmos. Sci*., 1:30;
973   https://doi.org/10.1038/s41612-018-0039-3.

974   Prenni, A. J., Harrington, J. Y., Tjernstöm, M., DeMott, P. J., Avramov, A., Long, C. N.,
975   Kreidenweis, S. M., Olsson, P. Q., and Verlinde, J.: Can ice-nucleating aerosols affect
976   arctic seasonal climate?, B. Am. Meteorol. Soc., 88, 541–550,
977   https://doi.org/10.1175/BAMS-88-4-541, 2007.

979   Quinn, P. K., et al. (2008), Short-lived pollutants in the Arctic: Their climate impact and
980   possible mitigation strategies, Atmos. Chem. Phys., 8(6), 1723–1735, doi:10.5194/acp-
981   8-1723-2008.
982

983 Randerson, J. T., and Coauthors, 2006: The impact of boreal forest fire on climate
984 warming. Science, 314, 1130–1132, doi:10.1126/science.1132075.

986 Ranjbar, K., O'Neill, N. T., Lutsch, E., McCullough, E. M., AboEl-Fetouh, Y., Xian, P., et
987 al. (2019). Extreme smoke event over the high Arctic. *Atmospheric Environment*, *218*,
988 117002. https://doi.org/10.1016/j.atmosenv.2019.117002

990 Ranjbar, K., O'Neill, N. T., and Aboel-Fetouh, Y.: Comment on "Short-cut transport path for
991 Asian dust directly to the Arctic: a case Study" by Huang et al. (2015) in Environ. Res. Lett.,
992 Atmos. Chem. Phys., 22, 1757–1760, https://doi.org/10.5194/acp-22-1757-2022, 2022.

994 Reid, J. S., Hyer, E. J., Prins, E. M., Westphal, D. L., Zhang, J., Wang, J., Christopher,
995 S. A., Curtis, C. A., Schmidt, C. C., Eleuterio, D. P., Richardson, K. A., and Hoffman, J.
996 P.: Global Monitoring and Forecasting of Biomass-Burning Smoke: Description of and
997 Lessons from the Fire Locating and Modeling of Burning Emissions (FLAMBE)
998 Program, IEEE J. Sel. Top. Appl., 2, 144–162, JSTARS-2009-00034, 2009.

1000 Reid, J. S., Koppmann, R., Eck, T. F., and Eleuterio, D. P.: A review of biomass burning
1001 emissions part II: intensive physical properties of biomass burning particles, Atmos.
1002 Chem. Phys., 5, 799–825, https://doi.org/10.5194/acp-5-799-2005, 2005.

1004 Rinke, A., Maturilli, M., Graham, R. M., Hatthes, H., Handorf, D., Cohen, L., Hudson, S.
1005 R. and Moore, J. C., (2017), Extreme cyclone events in the Arctic: Wintertime variability
1006 and trends. *Environ. Res. Lett.* **12** 094006

1008 Saha, A., et al. (2010), Pan-Arctic sunphotometry during the ARCTAS-A campaign of
1009 April 2008, Geophys. Res. Lett., 37, L05803, doi:10.1029/2009GL041375.

1011 Sand, M., T. K. Berntsen, Ø. Seland, and J. E. Kristjánsson (2013), Arctic surface
1012 temperature change to emissions of black carbon within Arctic or midlatitudes, J.
1013 Geophys. Res. Atmos., 118, 7788–7798, doi:10.1002/jgrd.50613.

1015 Serreze, M.C. and R.G. Barry, 2011: Processes and impacts of Arctic amplification: A
1016 research synthesis. Global and Planetary Change, **77** (1– 2), 85–96,
1017 doi:10.1016/j.gloplacha.2011.03.004.

1019 Serreze, M.C., Francis, J.A. The Arctic Amplification Debate. *Climatic Change* **76,** 241–
1020 264 (2006). https://doi.org/10.1007/s10584-005-9017-y

1022 Sharma, S., M. Ishizawa, D. Chan, D. Lavoué, E. Andrews, K. Eleftheriadis, and S.
1023 Maksyutov (2013), 16-year simulation of Arctic black carbon: Transport, source

1024 contribution, and sensitivity analysis on deposition, J. Geophys. Res. Atmos., 118, 943–
1025 964, doi:10.1029/2012JD017774.
1026
1027 Shi, Y., J. Zhang, J. S. Reid, E. J. Hyer, and N. C. Hsu, 2013: Critical evaluation of the
1028 MODIS Deep Blue aerosol optical depth product for data assimilation over North Africa.
1029 *Atmospheric Measurement Techniques*, **6,** 949-969.
1030
1031 Shi, Y., J. Zhang, J. S. Reid, B. Holben, E. J. Hyer, and C. Curtis, 2011: An analysis of
1032 the collection 5 MODIS over-ocean aerosol optical depth product for its implication in
1033 aerosol assimilation. *Atmos. Chem. Phys.*, **11,** 557-565.
1034
1035 Shindell, D. and Faluvegi, G.: Climate response to regional radiative forcing during the
1036 twentieth century, Nat. Geosci., 2, 294–300, https://doi.org/10.1038/ngeo473, 2009.
1037
1038 Schlosser, J. S., R. A. Braun, T. Bradley, H. Dadashazar, A. B. MacDonald, A. A.
1039 Aldhaif, M. A. Aghdam, A. H. Mardi, P. Xian, and A. Sorooshian (2017), Analysis of
1040 aerosol composition data for western United States wildfires between 2005 and 2015:
1041 Dust emissions, chloride depletion, and most enhanced aerosol constituents, J.
1042 Geophys. Res. Atmos., 122, 8951–8966, doi:10.1002/2017JD026547.
1043
1044 Skiles S. M., Flanner, M., Cook, J. M., Dumont, M. and Painter, T. (2018) Radiative
1045 forcing by light-absorbing particles in snow. Nature Climate Change, 8, 964-971.
1046 https://doi.org/10.1038/s41558-018-0296-5
1047
1048 Sogacheva, L., Popp, T., Sayer, A. M., Dubovik, O., Garay, M. J., Heckel, A., Hsu, N. C.,
1049 Jethva, H., Kahn, R. A., Kolmonen, P., Kosmale, M., de Leeuw, G., Levy, R. C., Litvinov, P.,
1050 Lyapustin, A., North, P., Torres, O., and Arola, A.: Merging regional and global aerosol
1051 optical depth records from major available satellite products, Atmos. Chem. Phys., 20,
1052 2031–2056, https://doi.org/10.5194/acp-20-2031-2020, 2020.
1053
1054 Stohl, A., et al. (2006), Pan-Arctic enhancements of light absorbing aerosol
1055 concentrations due to North American boreal forest fires during summer 2004, J.
1056 Geophys. Res., 111, D22214, doi:10.1029/2006JD007216.
1057
1058 Stohl, A., et al. (2007), Arctic smoke—Record high air pollution levels in the European
1059 Arctic due to agricultural fires in eastern Europe in spring 2006, Atmos. Chem. Phys.,
1060 7(2), 511–534, doi:10.5194/acp-7-511-2007.
1061
1062 Stone, R. S., G. P. Anderson, E. P. Shettle, E. Andrews, K. Loukachine, E. G. Dutton,
1063 C. Schaaf, and M. O. Roman III (2008), Radiative impact of boreal smoke in the Arctic:
1064 Observed and modeled, J. Geophys. Res., 113, D14S16,

doi:10.1029/2007JD009657.

Tomasi, C., Vitale, V., Lupi, A., Di Carmine, C., Campanelli, M., Herber, A., Treffeisen, R., Stone, R. S., Andrews, E., Sharma, S., Radionov, V., von Hoyningen-Huene, W., Stebel, K., Hansen, G. H., Myhre, C. L.,Wehrli, C., Aaltonen, V., Lihavainen, H., Virkkula, A., Hillamo, R., Ström, J., Toledano, C., Cachorro, V. E., Ortiz, P., de Frutos, A. M., Blindheim, S., Frioud, M., Gausa, M., Zielinski, T., Petelski, T., & Yamanouchi, T. (2007). Aerosols in polar regions: a historical overview based on optical depth and in situ observations. *Journal of Geophysical Research, Atmospheres, 112*, D16. https://doi.org/10.1029/2007JD008432.

Torres, O., Bhartia, P. K., Taha, G., Jethva, H., Das, S., Colarco, P., Krotkov, N., Omar, A., and Ahn, C.: Stratospheric Injection of Massive Smoke Plume From Canadian Boreal Fires in 2017 as Seen by DSCOVR-EPIC, CALIOP, and OMPS-LP Observations, J. Geophys. Res.-Atmos., 125, e2020JD032579, https://doi.org/10.1029/2020JD032579, 2020.

Tosca, M, J. Campbell, M. Garay, S. Lolli, F. Seidel, J. Marquis, and O. Kalashnikova (2017), Attributing accelerated summertime warming in the southeast United States to recent reductions in aerosol burden: indications from vertically-resolved observations. *Remote Sens.*, 9, 674, doi:10.3390/rs9070674.

Wang, Y., J. Jiang, H. Su, S. Choi, L. Huang, J. Guo and Y. Yung: Elucidating the Role of Anthropogenic Aerosols in Arctic Sea Ice Variations. J. Climate, 31(1), 99-114, 2018. https://doi.org/10.1029/2006JD007234

Warneke, C., Froyd, K. D., Brioude, J., Bahreini, R., Brock, C. A., Cozic, J., et al. (2010). An important contribution to springtime Arctic aerosol from biomass burning in Russia. *Geophysical Research Letters*, *37*, L01801. https://doi.org/10.1029/2009GL041816

Wendisch, M., Macke, A., Ehrlich, A., Lupkes, C., Mech, M., Chechin, D., et al. (2019). The Arctic cloud puzzle: Using ACLOUD/PASCAL multiplatform observations to unravel the role of clouds and aerosol particles in Arctic amplification. *Bulletin of the American Meteorological Society*, *100*, 841–871. https://doi.org/10.1175/BAMS-D-18-0072.1

Wex, H., Huang, L., Zhang, W., Hung, H., Traversi, R., Becagli, S., Sheesley, R. J., Moffett, C. E., Barrett, T. E., Bossi, R., Skov, H., Hünerbein, A., Lubitz, J., Löffler, M., Linke, O., Hartmann, M., Herenz, P., and Stratmann, F.: Annual variability of ice-nucleating particle concentrations at different Arctic locations, Atmos. Chem. Phys., 19, 5293–5311, https://doi.org/10.5194/acp-19-5293-2019, 2019.

1105
1106 Xian, P., J. S. Reid, J. F. Turk, E. J. Hyer and D. L. Westphal: Impact of models versus
1107 satellite measured tropical precipitation on regional smoke optical thickness in an
1108 aerosol transport model, *Geophys. Res. Lett.*, 36, L16805, doi:10.1029/2009GL038823,
1109 2009.
1110
1111 Xian, P., Reid J. S., Hyer, E., Sampson, C.R., Rubin,J., Ades M., et. al., Current state of
1112 the global operational aerosol multi-model ensemble: an update from the International
1113 Cooperative for Aerosol Prediction (ICAP), 2019, Quarterly J. of the Royal Met. Soc.
1114 https://doi.org/10.1002/qj.3497
1115
1116 Yang, Y., Wang, H., Smith, S. J., Easter, R. C., and Rasch, P. J.: Sulfate Aerosol in the
1117 Arctic: Source Attribution and Radiative Forcing, J. Geophys. Res.-Atmos., 123, 1899–
1118 1918, https://doi.org/10.1002/2017JD027298, 2018.
1119
1120 Yumimoto, K., Tanaka, T. Y., Oshima, N., and Maki, T.: JRAero: the Japanese
1121 Reanalysis for Aerosol v1.0, Geosci. Model Dev., 10, 3225–3253,
1122 https://doi.org/10.5194/gmd-10-3225-2017, 2017.
1123
1124 Zamora, L. M., Kahn, R. A., Cubison, M. J., Diskin, G. S., Jimenez, J. L., Kondo, Y.,
1125 McFarquhar, G. M., Nenes, A., Thornhill, K. L., Wisthaler, A., Zelenyuk, A., and Ziemba,
1126 L. D.: Aircraftmeasured indirect cloud effects from biomass burning smoke in the Arctic
1127 and subarctic, Atmos. Chem. Phys., 16, 715–738, https://doi.org/10.5194/acp-16-715-
1128 2016, 2016.
1129
1130 Zhang, J. L., and J. S. Reid, 2006: MODIS aerosol product analysis for data
1131 assimilation: Assessment of over-ocean level 2 aerosol optical thickness retrievals. *J.*
1132 *Geophys. Res.-Atmos.*, **111**.
1133
1134 Zhang, J. and Reid, J. S.: A decadal regional and global trend analysis of the aerosol
1135 optical depth using a data-assimilation grade over-water MODIS and Level 2 MISR
1136 aerosol products, Atmos. Chem. Phys., 10, 18879-18917, doi:10.5194/acpd-10-18879-
1137 2010, 2010.
1138
1139 Zhang, J., Reid, J. S., Alfaro-Contreras, R., and Xian, P.: Has China been exporting less particulate
1140 air pollution over the past decade?, *Geophys. Res. Lett.*, 44, 2941– 2948,
1141 doi:10.1002/2017GL072617, 2017
1142
1143 Zhang, J. L., J. S. Reid, D. L. Westphal, N. L. Baker, and E. J. Hyer, 2008: A system for
1144 operational aerosol optical depth data assimilation over global oceans. J. Geophys.
1145 Res., 113, D10208, doi:10.1029/2007JD009065.

1146
1147 Zhao, C., & Garrett, T. J. (2015). Effects of Arctic haze on surface cloud radiative
1148 forcing. *Geophysical Research Letters*, *42*, 557–564.
1149 https://doi.org/10.1002/2014GL062015
1150
1151 Zhang, Z.; Wang, L.; Xue, N.; Du, Z. Spatiotemporal Analysis of Active Fires in the
1152 Arctic Region during 2001–2019 and a Fire Risk Assessment Model. *Fire* **2021**, *4*, 57.
1153 https://doi.org/10.3390/fire4030057
1154
1155